Experimental Assessment of Structure-Borne Noise Excitation by Axial Piston Pumps

Zur Erlangung des akademischen Grades eines

Doktors der Ingenieurwissenschaften (Dr.-Ing.)

von der KIT-Fakultät für Maschinenbau
des Karlsruher Instituts für Technologie (KIT)

angenommene

Dissertation

von

M. Sc. Matthias Vogt

Tag der mündlichen Prüfung:	07. August 2026
Erster Gutachter:	Prof. Dr.-Ing. Marcus Geimer
Zweiter Gutachter:	Prof. Dr. rer. nat. Frank Gauterin

Karlsruher Institut für Technologie
Fakultät für Maschinenbau
Kaiserstraße 12
76131 Karlsruhe

Abstract

The continuous reduction of noise emissions from internal combustion engines, together with the increasing adoption of significantly quieter electric motors in battery-driven systems, has increased the demand for low-noise components in mobile machinery. While this development poses major challenges for component manufacturers, it also offers substantial potential for reducing the overall noise levels of mobile working machines. A fundamental prerequisite for the development of low-noise machinery is the reliable identification, assessment, and quantification of the contribution of individual noise sources.
One of the primary sources of noise in mobile machinery are hydraulic pumps, such as axial piston pumps. A challenge in experimentally assessing the noise contribution of hydraulic pumps arises from the fact that they emit all three types of noise: airborne noise (ABN), fluid-borne noise (FBN), and structure-borne noise (SBN). While well-established experimental source characterization methods exist for FBN excitation at the pump's discharge port and for ABN emissions through the pump housing, studies on SBN excitation at the mechanical mounting of hydraulic pumps are rare. Consequently, the characterization of SBN represents the missing link in the complete noise assessment of hydraulic pumps.
A method that has recently gained increasing attention, particularly in the automotive sector, is the In Situ Blocked Force method. This approach enables a robust characterization of SBN sources in their typical installation environment based on so-called blocked forces. Blocked forces are receiver-system-independent interface quantities, allowing for a source-specific description of SBN excitation and thus providing a promising basis for assessing the SBN excitation by axial piston pumps.
This thesis investigates the suitability of the In Situ Blocked Force method for characterizing the SBN excitation by an axial piston pump. In this context, different interface definitions are examined, and a preferred configuration is identified that allows intuitive interpretation of the excitation while remaining consistent across pump mounting geometries. Based on the blocked-force-based source characterization, simplified methods for assessing the SBN excitation by axial piston pumps are derived. These include two source-specific approaches, where the assessment metrics depend solely on the pump, and one receiver-dependent approach incorporating the dynamic behavior of an electrified excavator. These approaches aim to enable a straightforward evaluation of a pump's SBN excitation, facilitating the identification of critical operating points and comparison of different pumps. Through an extensive experimental study of a specific axial piston pump, the metrics are evaluated in terms of practicality, robustness, and explanatory capability.

***Keywords*:** Structure-Borne Noise Assessment, Axial Piston Pumps, Source Characterization, Blocked Forces, Transfer Path Analysis

Kurzfassung

Die kontinuierliche Reduzierung der Geräuschemissionen von Verbrennungsmotoren sowie der zunehmende Einsatz von, im Vergleich zu Verbrennungsmotoren, deutlich leiseren Elektromotoren in batteriebetriebenen Systemen haben die Nachfrage nach geräuscharmen Komponenten in mobilen Arbeitsmaschinen erhöht. Während diese Entwicklung für Komponentenhersteller Herausforderungen mit sich bringt, bietet sie zugleich ein großes Potenzial zur Senkung des Gesamtgeräuschpegels mobiler Arbeitsmaschinen. Eine grundlegende Voraussetzung für die Entwicklung geräuscharmer Maschinen ist die zuverlässige Identifikation, Bewertung und Quantifizierung des Beitrags einzelner Geräuschquellen.

Eine der wesentlichen Geräuschquellen in mobilen Arbeitsmaschinen sind Hydraulikpumpen, wie beispielsweise Axialkolbenpumpen. Eine zentrale Herausforderung bei der experimentellen Bewertung des Geräuschbeitrags von Hydraulikpumpen besteht darin, dass sie alle drei Arten von Geräuschen emittieren: Luftschall, Flüssigkeitsschall und Körperschall. Während für die Flüssigkeitsschallanregung am Hochdruckanschluss der Pumpe sowie für die Luftschallabstrahlung über das Pumpengehäuse etablierte experimentelle Methoden zur Quellencharakterisierung existieren, gibt es kaum Untersuchungen zur Körperschallanregung an der mechanischen Anbindung von Hydraulikpumpen. Folglich stellt die Charakterisierung des Körperschalls den fehlenden Baustein für die vollständige Geräuschbewertung von Hydraulikpumpen dar.

Eine Methode, die in jüngster Zeit insbesondere im Automobilbereich zunehmend an Bedeutung gewonnen hat, ist die In-situ-Blocked-Force-Methode. Dieser Ansatz ermöglicht eine robuste Charakterisierung von Körperschallquellen in ihrer typischen Einbausituation auf Basis sogenannter blockierter Kräfte. Blockierte Kräfte sind empfängerunabhängige Schnittstellenkenngrößen, die eine quellspezifische Beschreibung der Körperschallanregung erlauben und somit eine vielversprechende Grundlage für die Bewertung der Körperschallanregung durch Axialkolbenpumpen darstellen.

In dieser Arbeit wird die Eignung der In-situ-Blocked-Force-Methode zur Charakterisierung der Körperschallanregung einer Axialkolbenpumpe untersucht. In diesem Zusammenhang werden unterschiedliche Schnittstellendefinitionen analysiert und eine bevorzugte Konfiguration identifiziert, die sowohl eine intuitive Interpretation der Anregung ermöglicht als auch über verschiedene Pumpenbefestigungsgeometrien hinweg konsistent bleibt. Auf Basis der Quellencharakterisierung mittels blockierter Kräfte werden vereinfachte Methoden zur Bewertung der Körperschallanregung von Axialkolbenpumpen abgeleitet. Diese umfassen zwei quellspezifische Ansätze, bei denen die Bewertungsgrößen ausschließlich von der Pumpe abhängen, sowie ein empfängerabhängiger Ansatz, welcher das dynamische Verhalten eines elektrifizierten Baggers mitberücksichtigt. Die abgeleiteten Kenngrößen sollen eine einfache Bewertung der Körperschallanregung einer Pumpe ermöglichen und damit die Identifikation kritischer Betriebspunkte sowie den Vergleich unterschiedlicher Pumpen erleichtern. Im Rahmen einer umfangreichen experimentellen Untersuchung einer spezifischen Axialkolbenpumpe werden die Kenngrößen hinsichtlich ihrer Praktikabilität, Robustheit und Aussagekraft bewertet.

***Schlagworte*:** Körperschallbewertung, Axialkolbenpumpen, Quellcharakterisierung, Blockierte Kräfte, Transferpfadanalyse

Danksagung

Die vorliegende Arbeit entstand während meiner Tätigkeit als externer Doktorand in der Funktionsgruppenentwicklung von Axialkolbenpumpen bei Bosch Rexroth in Horb am Neckar in Zusammenarbeit mit dem Institutsteil für Mobile Arbeitsmaschinen des Karlsruher Instituts für Technologie.

Ein besonderer Dank gilt Prof. Dr.-Ing. Marcus Geimer für die Übernahme des Hauptreferats sowie Prof. Dr. rer. nat. Frank Gauterin für die Übernahme des Korreferats. Ich hatte das große Glück, dass Sie beide mich von Beginn meiner Zeit als Doktorand begleitet haben. Ihre Expertise in den Bereichen Hydraulik und Akustik hat sich dabei ideal ergänzt und mir eine hervorragende Betreuung meiner Arbeit ermöglicht. Gerade als externer Doktorand in der Industrie haben mir unsere Diskussionen immer wieder geholfen, den wissenschaftlichen Fokus der Arbeit im Blick zu behalten. Gleichzeitig haben Sie mir stets den Freiraum gegeben, neue Wege zu gehen, und damit maßgeblich dazu beigetragen, dass ich dieses Kapitel nun erfolgreich abschließen konnte. Zudem möchte ich Prof. Dr. rer. nat. habil. Hans Jürgen Seifert für die Übernahme des Prüfungsvorsitzes danken.

Mein Dank gilt auch meinen Kollegen und Freunden des Institutsteils für Mobile Arbeitsmaschinen. Sowohl während meiner Zeit als wissenschaftlicher Mitarbeiter als auch – und ganz besonders – während meiner Zeit als externer Doktorand habt Ihr mich stets unterstützt. Besonders hervorheben möchte ich Benjamin Kazenwadel, Marina Graf und Johannes Knapp, die mir bei den verschiedensten Anfragen, die oft von Horb aus kamen, immer tatkräftig zur Seite standen.

Ganz besonders möchte ich mich bei meinen Kollegen und Freunden bei Bosch Rexroth bedanken, die diese Untersuchung überhaupt erst möglich gemacht haben. Es ist ein großes Privileg, in einem Unternehmen zu arbeiten, in dem trotz des wirtschaftlichen Drucks auf technischen Fortschritt und Innovation gesetzt wird. Mein besonderer Dank gilt Peter Roos, Tobias Mosthaf und Stefan Haug für die hervorragende Betreuung meiner Arbeit, den Freiraum und das damit verbundene Vertrauen, das mir während meiner Untersuchungen entgegengebracht wurde. Ebenso danke ich den Kollegen des Bosch-Konzerns, insbesondere Jan Herrmann und dem *Bosch Sound Propagation*-Team sowie Kevin Wienen und Michael Sturm, für die fachliche Unterstützung und den unverzichtbaren Support mit Messtechnik und Auswerte-Tools. Ein besonderer Dank gilt auch Max Romeser und Felix Ruthmann für die wissenschaftliche und seelische Unterstützung während meiner Zeit als Doktorand, insbesondere aber auf Tagungen. Es macht vieles leichter, wenn man Doktoranden-Freunde hat, mit denen man seine Herausforderungen und Sorgen teilen kann!

Ein herzliches Dankeschön gilt meinen Eltern Johanna und Reiner, meinen Schwestern Andrea und Stefanie sowie all meinen Freunden, die während meines Studiums und meiner Promotion immer für mich da waren. Ohne Euren Rückhalt, Eure Unterstützung und vor allem Eure Nachsicht wäre diese Arbeit nicht möglich gewesen. Zum Schluss möchte ich mich ganz besonders bei meiner Partnerin Malina bedanken. Gerade wenn die Zweifel groß wurden, hast du mich aufgebaut und mir immer wieder den Mut gegeben, auf meine Fähigkeiten zu vertrauen.

Euch allen möchte ich auch für die vielen schönen Momente danken, die mir geholfen haben, die Arbeit einmal zu vergessen und neue Energie zu tanken. Am Ende blicke ich auf vier anstrengende, aber vor allem auch schöne Jahre zurück, in denen ich viel lernen durfte und unglaublich viel Unterstützung erfahren habe.

Karlsruhe, im August 2026 *Matthias Vogt*

Contents

Abbreviations and Symbols

Mathematical Notations

Scalar	Lower-case symbols: a, b, ω
Vector	Bold-face lower-case symbols: $\mathbf{a}, \mathbf{b}, \boldsymbol{\omega}$
Matrix	Bold-face capitals: $\mathbf{A}, \mathbf{B}, \boldsymbol{\Omega}$
a^*	Complex conjugate value of a complex scalar a
$\|\|\mathbf{a}\|\|$	Euclidean norm of vector $\mathbf{a}$
$\mathbf{A}^{\mathrm{T}}$	Transpose of matrix $\mathbf{A}$
$\mathbf{A}^{\mathrm{H}}$	Transpose and complex conjugate (Hermitian) of matrix $\mathbf{A}$
$\mathbf{A}^{-1}$	Standard inverse of matrix $\mathbf{A}$
$\mathbf{A}^{+}$	Pseudo inverse of matrix $\mathbf{A}$

Acronyms

ABN	Airborne noise
cTPA	Component-Based Transfer Path Analysis
DoF	Degree(s) of freedom
DIN	German Institute for Standardization (Deutsches Institut für Normung)
EN	European Norm
FBN	Fluid-borne noise
FBS	Frequency-Based Substructuring
FRF	Frequency response function
IDM	Interface displacement mode
ISO	International Organization for Standardization
OBV	On-Board Validation
RaLa	Reflectionless Termination (Reflexionsarmer Leitungsabschluss)
RMS	Root-Mean-Square
RSS	Root-Sum-Square
SBN	Structure-borne noise
SNR	Signal to noise ratio
SPL	Sound pressure level
TPA	Transfer Path Analysis

VAP	Virtual Acoustic Prototyping	
VP	Virtual point	
VPT	Virtual Point Transformation	

Latin Symbols

a	Acceleration	$\mathrm{m/s^2}$
f	Force	N
$\mathbf{F}$	Filter matrix of VPT	-
g	Actual interface force	N
H	Vibro-acoustic transfer function	Pa/N
L_F	Force level	dB
L_M	Torque level	dB
L_p	Sound pressure level	dB, dB(A)
L_W	Power level	dB
m	Generalized VP load	N, Nm
$\lVert\mathbf{m}_{\mathrm{T}}^{\mathrm{bl}}\rVert$	Load-based assessment metric for translational DoF	N
$\lVert\mathbf{m}_{\mathrm{R}}^{\mathrm{bl}}\rVert$	Load-based assessment metric for rotational DoF	Nm
n	Rotational speed	rpm
p	Pressure	Pa
p_{H}	Hydraulic pressure at the pump's discharge port	bar
P'	Active hydraulic pulsation/FBN power	W
$\widetilde{P}'_{\mathrm{p}}$	Source-specific active hydraulic pulsation/FBN power	W
P	Active mechanical SBN power	W
P_{Char}	Real part of Characteristic Power	W
q	Generalized VP velocity	m/s, 1/s
$\lVert\mathbf{q}_{\mathrm{T}}^{\mathrm{free}}\rVert$	Vector norm of the translational VP velocities	m/s
$\lVert\mathbf{q}_{\mathrm{R}}^{\mathrm{free}}\rVert$	Vector norm of the rotational VP velocities	1/s
Q	Volume flow	$\mathrm{m^3/s}$
$\mathbf{R}$	IDM matrix of VPT	-
S	Mechanical SBN power	W
$\mathbf{T}$	Transformation matrix of VPT	-
u	Generalized displacement quantity	m, m/s, $\mathrm{m/s^2}$
v	Velocity	m/s
V_d	Displacement volume hydraulic pump	$\mathrm{m^3}$
Y	Generalized mechanical admittance	m/N, m/s/N, $\mathrm{m/s^2/N}$
Z	Generalized mechanical dynamic stiffness	N/m, N/m/s, $\mathrm{N/m/s^2}$
Z'	Hydraulic impedance	$\mathrm{Pa/m^3/s}$

Greek Symbols

ρ	Consistency of VPT	-
ω	Angular frequency, angular velocity	1/s

Sub- and Superscripts

$(\cdot)_\mathrm{S}$	Source quantity
$(\cdot)_\mathrm{R}$	Receiver quantity
$(\cdot)_1$	Source internal excitation quantity
$(\cdot)_2$	Interface quantity
$(\cdot)_3$	Receiver quantity
$(\cdot)_4$	Indicator quantity
$(\cdot)_\mathrm{f}$	Indicates load DoF in the original coordinate system
$(\cdot)_\mathrm{m}$	Indicates load DoF in the VP coordinate system
$(\cdot)_\mathrm{q}$	Indicates displacement DoF in the VP coordinate system
$(\cdot)_\mathrm{u}$	Indicates displacement DoF in the original coordinate system
$(\cdot)_X$, $(\cdot)_Y$, $(\cdot)_Z$	Indicates translational VP DoF
$(\cdot)_{\theta_X}$, $(\cdot)_{\theta_Y}$, $(\cdot)_{\theta_Z}$	Indicates rotational VP DoF
$(\cdot)_\mathrm{1VP}$	Indicates single-VP configuration quantity
$(\cdot)_\mathrm{2VP}$	Indicates dual-VP configuration quantity
$(\cdot)_\mathrm{2VP\text{-}1}$	Indicates a quantity of the 1^st VP of the dual-VP configuration
$(\cdot)_\mathrm{2VP\text{-}2}$	Indicates a quantity of the 2^nd VP of the dual-VP configuration
$(\cdot)^\mathrm{bl}$	Blocked interface quantity
$(\cdot)^\mathrm{free}$	Free interface quantity
$(\cdot)^\mathrm{A}$	Quantity pertaining to Source **A**
$(\cdot)^\mathrm{B}$	Quantity pertaining to general receiver **B**
$(\cdot)^\mathrm{C}$	Quantity pertaining to general receiver **C**
$(\cdot)^\mathrm{R}$	Quantity pertaining to general test rig receiver **R**
$(\cdot)^{\mathrm{R_B}}$	Quantity pertaining to test rig receiver $\mathbf{R_B}$
$(\cdot)^{\mathrm{R_C}}$	Quantity pertaining to test rig receiver $\mathbf{R_C}$
$(\cdot)^\mathrm{E}$	Quantity pertaining to excavator receiver **E**
$(\cdot)^\mathrm{AB}$	Quantity pertaining to assembly **AB**
$(\cdot)^\mathrm{AC}$	Quantity pertaining to assembly **AC**
$(\cdot)^\mathrm{AR}$	Quantity pertaining to assembly **AR**
$(\cdot)^{\mathrm{AR_B}}$	Quantity pertaining to assembly $\mathbf{AR_B}$
$(\cdot)^{\mathrm{AR_C}}$	Quantity pertaining to assembly $\mathbf{AR_C}$
$(\cdot)^\mathrm{AE}$	Quantity pertaining to assembly **AE**

1 Introduction

1.1 Motivation

The reduction of greenhouse gas emissions to mitigate global climate change represents one of the central objectives of contemporary society. In line with this objective, increasingly stringent regulatory frameworks have been introduced, such as the European Green Deal [1], which aims to achieve climate neutrality within the European Union by 2050 and defines an intermediate target of at least a 55 % reduction in greenhouse gas emissions by 2030 compared to 1990. According to estimates published in 2024 [2], hydraulic machinery account for approximately 4 % of total greenhouse gas emissions, with mobile hydraulic machines contributing nearly one half of this share and therefore representing a significant contribution. As a consequence, manufacturers of mobile working machines face growing pressure to reduce emissions.
Emission reduction can be achieved through the development of more efficient drive systems and components, as well as through the transition to alternative, locally emission-free drive concepts, such as electrified powertrains [3]. However, the deployment of electric motors or quieter internal combustion engines fundamentally increases the acoustic requirements for the remaining drivetrain components of mobile working machines. While the absence of loud internal combustion engines reduces the absolute noise level of mobile working machines, the loss of their masking effect makes the noise emissions of other drivetrain components significantly more perceptible [4], [5].
A promising approach to meeting these higher acoustic requirements is the systematic identification of dominant noise sources and relevant noise transmission paths within mobile working machines, enabling the targeted application of noise mitigation measures. In electrified mobile working machines, hydraulic pumps—used to provide hydraulic power for traction or working functions—are frequently identified as dominant noise sources [6], [7] under many operating conditions and therefore offer significant potential for overall noise reduction. However, analyzing the noise contribution of hydraulic pumps is challenging, as they emit all three types of noise: airborne noise (ABN), fluid-borne noise (FBN), and structure-borne noise (SBN). For a targeted and effective analysis, these noise paths must be investigated separately. While established evaluation methods and standards exist for the characterization of ABN radiated from the pump housing and for FBN excitation at the pump's discharge port, no comparable standardized methodology for assessing SBN excitation at the pump mounting is available. Consequently, SBN represents the missing link in a comprehensive noise assessment of hydraulic pumps.
This situation may appear counterintuitive, as numerous previous studies [8]–[12] on

mobile machinery and industrial hydraulic systems have demonstrated that SBN transmission can contribute significantly to the overall noise radiation of hydraulic systems. A reason for the lack of standardized assessment approaches lies in the comparatively higher complexity of SBN description. Unlike ABN and FBN, which are characterized using scalar field quantities, SBN excitation generally requires a vectorial description involving multiple interface quantities. However, advances in SBN source characterization and *Transfer Path Analysis* (TPA) offer new opportunities to overcome these limitations. Further developed methods in these fields, such as the In Situ Blocked Force TPA, enable the description of SBN excitation of various machine types using receiver-independent interface quantities. This allows a source characterization that is conceptually comparable to established approaches for ABN and FBN.
Building on these source characterization concepts, this thesis aims to develop simplified assessment approaches for the straightforward evaluation of SBN excitation caused by axial piston pumps and to examine their suitability for practical application. Such assessment metrics provide the basis for identifying critical operating conditions and for comparing different pumps with respect to their SBN excitation, thereby enabling the derivation of appropriate mitigation measures. Furthermore, a detailed understanding of the pump's SBN excitation characteristics also enables system-level optimization, for example in mobile machinery. Once the source excitation characteristics are known, measures such as the design of decoupling elements and the configuration of pump mounting concepts can be pursued in a more systematic and application-oriented manner.

1.2 Terminology and Definitions

This section provides definitions of essential terms to ensure clarity and consistency in their application throughout the thesis.

- *Internal SBN Excitation vs. SBN Excitation*
  Throughout this work, it is important to clearly distinguish between *internal SBN excitation* and *SBN excitation.*
  Internal SBN excitation refers to the source-internal excitation mechanisms that generate SBN within the source itself. For an axial piston pump, for example, this includes the SBN excitation caused by the individual piston forces acting inside the pump.
  SBN excitation, in contrast, refers to the SBN excitation by the source at the interface to the receiving system. In the case of an axial piston pump, this corresponds, for example, to the loads acting at the mounting points of the pump.

- *Characterization vs. Assessment of SBN Sources*
  In this work, the terms *characterization* and *assessment* of SBN sources are used repeatedly, and they should be distinguished as follows:
  Characterization of a SBN source refers to the general objective of describing the excitation of a SBN source through appropriate interface quantities.
  Assessment of a SBN source, on the other hand, refers to the goal of being able to

evaluate the SBN excitation of a source in a straightforward manner by applying simplifications to the complete source description.

- *Blocked Forces vs. Blocked Load*
  The most important quantities for characterizing SBN sources in this work are the blocked forces. These are the forces acting at the source's mounting, i.e., at the interface, when any motion at the interface is completely constrained. The term blocked force is well established in structural dynamics and is frequently used in methods for source characterization, such as the In Situ Blocked Force TPA. In the context of this work, both blocked forces and blocked torques are employed to describe the SBN excitation. When both blocked forces and blocked torques are explicitly referred to, the collective term *blocked loads* is used. Conversely, when methods from the literature for characterizing SBN sources are discussed, the commonly used term *blocked force* is retained.

1.3 Structure of the Thesis

The content of this thesis is structured into six chapters.
After outlining the motivation and describing the overall structure of the thesis, Chapter 2 presents the state of the art relevant to this work. First, existing methods for the assessment of noise generated by hydraulic pumps are reviewed. Subsequently, general approaches for the characterization of SBN sources are introduced. At the end of this chapter, the research gap is identified and formulated in terms of three central research questions.
Chapter 3 introduces the theoretical foundations required to derive the assessment methods for the SBN excitation by an axial piston pump. These foundations can be further divided into TPA methods, the *Virtual Point Transformation* (VPT), and power-based source characterization approaches. Special focus is placed on the In Situ Blocked Force TPA to determine the blocked forces, which represent the fundamental quantities for all SBN assessment methods in this work.
In Chapter 4, the three approaches for assessing the SBN excitation by an axial piston pump are introduced, and the relationships required for their determination are presented. A distinction is made between source-specific and receiver-dependent assessment.
The results of the experimental investigations are presented in Chapter 5, where the SBN excitation of the axial piston pump is analyzed for a stationary operating point and for a rotational speed run-up. Finally, the different assessment methods are compared and discussed with respect to their practicality, robustness, and explanatory capability.
In the final chapter, Chapter 6, the main findings of this thesis are summarized and the research questions are answered. The chapter concludes with an outlook on potential directions for future research.

Parts of this work have already been published in [110]–[113].
Supporting work was carried out within two supervised student theses by Bünyamin Yakut [107] and Tom Böckle [108].

2 State of Research

This chapter provides an overview of the current state of research on noise assessment of hydraulic pumps, with a particular focus on axial piston pumps. It covers established methods for characterization ABN and FBN of hydraulic pumps and discusses SBN characterization approaches developed for other types of machinery but not yet adapted to hydraulic pumps. This review identifies the research gap that motivates the methodology proposed in this thesis.

The challenge in assessing the contribution of axial piston pumps to the overall noise of a mobile working machine lies in the fact that hydraulic pumps emit all three types of noise: ABN, FBN, and SBN. To enable a comprehensive assessment of the acoustic behavior of a pump, all three types of noise must be evaluated separately.[1]

Figure 2.1 illustrates the noise transfer within a mobile working machine caused by an axial piston pump, assuming that SBN transmitted through the hydraulic lines can be neglected.

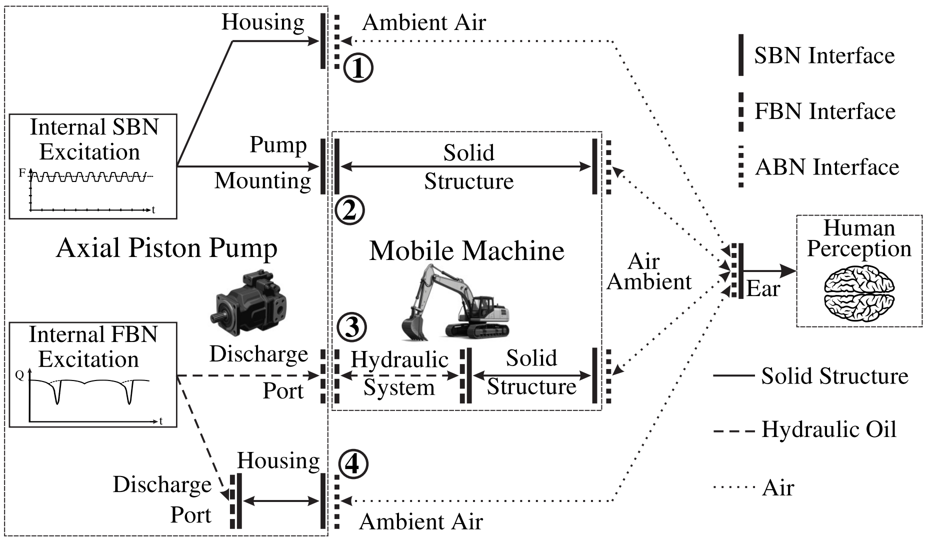

Figure 2.1: Noise transfer paths from the axial piston pump to the drivers ear in a mobile working machine

[1] In the literature, the terms *structure-borne sound* and *airborne sound* are often used instead of *structure-borne noise* (SBN) and *airborne noise* (ABN), as these are more general expressions. SBN and ABN are typically used when discussing sound that is considered disruptive or undesirable. In hydraulics, however, *fluid-borne noise* (FBN) is the common expression when dealing with sound issues within the hydraulic system. Given this and the fact that both structure-borne and airborne sound from hydraulic pumps are typically undesirable, this thesis will consistently use the terms SBN, FBN, and ABN.

The primary internal excitation mechanisms within an axial piston pump can be divided into an internal SBN excitation and an internal FBN excitation. These excitation mechanisms lead, on the one hand, to an ABN directly emitted from the pump housing ① ④ and, on the other hand, to FBN and SBN transmitted via the pump discharge port ③ and the pump mounting ② to the vehicle. The FBN excitation at the discharge port is commonly referred to as flow ripple or fluid pulsation. The SBN excitation at the pump mounting is the noise excitation that this thesis focuses on. Here, it is important to note that the term *internal SBN excitation* refers to the SBN excitation mechanisms within the pump, while the expression *SBN excitation* denotes the SBN excitation of the pump at the interface to the receiving structure.

The FBN and SBN excitations at the interface with the mobile working machine induce vibrations in the machine structure, which subsequently generate ABN. The overall noise at the driver's ear is then the sum of all four noise paths. For a targeted root cause analysis, all noise contributions must be evaluated separately. Therefore, the following section introduces existing methods for assessing the emitted ABN as well as the FBN and SBN excitation at the interface of hydraulic pumps.

2.1 Noise Assessment of Hydraulic Pumps

The primary focus of this thesis is the evaluation of hydraulic pumps with respect to the SBN excitation. However, the following section also provides an overview of various methods used to assess FBN and ABN. This is motivated by the observation that methods developed for the characterization of noise sources across different physical domains share fundamentally similar concepts, even though they have often been developed and studied independently.

The objective is to emphasize these analogies, thereby establishing a unified perspective on the different noise evaluation techniques applicable to hydraulic pumps. In addition, this overview helps to contextualize the structural-dynamic relationships introduced in Chapter 3 for the characterization of SBN sources. While these relationships may initially appear complex due to their vector representation, they are, in principle, closely analogous to the scalar relationships that govern hydraulic phenomena.

2.1.1 Fluid-Borne Noise Assessment

Flow pulsation—i.e., the FBN Excitation by the pump to the hydraulic system—is one of the main causes of noise emission in hydraulic systems [8]. The internal FBN excitation mechanism in an axial piston pump can be divided into kinematic pulsations, due to the finite number of displacement elements, and pulsations resulting from compressibility of the hydraulic oil. The compression-induced pulsations occur during the transition of a piston from the suction port to the discharge port of the pump, when the pressure in the piston chamber differs from that in the discharge port. In general, these pulsations are an order of magnitude higher than the kinematic flow pulsation. [13], [14] Since fluid pulsation can lead to not only noise issues but also other problems within the hydraulic system, various studies [15]–[19] have been conducted to characterize the FBN excitation of hydraulic pumps. An older, yet still extensive, overview of the various characterization methods is provided in [20]. The fundamental objective of such characterization techniques is to eliminate the influence of the receiving system, i.e., the hydraulic circuit connected to the pump, so that the intrinsic properties of the source can be evaluated. The combined system of the source and the connected hydraulic network can be represented in terms of its hydraulic impedances, as illustrated in Figure 2.2.

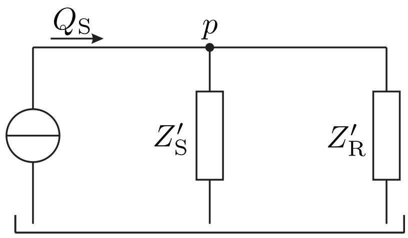

Figure 2.2: Impedance representation of a hydraulic circuit consisting of FBN source (Q_S, Z'_S) and circuit impedance Z'_R (adapted from ISO 10767-2:1999 [21])

In this representation, the pump is modeled as an ideal flow source Q_S in parallel with a source impedance Z'_S, which constitutes the hydraulic analogue of Norton's equivalent circuit for electrical current sources. Here, Q_S denotes the flow rate of the ideal flow source assumed at the discharge port of the pump, while Z'_S represents a complex hydraulic impedance comprising resistive, inertive, and capacitive components. The ideal volume flow Q_S corresponds to the flow rate if the source impedance Z'_S were infinitely high. However, due to the finite impedance of the source, the actual flow delivered to the hydraulic circuit does not exactly correspond to Q_S. The pressure p observed at the pump's discharge port is influenced not only by the source flow Q_S and the source impedance Z'_S, but predominantly by the impedance of the hydraulic circuit Z'_R. Therefore, p constitutes a system-dependent quantity that reflects the dynamic interaction between the pump and the connected hydraulic network.[20], [21]

2.1.1.1 Methods for Comprehensive Characterization

For a comprehensive characterization of hydraulic pumps with respect to FBN—for instance, when modeling pumps for dynamic hydraulic simulations—it is necessary to determine both Q_S and Z'_S [22]. Commonly used methods for this purpose are the *Secondary Source* method [23], [24], which formed the basis of ISO 10767-1:1996, and the *Two Pressures-Two Systems* method [25], [26], described in the revised edition of ISO 10767-1:2015.
These two methods are particularly relevant when the pulsation characteristics of a hydraulic pump are to be fully modeled. A major challenge, however, is that no measurement technology currently exists that can directly capture hydraulic flow pulsation with sufficient sampling frequency [22], [27], [28]. Therefore, both the Secondary Source method and the Two Pressures-Two Systems method employ multiple high-frequency pressure

measurements in combination with a wave propagation model of a well-defined test setup to calculate the quantities Q_S and Z'_S.
In the Secondary Source method, an additional excitation source is incorporated in the hydraulic system. In a first step, by exciting the system with this secondary source and measuring the responses at the multiple pressure transducers, the source impedance Z'_S of the pump under test can be determined. In the second step, with the secondary source turned off and only the test pump running, the source flow ripple Q_S is calculated from the measured pressure signals using the now-known source impedance.
In contrast, the Two Pressures–Two Systems method determines these quantities without an additional source by measuring pressure signals (typically at two or more locations) in two different, well-defined hydraulic system configurations. The variation in system impedance between these configurations enables the calculation of Z'_S and Q_S. Both approaches, Secondary Source and Pressures–Two Systems method, have been validated in several studies [27], [29], but they are also associated with significant experimental complexity and measurement effort.

2.1.1.2 Pressure-Ripple-Based Methods

Alternative approaches, which are primarily used for the experimental evaluation of pump pulsation characteristics, include the so-called *High-Impedance Pipe* method [30] and the *Reflectionless Termination (RaLa)* method (also called *Anechoic Termination* method) [13], [31]. Unlike the two previously mentioned methods, the objective here is not to determine Q_S and Z'_S. Instead, the connected hydraulic system, i.e., Z'_R, is designed in a way that the measured pressure at the discharge port p is largely independent of the downstream hydraulic circuit. In this case, p represents a pure source quantity. These methods have the significant advantage that the source-characterizing quantity is measured directly, rather than being derived from other quantities.

High-Impedance Pipe Method

The idea behind the High-Impedance Pipe Method—which also forms the basis of the standard ISO 10767-2:1999 [21]—is that, if the impedance of the downstream hydraulic circuit Z'_R is much greater than the pump source impedance Z'_S, the pressure at the pump outlet becomes independent of the hydraulic circuit and corresponds to the blocked acoustic pressure p^{bl}. Mathematically, this relationship can be derived by applying Kirchhoff's first law to the system shown in Figure 2.2. The pressure at the pump outlet can then be expressed as:

$$Q_S = \frac{p}{Z'_S} + \frac{p}{Z'_R} \quad \Rightarrow \quad p = \frac{Q_S Z'_S}{1 + \frac{Z'_S}{Z'_R}}. \tag{2.1}$$

If the condition $|Z'_R| \gg |Z'_S|$ is fulfilled, it follows that:

$$p = p^{bl} \approx Q_S Z'_S, \tag{2.2}$$

where it becomes immediately apparent that p^{bl} represents a pure source quantity. If Z'_{S} is known, the flow ripple Q_{S} can also be calculated based on Equation 2.2. [20]
When directly using the blocked pressure as an evaluation metric, it is important to note that p^{bl} is also affected by the source impedance Z'_{S}, which is primarily determined by the pump's discharge passageway. Therefore, a quantitative comparison of pumps with respect to FBN excitation using the High-Impedance Pipe method is only valid if their discharge passageways, or equivalently their source impedances Z'_{S}, are identical.
A method that follows the same principle but does not exactly match the test procedure specified in ISO 10767-2:1999 is the *Short Pipe End* method, which is described in detail in [32].

Reflectionless Termination Method (RaLa)
The alternative pressure-ripple-based approach is the RaLa method, which represents the hydraulic equivalent of an anechoic chamber. This method has the additional advantage that it enables a straightforward determination of the flow pulsation Q_{S}.
Figure 2.3 illustrates the schematic setup and the corresponding impedance representation of a typical test setup for the measurement-based characterization of flow pulsation. In this configuration, the pump delivers flow into a reference pipe, which is terminated by a throttle valve. Here, as in Figure 2.2, the pump is represented by a Norton equivalent model. The hydraulic system is modeled as a pipe with a characteristic impedance Z'_0 and a termination impedance Z'_{T} corresponding to the throttle. In a conventional setup, operation of the pump leads to the formation of a standing wave within the reference pipe, causing both flow and pressure pulsations to vary along the spatial x coordinate. The principle of the RaLa method is to adjust the termination impedance Z'_{T} such that it exactly matches the characteristic impedance of the pipe, i.e., $Z'_{\mathrm{T}} = Z'_{\mathrm{RaLa}} = Z'_0$ thereby eliminating reflections at the pipe termination and ensuring a reflection-free flow condition within the reference pipe.

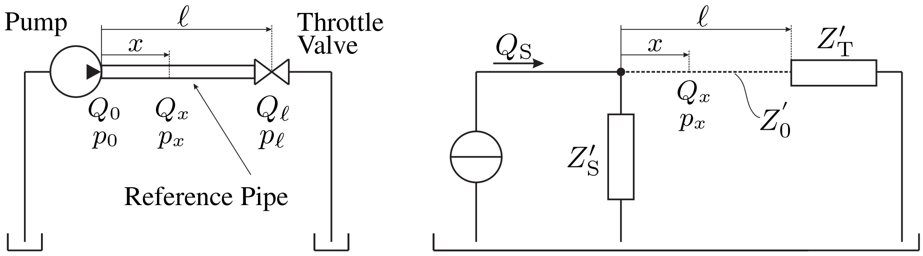

Figure 2.3: Typical test setup (left) and corresponding impedance representation (right) for the experimental characterization of FBN (adapted from [21] and [33])

For this purpose the throttle valve has to be replace by a RaLa, which is described in detail in multiple previous studies [13], [14], [20], [31], [34]. Therefore, the practical implementation will not be discussed further in this work.
If a reflection-free flow condition is established in the test rig using the RaLa, the pressure

ripple is the same at every location in the reference pipe and thus also at the discharge port of the pump. In this case p can be expressed as:

$$p = Z'_{\mathrm{RaLa}} Q_{\mathrm{S}}, \tag{2.3}$$

where Z'_{RaLa} can be computed from the orifice equation of the RaLa and corresponds to a real-valued, approximately frequency-independent proportionality factor. This relation allows the flow pulsation of the pump to be directly obtained from the measured pressure. It should be emphasized that Equation 2.3 implies that the flow through the RaLa corresponds to the total pump flow Q_{S}. To satisfy this condition, the measurement setup must ensure that $|Z'_{\mathrm{S}}| \gg |Z'_{\mathrm{RaLa}}|$.

2.1.1.3 Power-Based Methods

A further, less established yet noteworthy approach is the characterization of the flow pulsation of hydraulic pumps using the *Source Pulsation Power*, as proposed by Kojima in [33]. The objective of this method is to define a hydraulic equivalent—or more specifically, a FBN equivalent—to the sound power, which is commonly used for ABN characterization. As the previous source characterization metrics, this quantity also aims to characterize the pump itself, independently from the downstream hydraulic circuit. The experimental setup employed for this purpose is the same as in Figure 2.3.
The fundamental idea behind this approach is that the active component P' of the pulsation power is given by:[2]

$$P' = \frac{1}{2}\mathrm{Re}\{p_x Q_x^*\}, \tag{2.4}$$

where p_x denotes the pressure pulsation and Q_x the flow pulsation at position x in the reference pipe (see Figure 2.3). Furthermore, $\mathrm{Re}\{\cdot\}$ denotes the real part of a complex variable, and the superscript $(\cdot)^*$ represents the complex conjugate.
The active power P' can be decomposed into a progressive wave (outgoing) component P'_{p} and a regressive wave (reflected) component P'_{r}, such that:

$$P' = P'_{\mathrm{p}} - P'_{\mathrm{r}}. \tag{2.5}$$

As the regressive power arises from reflections within the hydraulic circuit, Kojima considers only P'_{p} as representative of the power generated inherently by the pump. However, since the pressure p_x depends on the hydraulic impedance of the measurement setup, P'_{p} remains influenced by the downstream hydraulic system. To compensate for this dependence, Kojima introduced a conversion factor K, which combines the specific impedance characteristics of the test setup such that multiplying P'_{p} by K eliminates all test-stand-related influences. The corrected, system-independent power quantity is then defined as:

$$\widetilde{P'_{\mathrm{p}}} = K P'_{\mathrm{p}}. \tag{2.6}$$

[2] In the referenced source [33], the active component of the pulsation power is denoted by W_a. However, to maintain consistency in the notation of power quantities throughout this thesis, the variable P' is used instead.

By introducing the conversion factor K, the pulsation power is effectively referenced to a standardized measurement configuration. This enables the direct comparison of pumps tested on different test benches—for instance, due to different displacement volumes of the pumps—on a consistent basis.

As evidenced by the large number of investigations and the variety of partially standardized methods, the FBN characterization of hydraulic pumps is a well-established research field. A thorough understanding of the capabilities and, in particular, the limitations of each method is crucial for selecting the most appropriate approach according to the specific research objective, while also considering the associated experimental effort.

2.1.2 Airborne Noise Assessment

Another well-studied topic is the ABN emission of axial piston pumps. Much of the literature addresses noise reduction measures, either through optimization of the pump housing [35]–[39] or by improving internal excitation mechanisms [40]–[45] to achieve lower noise levels. These studies have demonstrated that the dominant ABN emission from the pump housing originates from internal SBN excitation caused by pressure fluctuations in the piston chambers of the power unit. The superposition of the individual piston forces lead to three main SBN excitation mechanisms in the power unit: an axial force and, due to the eccentric point of action of this force, two swash plate torques (for a detailed description, see [14], [36], [46]). Other mechanical excitations—such as those caused by bearing irregularities or rotational imbalances—are typically of minor significance [40], [47], [48].
A further potential source of ABN is the pressure pulsation in the outlet channel (see 4 in Figure 2.1). However, Haarhaus [40] demonstrated that these pulsations contribute only marginally to the ABN emission of axial piston pumps, what is confirmed by recent investigations of He et al. [49].
The standard method for assessing ABN in the aforementioned publications is the determination of the airborne sound power radiated by the pump, which is briefly outlined in the following.

Airborne Sound Power
Similar to the characterization of FBN, several approaches exist for assessing ABN emissions. For hydraulic pumps, however, the determination of airborne sound power according to ISO 4412-1:1991 [50], defined in 1991, has become the predominant method.
The procedure and test setup specified in this standard aims to measure only the ABN directly emitted from the pump housing. ABN generated as a consequence of SBN excitation or FBN excitation (2 and 3 in Figure 2.1) are to be minimized as far as possible. Accordingly, specific requirements are imposed on the test setup to reduce these influences. Particular attention is given to the mechanical mounting of the pump and its coupling to the drive motor. The standard specifies that the mounting shall be designed to minimize noise radiated from surfaces other than the pump housing, such as the supporting structure.

Furthermore, the drive motor shall either be located outside the test space, with the pump driven via flexible couplings and an intermediate shaft, or be isolated within an acoustic enclosure.
Within ISO 4412-1:1991, for the determination of the sound power level, reference is made to ISO 3744:2010 [51], which defines procedures for calculating the sound power of machinery from microphone signals in various acoustic environments.
The A-weighted sound power level of a pump resulting from this procedure represents a single-value, pump-specific metric, enabling a straightforward and standardized assessment of ABN.

Acoustic Source Characterization
The ABN evaluation according to ISO 4412-1:1991 aims to ensure comparability between different pumps by standardizing the environmental conditions as much as possible. Another approach to characterizing ABN sources—one that has not yet been specifically standardized for hydraulic pumps but is commonly used in the context of Virtual Acoustic Prototyping (VAP)—is the *Acoustic Source Characterization* or *Acoustic Source Quantification* method. This method shares many similarities with the *In Situ Blocked Force* approach, which will be discussed in detail later for the characterization of SBN sources.
Similar to sound power determination, the objective of Acoustic Source Characterization is to identify ABN-describing quantities that are independent of the acoustic environment of the source. The key distinction, is that the quantities obtained through the Acoustic Source Characterization method can be combined with acoustic transfer functions. This enables the prediction of the ABN emitted by the source at any location within an acoustic environment, provided that the corresponding acoustic transfer function is known.
Hence, this approach is well suited for the development of virtual acoustic models of assembled systems. Vesikar, for instance, successfully applied this methodology in various publications for the acoustic analysis of a wheel loader [52], an excavator [53], and a tractor [54].

2.1.3 Structure-Borne Noise Assessment

As already mentioned in the introduction of this thesis, no established methods or standards currently exist for the assessment of SBN excitation by hydraulic pumps. In a few studies [55], [56], acceleration sensors mounted on the receiver structure have been used for evaluation of SBN. This represents a straightforward and practical approach but does not allow for a receiver-independent assessment of the SBN. The lack of standardized methods for characterizing the SBN emitted by hydraulic pumps is noteworthy, given that several investigations [8]–[12] have identified this specific noise component as a major contributor to the overall sound of hydraulic systems and mobile machinery.
One potential reason for this is the inherently more complex nature of SBN compared to FBN and ABN. For example, only longitudinal waves can propagate in fluids, whereas in solids multiple wave types (longitudinal, transverse, and bending) can occur simultaneously [57]. Consequently, for ABN and FBN the field variables pressure and acoustic particle

velocity (ABN) or volume flow (FBN) can be described using scalar quantities, whereas SBN generally requires vector quantities such as force and velocity vectors. Furthermore, in the case of ABN it can be reasonably assumed that the surrounding environment—i.e., the receiving system—has little influence on the characteristics of the source itself. This assumption does not hold for FBN. However, the characterization of hydraulic pumps considering FBN remains comparatively simple, as the acoustic propagation within hydraulic lines can typically be approximated as one-dimensional.
Since such simplifying assumptions generally cannot be made for SBN of hydraulic pumps, its characterization is correspondingly more complex. In other fields, such as automotive steering systems or heat pumps, the characterization of SBN excitation has long been of significant importance. Consequently, a few approaches for the characterization of specific types of SBN sources have been developed and standardized, which will be introduced in the following section.

2.2 Characterization of Structure-Borne Noise Sources

The objective of developing a general method for the characterization of SBN sources dates back to the 1980s. At that time, the characterization of ABN based on sound power was already standardized, and there was growing interest in defining an equivalent, preferably single-valued quantity for SBN. In this context, the ISO committee TC43 published a paper [58] proposing several potential approaches to address this problem, which were subsequently evaluated and discussed by various experts in acoustics. [59]
Based on this publication [58], the key requirements a suitable SBN source characterization method should fulfill are the following:

1. Comparison of structure-borne sound emissions of similar machines
2. Verification of compliance with prescribed limit values
3. Determination of input data for acoustic planning (e.g., prediction of sound levels under installed conditions)
4. Provision of the necessary data for the design and development of low-noise machinery

However, subsequent investigations revealed that no generally valid and at the same time simple description of SBN sources fulfilling all these requirements could be established. This limitation primarily arises from the inherent complexity of SBN and its strong dependence on boundary conditions such as machine type, mounting conditions, operating environment, and application. [57]
As a consequence, two different types of characterization approaches were developed. The first group comprises methods that are applicable to a wide variety of SBN sources and aim to comprehensively describe the SBN excitation by means of multiple interface quantities. The In Situ Blocked Force method, which was later standardized in ISO 20270-1:2019, represents such a type of characterization approach. In practice, however, these methods

suffer from the drawback that a large number of interface quantities are required for source description. As a result, a direct comparison between different SBN sources and straightforward verification of compliance with prescribed limit values—corresponding to the first two requirements listed above—are not readily possible.
For this reason, a second group of simplified characterization methods has also been developed to enable a more accessible description and assessment of SBN excitation. Such simplifications, however, cannot be applied universally to all types of SBN sources but are only valid for specific source types, depending on their physical properties and installation conditions. Exactly such simplified approaches are described in the standards ISO 9611:1996 and DIN EN 15657:2017. The standard ISO 9611:1996 [60] specifies a procedure for the characterization of SBN sources of resiliently mounted machinery, while DIN EN 15657:2017 [61] defines measurement techniques for SBN transmitted from building services equipment, such as heat pumps. The following quotation from ISO 9611:1996 summarizes the key aspects of SBN source characterization:

> *A major problem associated with the measurement of structure-borne sound emission is the choice of the quantities that characterize the "strength" of a source. The complete and fully accurate characterization of a source of structure-borne sound would involve an extremely large number of measurements; thus, one has somehow to trade accuracy against the simplicity of the method. In the context of standardization, emphasis is on simplicity; therefore an attempt has been made to describe "strength" by a limited number of frequency-dependent quantities.*

This statement highlights two main challenges and one primary objective in SBN source characterization:

- *Challenge 1:* Defining suitable quantities to describe the source.
- *Challenge 2:* A complete characterization requires an extremely large number of measurements/quantities.
- *Objective:* Achieving a simple yet representative description using a limited set of quantities.

The potential quantities related to *Challenge 1* are introduced in the following section and share many similarities with those used in FBN characterization. In contrast, *Challenge 2* reflects a fundamental difference between SBN and FBN. Due to the complexity and directional dependence of SBN, comprehensive characterization of SBN sources typically requires numerous measurements and source-describing quantities. The objective of the following standardized methods is therefore to simplify the source description by reducing the number of required quantities, which is only feasible for application-specific cases.

2.2.1 General Considerations

In order to define potential source-describing quantities—analogous to the FBN characterization discussed in Section 2.1.1—the impedance representation of a mechanical source-receiver system is introduced here, following the approach proposed in [59].

Therefore the concept of impedance in the context of SBN must be introduced in advance. In structural dynamics, a distinction is generally made between dynamic stiffness and admittance. Dynamic stiffness is defined as the frequency-dependent ratio between a force and a displacement quantity. It can therefore be interpreted as a complex frequency-dependent resistance to an excitation. Depending on the type of displacement quantity considered, different specific terms are used—namely dynamic stiffness, impedance, and apparent mass.
Admittance is the reciprocal of dynamic stiffness and thus serves as a measure of the system's susceptibility to vibrate. Similar to dynamic stiffness, specific terms for admittance are used depending on the chosen displacement variable. Table 2.1 provides an overview of the various designations. As can be seen from this table, impedance in the context of SBN is defined as the ratio of force to velocity.

Table 2.1: Overview of the definition of dynamic stiffness and admittance in structural dynamics according to [62]

Dynamic Stiffness	$Z(\omega)$	Unit	Admittance	$Y(\omega)$	Unit
Dynamic Stiffness	f/u	N/m	Receptance	u/f	m/N
Impedance	f/v	N/m/s	Mobility	v/f	m/s/N
Apparent Mass	f/a	N/m/s^2	Accelerance	a/f	m/s^2/N

Analogous to the FBN analysis, any mechanical system consisting of an active source and a passive receiver can be represented by means of an impedance representation. Figure 2.4 illustrates an exemplary one-dimensional mechanical source-receiver-system, together with the impedance representations for modeling the source either as a velocity source or as a force source. Although it was mentioned above that real mechanical systems generally cannot be considered one-dimensional, this special case is initially examined here. This simplifies the mathematical relationships, while the fundamental concept of the individual characterization approaches remains similar for the multidimensional case.

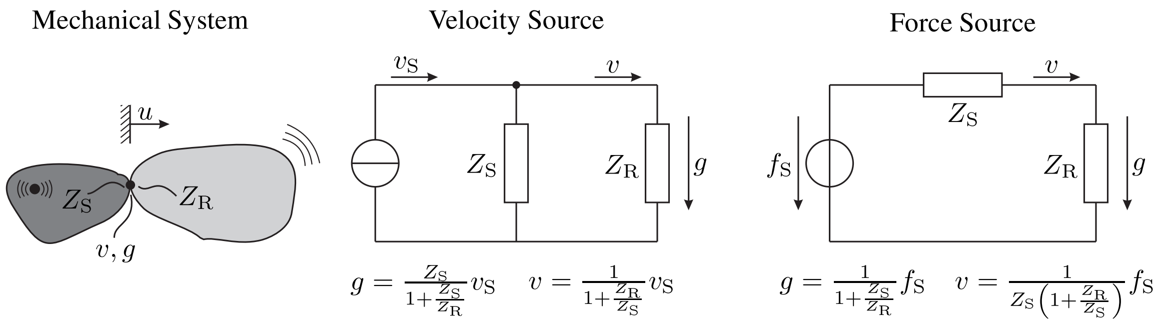

Figure 2.4: Impedance representation for an one-dimensional mechanical source-receiver-system (adapted from [59])

The left graph of the figure illustrates that internal SBN excitation of the source leads to forces g and velocities v at the interface between the source and the receiver. Similar to FBN, the real source can be modeled as an ideal source with source impedance. In

Figure 2.4, the ideal source quantities at the interface are denoted by the subscript $(\cdot)_\mathrm{S}$.[3] The resulting interface forces and velocities are determined by these ideal source quantities together with the source impedance Z_S and the receiver impedance Z_R.
As shown in Figure 2.4, the mechanical source can be represented either as an ideal velocity source or as an ideal force source. In the case of the velocity-based source description, the source is modeled—analogous to the FBN representation of a hydraulic pump—as an ideal flow source with a parallel source impedance Z_S, corresponding to a Norton-equivalent formulation. In the alternative force-based source description, it is modeled as an ideal effort source with the source impedance connected in series, according to Thévenin's theorem. Figure 2.4 further shows, below each impedance representations, the resulting relationships for v and g, as a function of the ideal source quantity and the impedances.
For a receiver-independent characterization of SBN, three special cases of the receiver impedance Z_R can be defined: $|Z_\mathrm{R}| \ll |Z_\mathrm{S}|$, $|Z_\mathrm{R}| \gg |Z_\mathrm{S}|$, $Z_\mathrm{R} \approx Z_\mathrm{S}$. By substituting these conditions into the equations given in Figure 2.4, simplified relationships for the velocity v and the force g, as well as the complex SBN power at the interface, can be derived. These relationships are identical for both source modeling approaches and are summarized in Table 2.2. The complex power S is given by the product of the complex conjugated force g^* and the velocity v, with a factor of $1/2$ if amplitudes are used instead of Root-Mean-Square (RMS) values[4] for the force and velocities.

Table 2.2: Special cases of receiver impedance Z_R for a mechanical source-receiver system

Z_R	**Velocity**	**Force**	**Power**
$\lvert Z_\mathrm{R}\rvert \ll \lvert Z_\mathrm{S}\rvert$	$\boxed{v \approx \frac{f_\mathrm{S}}{Z_\mathrm{S}} = v_\mathrm{S} = v^\mathrm{free}}$	$g \approx 0$	$S \approx 0$
$\lvert Z_\mathrm{R}\rvert \gg \lvert Z_\mathrm{S}\rvert$	$v \approx 0$	$\boxed{g \approx Z_\mathrm{S} v_\mathrm{S} = f_\mathrm{S} = f^\mathrm{bl}}$	$S \approx 0$
$Z_\mathrm{R} \approx Z_\mathrm{S}$	$v \approx \frac{g}{Z_\mathrm{S}} \approx \frac{v_\mathrm{S}}{2} = \frac{v^\mathrm{free}}{2}$	$g \approx Z_\mathrm{S} v \approx \frac{f_\mathrm{S}}{2} = \frac{f^\mathrm{bl}}{2}$	$\boxed{S \approx \frac{1}{2} \frac{f_\mathrm{S}{}^* v_\mathrm{S}}{4} = \frac{f^{\mathrm{bl}*} v^\mathrm{free}}{8}}$

For the case $|Z_\mathrm{R}| \ll |Z_\mathrm{S}|$, the interface force and, accordingly, the power vanish. The interface velocity v is then equal to that of the ideal velocity source v_S and can be interpreted as the free velocity v^free.
In contrast, for $|Z_\mathrm{R}| \gg |Z_\mathrm{S}|$, the motion at the interface is approximately completely suppressed, causing the velocity—and consequently the power—to vanish. The interface force g then becomes a pure source quantity and equals the ideal force excitation f_S, which can therefore be identified with the blocked force f^bl.
In the third case, when $Z_\mathrm{R} \approx Z_\mathrm{S}$, the velocities and forces at the interface are directly related through Z_S. The resulting power is then exactly one quarter of the power obtained by multiplying the blocked force and the free velocity. This relationship is of particular

3 In the referenced source [59], an overbar $\bar{(\cdot)}$ was used to denote the ideal source quantities. For consistency with the FBN characterization, this work uses the subscript $(\cdot)_\mathrm{S}$. Moreover, the variable g is used to denote the interface force instead of f, which might seem more reasonable at first glance. However, since g is the standard notation for the interface force in the later introduced framework of TPA, it is also used here.

4 For a harmonic signal, the RMS value equals the amplitude divided by $\sqrt{2}$. Using amplitudes instead of RMS values therefore introduces an additional factor of $1/2$ in the power expression.

interest for the later introduced Characteristic Power assessment approach.
Table 2.2 thus illustrates that different receiver-independent quantities arise for the various special cases of Z_R, which are potentially suitable for describing the SBN source. These quantities form the basis for the standardized methods for characterizing SBN sources presented in the following sections.

2.2.2 Source Characterization According to ISO 9611:1996

As discussed previously, the characterization of SBN excitation generally requires multiple interface quantities. A simplification of the source description by reducing the number of quantities is only possible by introducing additional assumptions, which can be justified only for specific types of SBN sources. One such approach is followed by the characterization method specified in ISO 9611:1996, which defines a procedure for characterizing resiliently mounted machines. The idea here is to mount the machine very softly so that the interface velocities can be assumed to be the free velocities.
Figure 2.5 illustrates the principal test setup for a machine characterized according to ISO 9611:1996. The machine contacts with the surrounding structure are assumed to behave as point contacts. These contact points, also called supports, are connected via resilient mounts (isolators) to a foundation, with the isolators being considered part of the receiving structure. Multiple accelerometers are placed near each contact point. Relative motion between the transducer signals at a support allows the determination of translational and rotational accelerations and velocities using Finite Difference methods. This is valid as long as rigid-body conditions between the transducers of a support are satisfied, which defines the method's upper frequency limit. The standard generally covers 20 to at least 1000 Hz, which, in the context of the standard, is regarded as covering the frequency range most relevant for many practical SBN applications.

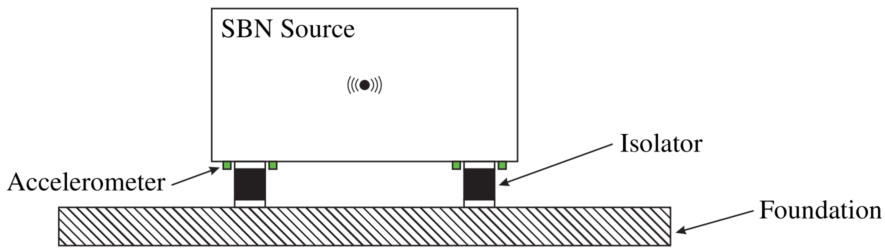

Figure 2.5: Typical test setup for measurements in accordance with ISO 9611:1996

Due to the relatively soft isolators compared to the machine structure, it can be assumed within a limited frequency range that $|Z_R| \ll |Z_S|$. Under this condition, the accelerations measured at the supports correspond to the free accelerations and can be converted into free translational velocities $\mathbf{v}^{\text{free}}$ and free angular velocities $\boldsymbol{\omega}^{\text{free}}$. These quantities are vectorial, as up to three velocities and three angular velocities can be determined at each support.
A crucial requirement of the approach is that the coupling and phase relationships between different supports can be neglected, allowing each support to be treated as an independent

SBN source. This condition depends on the support spacing and is generally satisfied only above a certain frequency. Accordingly, the standard advises caution for results below approximately 200 Hz.
If all the above conditions are met for the frequency range of interest, the determined free velocities serve as receiver-independent quantities to characterize the source. For machines with multiple contact points, however, this results in many different velocity components describing the source. To reduce the number of quantities, the standard proposes energy-based averaging of all support velocity components in each coordinate direction, resulting in a maximum of six frequency-dependent velocities describing the source. This consolidation ignores phase relations between the combined velocities. However, as mentioned above, neglecting coupling and phase relationships between different supports is a necessary condition for the validity of the method.

2.2.3 Source Characterization According to DIN EN 15657:2017

A more recent and product-specific standard is DIN EN 15657:2017, which specifies various methods for the characterization of SBN emitted by building service equipment, such as heating and cooling units, fans, and sanitary installations. The sources considered in this standard must be connectable to receiver plates, or in other words, it must be possible to mount and operate the source on such a plate.
The objective of this standard is to determine the SBN power transmitted from a source into a receiver, which is given by the real part of the complex SBN power S and, in the one-dimensional case, can be expressed by

$$P = \frac{1}{2}\mathrm{Re}\{g^{*}v\}. \tag{2.7}$$

As the interface forces g and the interface velocities v depend on the receiver behavior, so P also represents a receiver-dependent quantity. In the standard, the determination of the transmitted power P is carried out in two steps:

1. Characterization of the source using free velocities or blocked forces together with the source point mobility at the interface (the reciprocal of the point impedance)[5]
2. Characterization of the receiver behavior at the interface by determining the point mobility of the receiver at the interface

In the standard, several simplifications are introduced, which are made possible primarily by restricting the scope of application. As in ISO 9611:1996, the source is assumed to be connected to the receiver through several discrete point contacts. Moreover, only the vibration component in the normal direction to the plate surface is considered relevant for the transmitted power, which represents a substantial simplification of the problem. It is also assumed that the individual point mobilities at the contact points can be combined

[5] A *point mobility* describes the mobility at a specific location, i.e., the ratio between velocity and force at the same point. In addition, transfer mobilities between spatially separated points can be defined. These are introduced later in the thesis and are not relevant at this stage.

into a single mobility, which, in the terminology of the standard, is referred to as *Equivalent Point Mobility*. Consequently, both the source and the receiver can each be represented by one Equivalent Point Mobility. Similarly, it is assumed that the free velocities and blocked forces can be combined energetically into one *Equivalent Free Velocity* and one *Equivalent Blocked Force*. Thus, both steps—source characterization and receiver point mobility determination—reduce to a one-dimensional problem.
Particularly relevant for this thesis is the first step, since the source characterization is performed using methods that yield a receiver-independent description of the source. Two different procedures are proposed for this purpose: a direct and an indirect method. The direct method is based on the procedure described in ISO 9611:1996, whereas the indirect method is based on the so-called *Reception Plate* method [63]–[65], which will be discussed in detail in the following.
Application of the reception plate method relies on the simplifying assumptions outlined above. In particular, it is assumed that only the vibration in the direction normal to the plate surface is relevant, and that the free velocities, blocked forces, and point mobilities can each be represented as one-dimensional quantities. The method determines these quantities through a three-step procedure involving two distinct reception plates. Figure 2.6 illustrates the schematic layout of the reception plate method. The green squares represent the randomly distributed measurement locations, which are typically accelerometers.

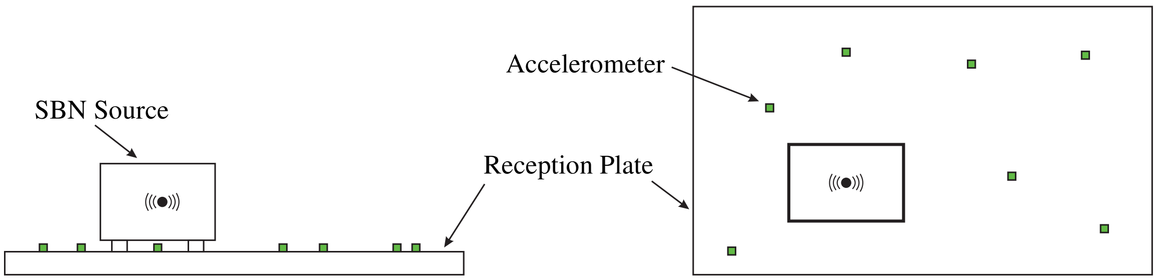

Figure 2.6: Schematic layout of the test setup for the reception plate method, adapted from [66]

In the first step of the method, the source is rigidly mounted on a high-mobility plate ($|Y_\mathrm{R}| \gg |Y_\mathrm{S}|$, or equivalently, low impedance $|Z_\mathrm{R}| \ll |Z_\mathrm{S}|$), such as a thin steel plate. The source is operated, and plate accelerations are measured at several randomly placed points (see 2.6). Based on the measured accelerations and the structural dynamic properties of the plate, the SBN power transmitted to the reception plate is obtained. Using the transmitted power and the known plate mobility, the Equivalent Free Velocity of the source can then be computed.
In the second step, the source is mounted on a low-mobility plate ($|Y_\mathrm{R}| \ll |Y_\mathrm{S}|$, i.e., high impedance $|Z_\mathrm{R}| \gg |Z_\mathrm{S}|$), such as a concrete plate. Analogously, the Equivalent Blocked Force is derived from the measured responses and plate properties.
Finally, the Equivalent Point Mobility of the source is determined from the ratio of Equivalent Free Velocity to Equivalent Blocked Force, as the two are directly related through the source point mobility or impedance (see Table 2.2). This procedure allows the determination of all relevant source quantities, which are expressed as single-valued parameters,

thereby allowing a compact and practical characterization of the installed SBN source. Consequently, DIN EN 15657:2017 provides a standardized and practically applicable framework for SBN characterization, which, however, depends on several simplifying assumptions to remain feasible.

The two standards presented for a simplified characterization of SBN sources are fundamentally similar in that both assume the source is connected to the receiver structure through several point-like contact interfaces. However, additional assumptions are made—such as in ISO 9611:1996, where the individual contact points have to be mounted resiliently to the receiver, or in DIN EN 15657:2017, where only the vibration component in the normal direction is considered relevant.

For hydraulic pumps, however, it is expected that the simplifying assumptions from these standards do not hold for the contact between the pump and the corresponding receiver structures. Hydraulic pump interfaces are typically characterized by flange-like steel-to-steel contacts with multiple closely spaced bolting points. Under such configurations, it is reasonable to assume that:

- The individual contact points are strongly coupled
- Excitation occurs in multiple spatial directions
- Both forces and torques contribute significantly to the SBN excitation

Furthermore, the pump is driven by an external motor rather than by internal combustion or other self-excited processes, which makes it impossible to drive it on a receiver plate. Given these considerations, it can be concluded that, the assumptions made in ISO 9611:1996 and DIN EN 15657:2017 are not directly applicable to hydraulic pumps. Thus, a comprehensive analysis of the SBN excitation by such pumps is required as a basis for identifying suitable simplifications.

A possible approach to provide such a comprehensive description is the In Situ Blocked Force method standardized in ISO 20270-1:2019 [67]. Similar to the reception plate method, it represents an indirect approach for determining blocked forces, but it requires considerably fewer restrictive assumptions. The method is highly flexible and can be applied to a wide range of SBN sources [68]–[76]. For this reason, it has gained increasing popularity in the automotive industry in recent years, ultimately leading to its standardization in 2019. The application of this method constitutes one of the core elements of this work and will therefore be introduced in detail in Chapter 3.

Based on the comprehensive description of the SBN excitation obtained by means of the In Situ Blocked Force method, simplified SBN assessment approaches are subsequently derived in this thesis. In this way, the In Situ Blocked Force method serves as a fundamental framework from which application-specific simplifications for hydraulic pumps can be systematically developed.

As stated at the beginning of this chapter, the methods introduced for the evaluation of FBN and ABN of hydraulic pumps are not strictly required for the development of a methodology to assess SBN excitation. Nevertheless, these approaches have been included for several reasons. First, these methods provide a basis for understanding how the characterization of SBN differs from that of the other two noise types, primarily due to its multidimensional excitation characteristics. While the characterization of ABN also differs substantially from that of SBN, the approaches used for characterizing FBN and SBN excitation are highly comparable. In both cases, the primary objective is to eliminate the influence of the receiver system in order to obtain source-specific quantities that are independent of the test environment. Therefore, by introducing methods for characterizing FBN, this chapter aims to facilitate a clearer understanding of the underlying concepts of SBN characterization, which are often perceived as more complex. This is expected to be particularly beneficial for readers with a background in hydraulics. Finally, this chapter provides an overview of the currently established methods for the noise assessment of hydraulic pumps, thereby placing the SBN-focused methodology developed in this work within a broader methodological context.

2.3 Research Gap

As the previous sections of this chapter have shown, the characterization of the SBN excitation represents the missing link for a comprehensive noise assessment of hydraulic pumps. Existing standards for the assessment of SBN sources—primarily developed for other types of machinery—are of limited applicability, as their underlying assumptions are not expected to hold for hydraulic pumps.

To address this gap, this work investigates various approaches for the experimental assessment of SBN excitation by hydraulic pumps. A central objective is to simplify the SBN excitation of the pump to enable a straightforward assessment. In addition, the strengths and limitations of the investigated methods are systematically analyzed with respect to their applicability, robustness, and validity ranges.

Although the experimental investigations presented in this work are limited to an axial piston pump, the developed approaches are designed with the intention of being applicable to other hydraulic pump types. This assumption is supported by the standardized mechanical mounting interfaces of hydraulic pumps defined in ISO 3019-1:2001 [77], which provide a common structural connection to the receiver system.

Based on these considerations, the objectives of the present investigations are guided by the following research questions:

- Is the In Situ Blocked Force method according to ISO 20270-1:2019 suitable for experimentally characterizing the structure-borne noise excitation by an axial piston pump?
- What is an appropriate interface definition for describing the structure-borne noise excitation by an axial piston pump?
- How can the structure-borne noise excitation by an axial piston pump, described using multiple interface quantities, be summarized into a straightforward evaluation metric?

The first research question is addressed through the implementation of the In Situ Blocked Force method for an axial piston pump, enabling an evaluation of its suitability for SBN source characterization of hydraulic pumps. The second research question concerns the definition of an appropriate source-receiver interface. Here, the goal is to establish an adequate compromise between accuracy and practical applicability of the interface description. Based on this, several approaches for aggregating the interface quantities to enable a simplified assessment of the SBN excitation are proposed. By analyzing the resulting assessment metrics based on an experimental investigation of an axial piston pump, the third research question is subsequently addressed.

Overall, the objective of this research is not to define a single optimal assessment metric, but rather to systematically investigate the advantages and limitations of different approaches. The results are intended to provide guidance for selecting a suitable method depending on specific application requirements and boundary conditions.

3 Theoretical Framework for Structure-Borne Noise Source Characterization

As discussed in detail in the previous chapter, the original goal of developing a universal and at the same time straightforward method for the characterization of SBN sources could not be achieved. Instead, two main approaches were pursued. On the one hand, application-specific methods were developed and standardized to enable simplified evaluation, e.g., ISO 9611:1996 and DIN EN 15657:2017.

On the other hand, methods were designed to comprehensively describe the source with the specific objective of characterizing SBN sources in such a way that the radiated sound in the installed condition can be predicted. Thus, the focus here is shifted from simplification toward a comprehensive representation of the source behavior, enabling reliable sound prediction. Such methods form the basis for Virtual Acoustic Prototyping (VAP), where a digital model is used to represent the acoustic behavior of a system. A thorough overview of the historical developments that enabled the concept of VAP is provided in [59].

A major breakthrough in the realization of VAP was achieved in 2009 with the publication of the In Situ Blocked Force method by Moorhouse et al. [78]. This method forms the basis of the current standard ISO 20270-1:2019—*Characterization of sources of structure-borne sound and vibration—Indirect measurement of blocked forces*. In contrast to other approaches, the In Situ Blocked Force method imposes fewer restrictions on the source-receiver interface and is therefore applicable to a wide range of SBN sources [68]–[76].

Since the In Situ Blocked Force method belongs to the broader framework of Transfer Path Analysis (TPA), the following section provides an introduction to TPA as applied to SBN sources. This is followed by a description of the Virtual Point Transformation (VPT), which provides the basis for a distinct definition of the source-receiver interface. The chapter concludes with the introduction to power-based source characterization approaches.

3.1 Introduction to Transfer Path Analysis

The general objective of TPA is to investigate the transmission paths through which noise is transferred from one or more sources to a receiver. In this way, noise-critical sources, excitation degrees of freedom (DoF), or dominant transmission paths can be identified and analyzed. Based on this understanding, targeted noise reduction measures can subsequently be implemented. A comprehensive overview of the various TPA methodologies

can be found in [79]. The notation and theoretical framework introduced in the following are also based on this reference.
Before introducing the TPA concept in detail, it is important to note that problems in experimental structural dynamics are typically formulated in terms of admittances $Y(\omega)$ rather than impedances $Z(\omega)$, unlike in Section 2.2.1. Although impedance and admittance are physically related through inversion, admittances are preferred in practice because they are easier to measure. The admittance between an excitation point to multiple receiver points can be obtained by exciting the structure with an impact hammer or shaker and measuring the vibration response with multiple accelerometers. By contrast, determining impedance would require imposing a prescribed movement at the excitation point while constraining the vibrations at all receiver DoF and measuring the resulting force, which is impractical. Therefore, admittance is considerably easier to determine experimentally, and problem formulations in this field predominantly use the admittance description. [80]

Figure 3.1 illustrates the general transfer path problem applied to a hydraulic pump **A** connected to a arbitrary receiver system **B** such as mobile working machine (illustrated here only by the motor flange). In addition to the mounting points, the pump is also connected to the receiver via hydraulic hoses or pipes, indicated in red and blue in Figure 3.1. These interfaces are not considered here.

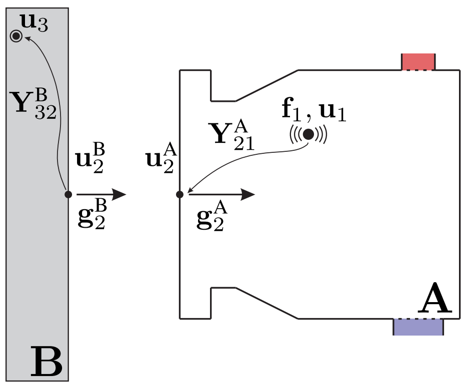

Figure 3.1: General transfer path problem applied to a hydraulic pump

The system in Figure 3.1 consists of three nodes: the excitation point within the source **1**, the interface **2**, and an arbitrary point on the receiver **3**. The internal excitation at node **1** is described by the force $\mathbf{f}_1$ and the displacement quantity $\mathbf{u}_1$. In the following the variable u is used, in accordance with standard practice in the literature, as a generalized displacement variable and may denote displacement, velocity, or acceleration. The response at the receiver point to the excitation at **1** is denoted by $\mathbf{u}_3$. At the interface, the displacement quantities on the source and receiver sides are described by $\mathbf{u}^{\mathrm{A}}_2$ and $\mathbf{u}^{\mathrm{B}}_2$, respectively, and the interface forces by $\mathbf{g}^{\mathrm{A}}_2$ and $\mathbf{g}^{\mathrm{B}}_2$. At this point, it is important to note that the superscript indicates the component to which the quantity refers. Accordingly, $(\cdot)^{\mathrm{A}}$ represents a source quantity, while $(\cdot)^{\mathrm{B}}$ denotes a receiver quantity. The superscript $(\cdot)^{\mathrm{AB}}$ indicates that the quantity is associated with the assembled system. The structural dynamic behavior of a node itself, as well as the transfer behavior between two nodes, is described using

admittances $\mathbf{Y}$. As the transmission of SBN is a typically multidimensional problem, forces and velocities at the nodes are described by column vectors, and the transfer behavior is represented using admittance matrices, both denoted by bold symbols.
The described transfer path problem can be represented by the following system of equations:

$$\underbrace{\begin{bmatrix}\mathbf{u}_1\\ \mathbf{u}_2^{\mathrm{A}}\\ \mathbf{u}_2^{\mathrm{B}}\\ \mathbf{u}_3\end{bmatrix}}_{\mathbf{u}} = \underbrace{\begin{bmatrix}\mathbf{Y}_{11}^{\mathrm{A}} & \mathbf{Y}_{12}^{\mathrm{A}} & \mathbf{0} & \mathbf{0}\\ \mathbf{Y}_{21}^{\mathrm{A}} & \mathbf{Y}_{22}^{\mathrm{A}} & \mathbf{0} & \mathbf{0}\\ \mathbf{0} & \mathbf{0} & \mathbf{Y}_{22}^{\mathrm{B}} & \mathbf{Y}_{23}^{\mathrm{B}}\\ \mathbf{0} & \mathbf{0} & \mathbf{Y}_{32}^{\mathrm{B}} & \mathbf{Y}_{33}^{\mathrm{B}}\end{bmatrix}}_{\mathbf{Y}} \underbrace{\left(\begin{bmatrix}\mathbf{f}_1\\ \mathbf{0}\\ \mathbf{0}\\ \mathbf{0}\end{bmatrix} + \begin{bmatrix}\mathbf{0}\\ \mathbf{g}_2^{\mathrm{A}}\\ \mathbf{g}_2^{\mathrm{B}}\\ \mathbf{0}\end{bmatrix}\right)}_{(\mathbf{f}+\mathbf{g})}, \tag{3.1}$$

where the subsystem admittance matrices $\mathbf{Y}^{\mathrm{A}}$ and $\mathbf{Y}^{\mathrm{B}}$ are arranged in a block-diagonal format. The admittances matrices with identical indices describe the point admittances at the nodes, while those with different indices represent the transfer admittances between the nodes.
For an assembled system, assuming a rigid behavior of the interface, the compatibility condition and the equilibrium condition at the interface must be satisfied. The compatibility condition states that the displacement on both sides of the interface must be identical, i.e., $\mathbf{u}_2^{\mathrm{B}} = \mathbf{u}_2^{\mathrm{A}}$. The equilibrium condition, which is fundamentally based on Newton's Third Law, asserts that the interface forces on the receiver side must be equal in magnitude and opposite in direction to the forces on the source side, i.e., $\mathbf{g}_2^{\mathrm{B}} = -\mathbf{g}_2^{\mathrm{A}}$. By employing Equation 3.1 in conjunction with the compatibility and equilibrium conditions, it is possible to forecast the response at the receiver $\mathbf{u}_3$ to an excitation at node **1**, provided that the excitation and the admittances of the subsystems are known.
Although predicting the response at the receiver using the internal excitation, as just described, is theoretically possible, it presents certain practical issues. In particular, the internal forces $\mathbf{f}_1$ are typically unknown with regard to their position, orientation, and magnitude. Consequently, it is not possible to define the transfer behavior, i.e., the admittances $\mathbf{Y}_{11}^{\mathrm{A}}$ and $\mathbf{Y}_{21}^{\mathrm{A}}$. A solution to this problem is to find an alternative description of the source activity that: a) is capable of physically representing the internal forces (i.e., inducing the same vibration in the structure), b) has known positions, and c) has magnitudes that can be practically determined [57].
The objective of source characterization as part of TPA is to determine such an alternative representation of the source. This is typically achieved by utilizing the interface quantities measured at interface **2** (see Figure 3.1). The TPA approaches presented in the following differ primarily in the interface quantities used to describe the source and how the response at the receiver $\mathbf{u}_3$ can be predicted based on these interface quantities.

3.1.1 Classical Transfer Path Analysis

In the first investigations in the field of TPA, the objective was to describe the source activity using the forces acting at the interface $\mathbf{g}_2^{\mathrm{A}}$ and $\mathbf{g}_2^{\mathrm{B}}$, whereby $\mathbf{g}_2^{\mathrm{A}}$ and $\mathbf{g}_2^{\mathrm{B}}$ differ only in sign due to the equilibrium condition. From the fourth row of Equation 3.1, it follows that:

$$\mathbf{u}_3 = \mathbf{Y}^{\mathrm{B}}_{32}\mathbf{g}^{\mathrm{B}}_2. \tag{3.2}$$

From this, it can be seen that the response at the receiver $\mathbf{u}_3$ is determined by the interface force $\mathbf{g}^{\mathrm{B}}_2$ and the transfer behavior from the interface to the receiver point $\mathbf{Y}^{\mathrm{B}}_{32}$. This type of TPA is referred to as *Classical TPA*.
In practice, the transfer behavior is usually determined using impact hammer or shaker measurements. When measuring $\mathbf{Y}^{\mathrm{B}}_{32}$, the source must be decoupled, as only the transfer behavior of the receiver itself (denoted by the superscript $(\cdot)^{\mathrm{B}}$) is required. This can be impractical or, depending on the connection, even impossible in practice. Furthermore, the classical TPA has the fundamental drawback, that the interface forces $\mathbf{g}^{\mathrm{B}}_2$ used in this approach are influenced not only by source but also by the structural dynamic behavior of the receiver. As a result, these forces do not represent a pure source quantity, making them not transferable to other receiver systems and unsuitable for evaluating the source itself.

3.1.2 Component-Based Transfer Path Analysis

The limitations of Classical TPA are overcome in *Component-Based Transfer Path Analysis* (cTPA). The primary goal of cTPA approaches is to describe the source using receiver-independent interface quantities. Figure 3.2 shows an overview of the most common source characterization methods in cTPA, which are introduced in the following.

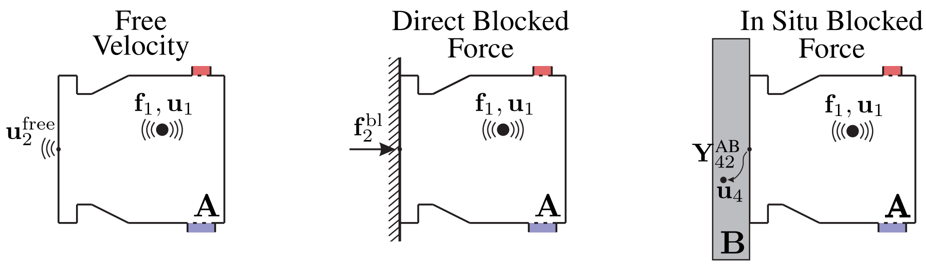

Figure 3.2: Source characterization methods in cTPA

3.1.2.1 Free Velocity

The most obvious method to characterize a source without receiver system influence is to determine an interface quantity when the source is freely vibrating, i.e., not connected to any receiver system. In this case, the force at the interface vanishes, i.e., $\mathbf{g}^{\mathrm{A}}_2 = 0$. The velocity at the interface is referred to as the free velocity, $\mathbf{u}^{\mathrm{free}}_2$. Under this condition, the second row of Equation 3.1 becomes:

$$\mathbf{u}^{\mathrm{free}}_2 = \mathbf{Y}^{\mathrm{A}}_{21}\mathbf{f}_1, \tag{3.3}$$

from which it is evident that the free velocity depends solely on source quantities, thereby allowing for a description of the source excitation at the interface. Although the characterization of SBN sources using free velocities is theoretically possible, this method is not applicable to every kind of source. This is primarily because the source must be operated under free conditions. For hydraulic pumps in particular, this is not practical, as it would eliminate any means of driving the pump.

3.1.2.2 Direct Blocked Force

Another method for eliminating environmental influences is to attach the source to a receiver with infinite mechanical impedance (e.g., very high mass and high stiffness compared to the source). In this scenario, the velocity at the interface vanishes, i.e., $\mathbf{u}_2^{\mathrm{A}} = \mathbf{u}_2^{\mathrm{B}} = 0$. The force at the interface is then referred to as the blocked force $\mathbf{f}_2^{\mathrm{bl}}$. Under these conditions, the second row of Equation 3.1 becomes:

$$0 = \mathbf{Y}_{21}^{\mathrm{A}}\mathbf{f}_1 + \mathbf{Y}_{22}^{\mathrm{A}}\mathbf{g}_2^{\mathrm{A}} \quad \text{for} \quad \mathbf{f}_2^{\mathrm{bl}} = \mathbf{g}_2^{\mathrm{bl}} = -\mathbf{g}_2^{\mathrm{A}} \tag{3.4}$$

$$\Rightarrow \mathbf{f}_2^{\mathrm{bl}} = \left(\mathbf{Y}_{22}^{\mathrm{A}}\right)^{-1} \mathbf{Y}_{21}^{\mathrm{A}}\mathbf{f}_1. \tag{3.5}$$

From this, it can be seen that the blocked forces depend solely on source quantities, making them an appropriate receiver-independent interface quantity as well. Furthermore, by substituting the term $\mathbf{Y}_{21}^{\mathrm{A}}\mathbf{f}_1$ in Equation 3.3 with the relationship from Equation 3.5, it can be seen that the blocked forces and the free velocities are directly related through the equation:

$$\mathbf{u}_2^{\mathrm{free}} = \mathbf{Y}_{22}^{\mathrm{A}}\mathbf{f}_2^{\mathrm{bl}}. \tag{3.6}$$

Thus, if the free velocities cannot be measured directly, they may alternatively be determined from the blocked forces and the point admittance of the source $\mathbf{Y}_{22}^{\mathrm{A}}$.
There are several methods for determining the blocked forces. The most obvious method is direct measurement using force transducers between the source and a receiver with sufficient impedance. Nevertheless, previous studies [81], [82] have demonstrated that the condition of sufficiently high receiver stiffness can only be met within a limited frequency range. Furthermore, mounting force transducers between the source and the receiver presents several challenges. Firstly, the stiffness of the force transducers must be sufficiently high to meet the stiffness requirements. Secondly, the sensors must not alter the contact area of the interface. While this is less of an issue for point contacts, it becomes a significant challenge for surface-like interfaces, as is typically the case for hydraulic pumps. Moreover, directly measuring torques and in-plane forces is difficult to achieve due to the complex sensor alignment. Consequently, direct measurement of blocked forces is impractical for many applications, including hydraulic pumps.

3.1.2.3 In Situ Blocked Force

Another method is the aforementioned In Situ Blocked Force method. This approach allows for the determination of blocked forces "in situ", meaning in the typical installation

condition of the source.
Moorhouse et al. demonstrated that the blocked force can be determined using the following relationship (for a detailed derivation, see [78] or [79]):

$$\mathbf{f}_2^{\mathrm{bl}} = \left(\mathbf{Y}_{42}^{\mathrm{AB}}\right)^{-1} \mathbf{u}_4. \tag{3.7}$$

This relationship states that the receiver-independent blocked forces $\mathbf{f}_2^{\mathrm{bl}}$ can be determined by multiplying the vibration responses at additional receiver points $\mathbf{u}_4$ with the inverted transfer behavior $\mathbf{Y}_{42}^{\mathrm{AB}}$ from the interface to the additional receiver points in the coupled state (denoted by the superscript $(\cdot)^{\mathrm{AB}}$). Since these additional receiver points $\mathbf{u}_4$ are not used as target quantities for purposes such as predictions, but rather for determining the blocked forces, they are usually referred to as indicators (see Figure 3.2).
From Equation 3.7, it follows that the measurement procedure for determining the blocked forces using the In Situ Blocked Force method consists of the following two steps:

- **Step 1:** Determination of the admittance matrix $\mathbf{Y}_{42}^{\mathrm{AB}}$ from the interface to the indicator points in the assembled system. For this purpose, the structure is excited in the vicinity of the interface using an impulse hammer or a shaker, and the responses at the indicator points are recorded with accelerometers.
- **Step 2:** Measurement of the operational response $\mathbf{u}_4$ at the same indicator points while the source is active. The accelerometers remain in the identical positions used during the impulse hammer or shaker excitation.

The blocked forces during operation of the source are subsequently computed using Equation 3.7 at the excitation locations defined in Step 1. This procedure enables the determination of the blocked forces without separating the source and receiver at any step of the process, thereby allowing for in situ characterization of the source.
It should be noted that the standard inverse $(\cdot)^{-1}$ in Equation 3.7 is often replaced by a pseudoinverse $(\cdot)^{+}$, as the admittance matrix $\mathbf{Y}_{42}^{\mathrm{AB}}$ is not necessarily a square matrix. In this case, the matrix inversion is carried out using a least-squares optimization procedure, which additionally mitigates the effects of measurement uncertainties and noise (for a detailed explanation, see [83]). Therefore, the standard ISO 20270-1:2019 recommends a two- to threefold overdetermination of the matrix $\mathbf{Y}_{42}^{\mathrm{AB}}$, whereas Haeussler [62] suggest an overdetermination factor of at least 1.5. In cases where such overdetermination cannot be ensured, regularization techniques—such as *Truncated Singular Value Decomposition* or *Tikhonov Regularization*—may be employed to stabilize the matrix inversion. A comprehensive overview and evaluation of different regularization approaches for the In Situ Blocked Force method is provided in [62].
Figure 3.3 visually highlights the crucial difference between describing the interface excitation using actual interface forces $\mathbf{g}_2$ (Classical TPA) and blocked forces $\mathbf{f}_2^{\mathrm{bl}}$ (cTPA). When the source is fully characterized by the corresponding interface quantity, both methods ultimately lead to the original vibration response at the receiver. In classical TPA, the interface forces are combined with the admittance $\mathbf{Y}_{32}^{\mathrm{B}}$ of the receiver only, whereas in component-based TPA, the blocked forces are applied to the coupled system $\mathbf{Y}_{32}^{\mathrm{AB}}$.

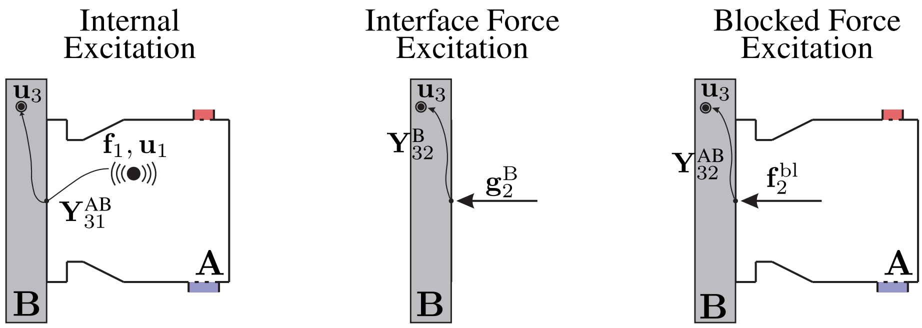

Figure 3.3: Description of the source excitation with Interface Forces and Blocked Forces (adapted from [59])

3.1.3 Quality Criteria for the In Situ Blocked Force Method

An essential aspect of the practical applicability of a TPA method is the ability to verify the quality of the obtained results. The In Situ Blocked Force method is also particularly advantageous in this respect, as it provides two practical validation approaches, namely *On-Board Validation* and *Transferability Validation*, which are introduced in this section. Achieving reliable results according to these quality criteria requires that the transfer admittance $\mathbf{Y}_{42}^{AB}$ is determined with sufficient accuracy. Common quality indicators such as *Coherence*, *Reciprocity*, and *Passivity* can be used for this purpose. Since these represent general criteria for the experimental characterization of transfer behavior, they are not discussed further here. A detailed discussion can be found in [57], [62], [80], [83], [84].

3.1.3.1 On-Board Validation

The most straightforward and particularly easy-to-apply method for in situ determination of blocked forces is the *On-Board Validation* (OBV), which is also an essential part of ISO 20270-1:2019. In this approach, the blocked forces, determined via Equation 3.7, are used to make a prediction for the receiver $\mathbf{u}_3$:

$$\mathbf{u}_3 = \mathbf{Y}_{32}^{AB}\mathbf{f}_2^{bl}. \tag{3.8}$$

The required transfer admittance $\mathbf{Y}_{32}^{AB}$ and vibration response $\mathbf{u}_3$ are typically obtained simultaneously with $\mathbf{Y}_{42}^{AB}$ and $\mathbf{u}_4$, which makes the procedure straightforward to apply. The source characterization based on blocked forces can then be validated by comparing the predicted vibrations $\mathbf{u}_3$ at the receiver locations with the corresponding measured responses. This validation is particularly valuable for assessing whether the selected number of interface loads is sufficient to represent the source dynamics accurately. Furthermore, OBV can assist in identifying potential errors or inconsistencies arising from the inversion of the admittance matrix $\mathbf{Y}_{42}^{AB}$.

In addition to OBV performed during actual source operation, an alternative OBV procedure using artificial excitation is often employed. In this case, the source remains inactive, and a controlled excitation—such as an impact hammer or shaker input—is applied directly to the source structure (e.g., the pump housing). This approach provides a well-defined and broadband input that is free from the complex characteristics of operational excitation mechanisms. Consequently, OBV with artificial excitation enables a straightforward assessment of whether excitations originating from the source side can, in principle, be represented by blocked forces. However, it does not account for the specific operational excitation mechanisms of the source.

3.1.3.2 Transferability Validation

As discussed in the previous section, OBV provides a straightforward criterion for evaluating blocked forces. However, a satisfactory OBV result represents a necessary but not sufficient condition for ensuring the validity of the blocked force description. While OBV verifies the accuracy of the source description and the matrix inversion process for one assembly, it does not confirm whether the blocked forces are independent of the receiving structure. This independence is a fundamental requirement for a meaningful source description in cTPA.

To assess this property, the concept of transferability is employed. The *Transferability Validation* examines whether the blocked forces determined on one receiving system can be successfully applied to another. In practice, this involves determining the blocked forces for an identical source excitation in two different assemblies, denoted as **AB** and **AC**. If the condition of receiver independence is fulfilled, the response at the receiver points $\mathbf{u}_3$ of assembly **AC** can be predicted using the blocked forces obtained from assembly **AB**. Or mathematically expressed:

$$\mathbf{u}_3^{\mathrm{AC}} = \mathbf{Y}_{32}^{\mathrm{AC}} \mathbf{f}_2^{\mathrm{eq,AB}}. \tag{3.9}$$

It should be noted that discrepancies between measured and predicted responses may arise not only from insufficient interface modeling or numerical inaccuracies, but also from differences in the excitation mechanism itself. Therefore, it is essential to ensure that the operating conditions are as similar as possible across both experimental setups. For hydraulic pumps, in particular, this includes maintaining identical pressure levels and rotational speeds. Furthermore, the passive properties on the source side, such as the hose configuration, should be kept consistent between the two assemblies to minimize systematic deviations.

3.2 Interface Description and Virtual Point Transformation

In the previous section, various methods were introduced to describe a SBN source using receiver-dependent or receiver-independent interface quantities. In these approaches, either forces or displacement-related interface quantities, such as free velocities or blocked forces, may be employed to describe the source. The underlying principle of these methods is that both the compatibility condition of the displacements and the equilibrium condition of the forces at the interface must be satisfied.

For a simple point contact, it is trivial that these conditions must hold at the contact point. In the case of SBN sources coupled through one or more point-like contacts, as assumed in standards ISO 9611:1996 and DIN EN 15657:2017, the definition of the interface is therefore typically clear. However, for flange-type connections, such as the attachment of a gearbox or a hydraulic pump with a mounting flange according to ISO 3019-1:2001, the interface definition is not unique, as these connections represent line or surface contacts rather than discrete points. In such cases, the definition of the interface requires special attention, since it usually must be simplified in a way that still provides a sufficiently accurate representation of the source.

Furthermore, particularly for experimental receiver-independent source-characterization methods, it is essential that the interface quantities are not influenced by the specific measurement setup but are uniquely defined by the source itself. This is particularly significant for the In Situ Blocked Force method, where the source-receiver coupling prevents direct access to the interface. Consequently, the determination of $\mathbf{Y}_{42}^{\mathrm{AB}}$ (Step 1 in Section 3.1.2.3) typically involves exciting the region surrounding the interface on the receiver side using an impact hammer or a shaker. As described earlier, the blocked forces are then obtained at these excitation points on the receiving structure. Thus, the blocked forces, in their original form, are dependent on the receiver geometry around the interface, making them unsuitable for receiver-independent source characterization.

The general objective of a distinct interface definition is therefore to establish interface quantities that are clearly defined by the source while allowing for a sufficiently accurate description of its dynamic behavior. For the special case of the investigated axial piston pump, this aspect is analyzed in greater detail later in this thesis and forms the focus of the second research question.

Several approaches have been proposed in the literature to achieve a distinct interface definition for structural dynamic source-receiver systems. The most prominent among them are the *Equivalent Multi-Point Connection* method, the *Finite Difference* method, and the *Virtual Point Transformation* (VPT) method, which are described in detail in [83]. As discussed therein, the VPT method offers significant advantages over the Equivalent Multi-Point Connection and Finite Difference methods in terms of applicability and robustness. Therefore, only the VPT method is introduced and applied in the following sections.

3.2.1 Virtual Point Transformation

The concept of VPT, introduced by van der Seijs et al. [85], originates from the field of dynamic substructuring, where a precise definition of interfaces between subsystems is essential. As schematically illustrated in Figure 3.4, VPT aims to map interface quantities (interface DoF) $\mathbf{u}, \mathbf{f}$ onto a set of interface displacement modes (IDMs) $\mathbf{q}, \mathbf{m}$ that offer a precise interface description. When IDMs correspond to the six DoF (3 translational and 3 rotational) of a virtual point (VP), they are also known as rigid interface modes or VP DoF. This projection of interface quantities onto VPs allows for a clear definition of an interface, even at locations that are not directly accessible, such as with an impact hammer or accelerometer. Typically, physically significant points, like joint points or bolting points, are chosen as VPs.

The projection of n_{u} displacement- and n_{f} force-interface DoF onto n_{m} VP DoF can be

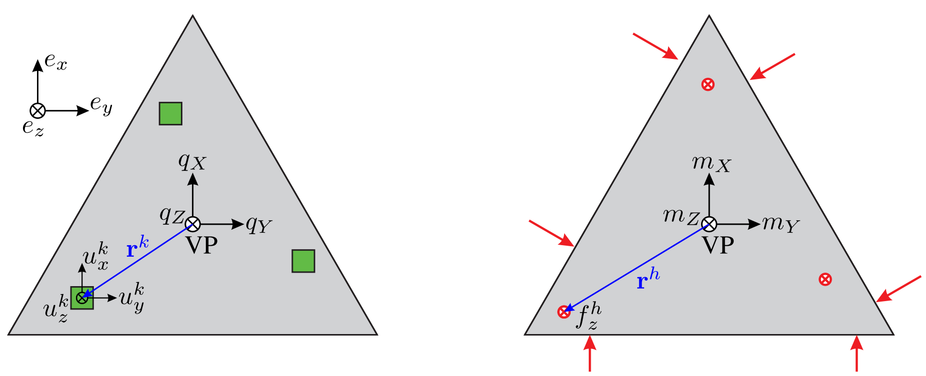

Figure 3.4: Schematic illustration of the VPT, adapted from [85]

accomplished using the IDM matrices $\mathbf{R}_\mathrm{u}$ and $\mathbf{R}_\mathrm{f}$.[1] The IDM matrix for the displacements, $\mathbf{R}_\mathrm{u} \in \mathbb{R}^{n_\mathrm{u} \times n_\mathrm{m}}$, contains the spatial positions and orientations of n_u measured displacement quantities relative to the VP locations. Similarly, the IDM matrix $\mathbf{R}_\mathrm{f} \in \mathbb{R}^{n_\mathrm{f} \times n_\mathrm{m}}$ contains the spatial positions and orientations of the n_f measured forces relative to the VP locations. Although in theory only seven measured displacement and force DoF are sufficient to determine the six DoF of a single VP, it is common practice to use at least nine DoF to achieve a sufficient overdetermination of the transformation matrices. For a detailed explanation of this and a comprehensive description of the construction of the IDM matrices, see [81], [83], [85].

The projection of displacement quantities onto the VP displacements can be described by the following equation:

$$\mathbf{u} = \mathbf{R}_\mathrm{u}\mathbf{q} + \boldsymbol{\mu} \quad \text{with} \quad \mathbf{q} \in \mathbb{C}^{n_\mathrm{m}}, \tag{3.10}$$

where $\mathbf{q}$ includes three translational and three rotational displacement quantities for each VP. The term $\boldsymbol{\mu}$ represents the residuals, i.e., the motion that cannot be captured by the VP. These are typically flexible interface modes that cannot be represented as the VPT assumes a rigid interface behavior.

Similar to the interface velocities, the projection of the forces onto the VP loads, i.e. VP forces and and VP torques, can be achieved as follows:

$$\mathbf{m} = \mathbf{R}_\mathrm{f}^\mathrm{T}\mathbf{f} \quad \text{with} \quad \mathbf{m} \in \mathbb{C}^{n_\mathrm{m}}, \tag{3.11}$$

where $\mathbf{m}$ includes three forces and three torques for each VP. Note that Equation 3.11 requires no residual term $\boldsymbol{\mu}$, as the virtual loads are, in fact, a direct result of the applied forces [81].

[1] In the original coordinates, it is common that the number of displacement-related DoF n_u (typically corresponding to the number of acceleration sensor signals) differs from the number of force-related DoF n_f (corresponding to the excitation points, e.g., impact hammer locations). In contrast, in VP coordinates each VP is typically described by exactly six displacement DoF and six corresponding load DoF. Therefore, for both VP displacements and loads, the number of DoF is denoted uniformly by n_m.

The relations in Equations 3.10 and 3.11 can be reformulated using the pseudo-inverse, yielding[2]:

$$\mathbf{q} = (\mathbf{R}_\mathrm{u})^+\mathbf{u} = \mathbf{T}_\mathrm{u}\mathbf{u}, \tag{3.12}$$

$$\mathbf{f} = (\mathbf{R}_\mathrm{f}^\mathrm{T})^+\mathbf{m} = \mathbf{T}_\mathrm{f}^\mathrm{T}\mathbf{m}, \tag{3.13}$$

where $\mathbf{T}_\mathrm{u} \in \mathbb{R}^{n_\mathrm{m}\times n_\mathrm{u}}$ and $\mathbf{T}_\mathrm{f} \in \mathbb{R}^{n_\mathrm{m}\times n_\mathrm{f}}$ are commonly referred to as the transformation matrices of the VPT. It should be noted that in the original publication by van der Seijs et al. [85], an additional weighting matrix $\mathbf{W}$ is introduced (i.e., a weighted pseudo-inverse), which allows the specification of the relative importance of individual DoF in the transformation. However, this feature was not employed in this work, and the formulation is therefore expressed without $\mathbf{W}$.
Using $\mathbf{T}_\mathrm{u}$ and $\mathbf{T}_\mathrm{f}$, not only the interface quantities themselves but also admittance matrices $\mathbf{Y}_\mathrm{uf} \in \mathbb{C}^{n_\mathrm{u}\times n_\mathrm{f}}$ can be transformed into VP coordinates:

$$\mathbf{Y}_\mathrm{qm} = \mathbf{T}_\mathrm{u}\mathbf{Y}_\mathrm{uf}\mathbf{T}_\mathrm{f}^\mathrm{T} \quad \text{with} \quad \mathbf{Y}_\mathrm{qm} \in \mathbb{C}^{n_\mathrm{m}\times n_\mathrm{m}}, \tag{3.14}$$

where the subscripts $(\cdot)_\mathrm{u}$ and $(\cdot)_\mathrm{f}$ denote displacement and force quantities in the original coordinates, while $(\cdot)_\mathrm{q}$ and $(\cdot)_\mathrm{m}$ refer to those in VP coordinates.
Besides transforming an entire admittance matrix, it is also possible to transform only the displacement or only the force quantities into VP coordinates:

$$\mathbf{Y}_\mathrm{qf} = \mathbf{T}_\mathrm{u}\mathbf{Y}_\mathrm{uf} \quad \text{with} \quad \mathbf{Y}_\mathrm{qf} \in \mathbb{C}^{n_\mathrm{m}\times n_\mathrm{f}}, \tag{3.15}$$

$$\mathbf{Y}_\mathrm{um} = \mathbf{Y}_\mathrm{uf}\mathbf{T}_\mathrm{f}^\mathrm{T} \quad \text{with} \quad \mathbf{Y}_\mathrm{um} \in \mathbb{C}^{n_\mathrm{u}\times n_\mathrm{m}}. \tag{3.16}$$

This is particularly advantageous for the In Situ Blocked Force TPA. Instead of first determining the blocked forces using Equation 3.7 and subsequently transforming them into VP coordinates via Equation 3.11, the matrix $\mathbf{Y}_{42,\mathrm{uf}}^\mathrm{AB}$ can be directly transformed into $\mathbf{Y}_{42,\mathrm{um}}^\mathrm{AB}$ using Equation 3.16. Thus, only the forces are transformed into VP coordinates, while the displacement quantities remain in the original coordinate system, which is sufficient for the In Situ Blocked Force method since the blocked loads alone are required to characterize the source. Using $\mathbf{Y}_{42,\mathrm{um}}^\mathrm{AB}$, the blocked loads can then be determined directly in VP coordinates via the following modified In Situ Blocked Force relation:

$$\mathbf{m}_2^\mathrm{bl} = \left(\mathbf{Y}_{42,\mathrm{um}}^\mathrm{AB}\right)^+ \mathbf{u}_4. \tag{3.17}$$

This procedure has the advantage that, by transforming only the forces into VP coordinates, the overdetermination of $\mathbf{Y}_{42,\mathrm{um}}^\mathrm{AB}$ is higher than that of $\mathbf{Y}_{42,\mathrm{uf}}^\mathrm{AB}$. Consequently, the recommended 1.5-fold overdetermination of $\mathbf{Y}_{42}^\mathrm{AB}$ can be achieved with fewer indicator signals $\mathbf{u}_4$. This can be demonstrated with the following example:

[2] Since $\mathbf{R}_\mathrm{u}$ and $\mathbf{R}_\mathrm{f}^\mathrm{T}$ are generally overdetermined, the pseudo-inverse is used to compute the transformation matrices $\mathbf{T}_\mathrm{u}$ and $\mathbf{T}_\mathrm{f}^\mathrm{T}$ in a least-squares sense. For the displacements, this minimizes the residuals $\boldsymbol{\mu}$, such that the measured motions are best approximated by rigid-body motion at the virtual point. For the forces, the transformation provides the equivalent forces and torques at the virtual point consistent with the measured force distribution.

Example - Number of indicator sensors depending on the application of VPT

This simple example illustrates how applying the VPT either before or after the blocked load calculation can significantly reduce the number of required accelerometers.

To determine the 6 blocked loads of one VP, typically **9** excitation points are required.

Approach 1 - VPT after blocked load calculation:

1. *Determination of blocked forces via Equation 3.7:*
   For a 1.5-fold overdetermination of $\mathbf{Y}^{AB}_{42,uf}$, at least **14** sensor signals are required.
2. *Transformation of blocked forces into VP coordinates via Equation 3.11:*
   9 blocked forces are transformed into 6 VP blocked loads.

$\Rightarrow$ **5 triaxial accelerometers required.**

Approach 2 - VPT before blocked load calculation:

1. *One-sided transformation of the admittance matrix via Equation 3.16:*
   $\mathbf{Y}^{AB}_{42,uf} \in \mathbb{C}^{n_u \times 9}$ is transformed into $\mathbf{Y}^{AB}_{42,um} \in \mathbb{C}^{n_u \times 6}$.
2. *Determination of blocked loads via Equation 3.17:*
   For a 1.5-fold overdetermination of $\mathbf{Y}^{AB}_{42,um}$, at least **9** sensor signals are required.

$\Rightarrow$ **3 triaxial accelerometers required.**

Result:
By applying the VPT before the blocked load calculation, the number of required accelerometers can be reduced by **40%**.

3.2.2 Quality Criteria for the Virtual Point Transformation

A further advantage of the VPT is that it enables a quantitative assessment of the transformation quality through the *Consistency* criteria, which were also introduced by van der Seijs [81], [85]. Two types of Consistency are distinguished: *Sensor Consistency* and *Impact Consistency*, both based on the same underlying concept.
The VPT relies on the assumption that the rigid-body condition is satisfied for the interface or for the portion of the interface that is aggregated into one VP. Typically, the validity of the VPT is constrained by an upper frequency limit, which varies depending on the specific application. The Consistency criteria are designed to assess whether this validity is met. The fundamental concept underlying these criteria can be explained as follows.
During the transformation of measured signals into VP coordinates, only those signals are correctly transformed for which the rigid-body condition is satisfied. The basic idea for the determination of the Consistency criteria is therefore to first transform the measured admittance matrix $\mathbf{Y}_{uf}$ into VP coordinates using Equation 3.14, yielding $\mathbf{Y}_{qm}$, and then to apply the inverse transformation to obtain a reconstructed admittance matrix $\tilde{\mathbf{Y}}_{uf}$. The

tilde indicates that the respective quantity has been back-transformed. Mathematically, this procedure can be expressed as:

$$\tilde{\mathbf{Y}}_{\mathrm{uf}} = \mathbf{R}_{\mathrm{u}}\mathbf{Y}_{\mathrm{qm}}\mathbf{R}_{\mathrm{f}}^{\mathrm{T}} = \underbrace{\mathbf{R}_{\mathrm{u}}\mathbf{T}_{\mathrm{u}}}_{\mathbf{F}_{\mathrm{u}}}\,\mathbf{Y}_{\mathrm{uf}}\,\underbrace{\mathbf{T}_{\mathrm{f}}^{\mathrm{T}}\mathbf{R}_{\mathrm{f}}^{\mathrm{T}}}_{\mathbf{F}_{\mathrm{f}}^{\mathrm{T}}} \quad \text{with} \quad \tilde{\mathbf{Y}}_{\mathrm{uf}} \in \mathbb{C}^{n_{\mathrm{u}}\times n_{\mathrm{f}}}. \tag{3.18}$$

As long as the rigid-body condition is satisfied, $\tilde{\mathbf{Y}}_{\mathrm{uf}} = \mathbf{Y}_{\mathrm{uf}}$ holds. When the rigid-body assumption is violated, the equality no longer holds, and $\tilde{\mathbf{Y}}_{\mathrm{uf}}$ represents a reconstructed admittance matrix that contains only the rigid-body dynamics, whereas flexible interface dynamics are filtered out. The matrices $\mathbf{F}_{\mathrm{u}} \in \mathbb{R}^{n_{\mathrm{u}}\times n_{\mathrm{u}}}$ and $\mathbf{F}_{\mathrm{f}} \in \mathbb{R}^{n_{\mathrm{f}}\times n_{\mathrm{f}}}$ can therefore be interpreted as filter matrices.

3.2.2.1 Sensor Consistency

In analogy to the admittance matrix $\mathbf{Y}_{\mathrm{uf}}$, the measured displacement responses can also be filtered, in this case using $\mathbf{F}_{\mathrm{u}}$ only. Let $\mathbf{f}$ denote a vector of excitation forces applied at multiple locations on the structure, with each component corresponding to a unit force ($f_i = 1$). The unfiltered displacement response $\mathbf{u}$ and the filtered response $\tilde{\mathbf{u}}$ are then given by:

$$\mathbf{u} = \mathbf{Y}_{\mathrm{uf}}\mathbf{f} \quad \text{with} \quad \mathbf{u} \in \mathbb{C}^{n_{\mathrm{u}}}, \tag{3.19}$$

$$\tilde{\mathbf{u}} = \mathbf{F}_{\mathrm{u}}\mathbf{Y}_{\mathrm{uf}}\mathbf{f} \quad \text{with} \quad \tilde{\mathbf{u}} \in \mathbb{C}^{n_{\mathrm{u}}}, \tag{3.20}$$

where $\tilde{\mathbf{u}}$ contains only the rigid body dynamics of the sensor signals. A comparison between the filtered and unfiltered responses provides an indication of how well the rigid-body condition is satisfied for the sensor signals. A simple metric to compare $\mathbf{u}$ and $\tilde{\mathbf{u}}$ is the *Overall Sensor Consistency*, introduced in [81]. It is defined as the ratio of the norms of the two vectors:

$$\rho_{\mathrm{u}}(\omega) = \frac{||\tilde{\mathbf{u}}(\omega)||}{||\mathbf{u}(\omega)||}. \tag{3.21}$$

The resulting frequency-dependent function $\rho_{\mathrm{u}}(\omega)$ takes values between 0 and 1. A value of 1 indicates that the sensor motion can be fully represented by the VP motion, and that the rigid-body condition is perfectly satisfied. A reduction in Consistency indicates that the measured motion can no longer be fully described by VP motion, which typically occurs when flexible interface modes arise. Additionally, poor Sensor Consistency may indicate unsuitable sensor positioning or errors within the IDM matrix $\mathbf{R}_{\mathrm{u}}$.

3.2.2.2 Impact Consistency

Similar to Sensor Consistency, an Impact Consistency metric can be introduced. The unfiltered and filtered responses, $\mathbf{y}$ and $\tilde{\mathbf{y}}$, to the excitation forces $\mathbf{f}$ are then obtained using the filter matix $\mathbf{F}_{\mathrm{f}}$:

$$\mathbf{y} = \mathbf{Y}_{\mathrm{uf}}\mathbf{f} \quad \text{with} \quad \mathbf{y} \in \mathbb{C}^{n_{\mathrm{u}}}, \tag{3.22}$$

$$\tilde{\mathbf{y}} = \mathbf{Y}_{\mathrm{uf}}\mathbf{F}_{\mathrm{f}}^{\mathrm{T}}\mathbf{f} \quad \text{with} \quad \tilde{\mathbf{y}} \in \mathbb{C}^{n_{\mathrm{u}}}. \tag{3.23}$$

The *Overall Impact Consistency* is then defined as:

$$\rho_{\mathrm{f}}(\omega) = \frac{||\tilde{\mathbf{y}}(\omega)||}{||\mathbf{y}(\omega)||}. \tag{3.24}$$

This metric is likewise frequency-dependent and provides a complementary measure for assessing the validity of the rigid-body assumption at the excitation side.

3.3 Power-Based Approaches

As can be seen from the VPT, a comprehensive description of a single point contact already necessitates six DoF. Consequently, the characterization of SBN sources often requires a substantial number of DoF. The goal for many years has therefore been to simplify the characterization of SBN and to obtain a simple, universally applicable assessment metric, similar to sound power in ABN.
However, practical experience indicates that no universally valid single metric for SBN can be defined. Nevertheless, for specific applications such as those considered in the standard DIN EN 15657:2017, reduced-order source descriptions can be sufficiently accurate, especially if the focus is on a straightforward description of the source. In this context, power-based approaches constitute a promising strategy, particularly when the aim is to represent SBN excitation through a single-valued, frequency-dependent metric that combines translational and rotational DoF.
The key difference between the characterization of ABN sources and SBN sources using power quantities arises from the influence of the receiving system. For ABN power, it is generally assumed that the receiving system has negligible influence on the radiated sound power. In contrast, the transmitted SBN power highly depends on the mechanical properties of the receiver. It is evident that the surrounding air hardly influences the surface motion of a machine that generates ABN, whereas the mechanical mounting conditions of the machine substantially determine the transmitted SBN.
However, since the receiver is often unknown in technical applications, receiver-independent power quantities for the characterization of SBN sources have been introduced in the literature. Although these inherently neglect receiver behavior, which is an important influencing factor for transmitted SBN, they remain justified from a practical standpoint for evaluating the source strength independent of the receiver.
The following sections introduce the fundamentals of SBN power and subsequently present the concept of *Characteristic Power*, which represents the most promising receiver-independent power approach. The explanations and relationships provided here follow the recently published book *Experimental Vibro-Acoustics* [83] by Meggitt and Moorhouse, which provides a comprehensive overview of power-based approaches.

3.3.1 General Concepts of Structure-Borne Noise Power

The SBN power, commonly referred to as the complex power, of an interface with multiple DoF is defined as:

$$S_2 = \frac{1}{2}\mathbf{g}_2^{\mathrm{H}}\mathbf{v}_2, \tag{3.25}$$

where the subscript $(\cdot)_2$ designates quantities associated with the interface. The vector $\mathbf{v}$ is used here instead of a general displacement vector $\mathbf{u}$, as it explicitly represents velocity. In this context, $\mathbf{Y}$ denotes the mobility, i.e., the frequency-dependent ratio of velocity to force (see Table 2.1). The superscript $(\cdot)^{\mathrm{H}}$ indicates the Hermitian transpose, which involves transposition followed by complex conjugation. Since both $\mathbf{g}_2$ and $\mathbf{v}_2$ are column vectors, Equation 3.25 represents the scalar product of the complex-conjugated interface forces with the interface velocities. Consequently, the total complex power is obtained by summing the power contributions of the individual DoF. Similar to the SBN power in Section 2.2.1, Equation 3.25 also includes the factor 1/2, as amplitude values of forces and velocities are used instead of RMS values. In some literature, RMS values are used, in which case the factor 1/2 is omitted.
Analogous to the pulsation power of the FBN in Section 2.1.1.3, the complex SBN power S_2 can be decomposed into reactive and active components. The active component represents the net power delivered to the receiver, while the reactive component corresponds to power that oscillates between source and receiver without contributing to net transfer. The imaginary part of the complex power yields the reactive component, while the real part yields the active component. Thus, the net SBN power transmitted to the receiver is given by:

$$P_2 = \frac{1}{2}\mathrm{Re}\{\mathbf{g}_2^{\mathrm{H}}\mathbf{v}_2\}. \tag{3.26}$$

In a physically meaningful system, the total active complex power P_2 must be positive, as power is transferred only from the active source to the passive receiver. However, the power contributions of individual DoF can be negative.
A key aspect of SBN transmission, and thus also for the value of P_2, is the mobility (or impedance) ratio between source and receiver. Understanding how this ratio influences power transmission is fundamental to the design of effective vibration isolation strategies. To investigate this, Equation 3.25 must be reformulated into a component-based representation in which only quantities specific to either the source or the receiver appear. For the multidimensional case, the following relationships are obtained:

$$S_2 = \frac{1}{2}\left(\left(\mathbf{f}_2^{\mathrm{bl}}\right)^{\mathrm{H}}\left(\mathbf{Y}_{22}^{\mathrm{A}}\right)^{\mathrm{H}}\left(\mathbf{Y}_{22}^{\mathrm{B}}+\mathbf{Y}_{22}^{\mathrm{A}}\right)^{-\mathrm{H}}\right)\left(\mathbf{Y}_{22}^{\mathrm{B}}\left(\mathbf{Y}_{22}^{\mathrm{B}}+\mathbf{Y}_{22}^{\mathrm{A}}\right)^{-1}\mathbf{Y}_{22}^{\mathrm{A}}\mathbf{f}_2^{\mathrm{bl}}\right), \tag{3.27}$$

$$S_2 = \frac{1}{2}\left(\left(\mathbf{v}_2^{\mathrm{free}}\right)^{\mathrm{H}}\left(\mathbf{Y}_{22}^{\mathrm{B}}+\mathbf{Y}_{22}^{\mathrm{A}}\right)^{-\mathrm{H}}\right)\left(\mathbf{Y}_{22}^{\mathrm{B}}\left(\mathbf{Y}_{22}^{\mathrm{B}}+\mathbf{Y}_{22}^{\mathrm{A}}\right)^{-1}\mathbf{v}_2^{\mathrm{free}}\right), \tag{3.28}$$

where the first expression corresponds to the formulation using blocked forces $\mathbf{f}_2^{\mathrm{bl}}$ and the second to that using free velocities $\mathbf{v}_2^{\mathrm{free}}$ (a detailed derivation of the relationships can be found in [83], [86]).

For the one-dimensional case, the formulation simplifies considerably, and the representation based on free velocities becomes:

$$S_2 = \frac{1}{2}\left|v^{\text{free}}\right|^2 \frac{Y_{22}^{\text{B}}}{\left|Y_{22}^{\text{B}} + Y_{22}^{\text{A}}\right|^2}. \tag{3.29}$$

Using this expression, the transmitted power can be evaluated as a function of the ratio $Y_{22}^{\text{B}}/Y_{22}^{\text{A}}$, as illustrated in Figure 3.5. The figure displays the qualitative behavior of the relationship for a constant value of v^{free} and different relative phases φ between the mobilities Y_{22}^{A} and Y_{22}^{B}. All curves exhibit a maximum at $Y_{22}^{\text{B}}/Y_{22}^{\text{A}} = 1$. Increasing mismatch between the mobilities reduces the transmitted power. Consequently, low SBN transmission can be achieved by mounting a machine more softly (e.g., via resilient mounts) or more stiffly (e.g., on a concrete foundation) than the mobility of the source. Moreover, maximum transmission at $Y_{22}^{\text{B}}/Y_{22}^{\text{A}} = 1$ occurs when the relative phase approaches π, which corresponds to the case where the point mobility of the receiver equals the complex conjugate of the point mobility of the source, thus $Y_{22}^{\text{B}} = \left(Y_{22}^{\text{A}}\right)^*$. The additionally marked points in the plot are specific power values, which will be discussed in the next section.

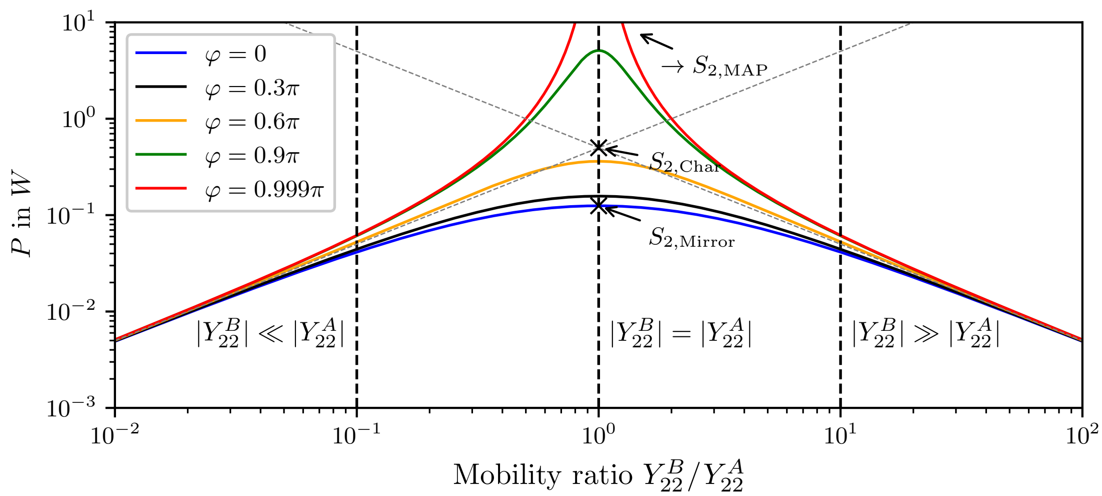

Figure 3.5: Transferred power as a function of the ratio $Y_{22}^{\text{B}}/Y_{22}^{\text{A}}$ for different relative phases φ between the mobilities, adapted from [83] and [86]

The challenge when dealing with SBN transmission is that the mobilities Y_{22}^{B} and Y_{22}^{A} are frequency dependent. Their values typically match over certain portions of the frequency spectrum, leading to efficient power transmission at those frequencies. To minimize SBN transmission within a source-receiver-system, the dominant excitation of the source should therefore lie in frequency ranges where transmission efficiency is low.
This analysis highlights that transmitted SBN power strongly depends on the receiver system. However, during component development, the connected receiver system is typically unknown and cannot be accounted for. Therefore several concepts have been introduced to obtain receiver-independent SBN power metrics. These approaches focus less on determining actual power delivery, but rather on providing a single-valued receiver-independent evaluation metric for comparing different sources.

3.3.2 Introduction to Characteristic Power

Already in 2001, well before the publication of the In Situ Blocked Force method, Moorhouse proposed a framework for receiver-independent source characterization [86]. In this work, three source-specific power metrics were introduced: the *Maximum Available Power*, the *Mirror Power*, and the *Characteristic Power*.
The Maximum Available Power $S_{2,\mathrm{MAP}}$ is obtained when the receiver mobility is the complex conjugate of the source mobility, i.e., $\mathbf{Y}_{22}^{\mathrm{B}} = \left(\mathbf{Y}_{22}^{\mathrm{A}}\right)^{*}$. Substituting this condition into Equation 3.28 yields:

$$S_{2,\mathrm{MAP}} = \frac{1}{8}\left(\mathbf{v}_2^{\mathrm{free}}\right)^{\mathrm{H}} \mathrm{Re}\left\{\mathbf{Y}_{22}^{\mathrm{A}}\right\}^{-1} \left(\mathbf{Y}_{22}^{\mathrm{A}}\right)^{*} \mathrm{Re}\left\{\mathbf{Y}_{22}^{\mathrm{A}}\right\}^{-1} \mathbf{v}_2^{\mathrm{free}}, \tag{3.30}$$

which is a power quantity that solely depends on source properties and is therefore receiver-independent. As can be seen in the upper figure for the one-dimensional case, the power becomes maximal for $\varphi \to \pi$ and thus $Y_{22}^{\mathrm{B}} \to \left(Y_{22}^{\mathrm{A}}\right)^{*}$, which explains why this power is the Maximum Available Power.
The Mirror Power $S_{2,\mathrm{Mirror}}$ corresponds to the power transmitted if the source is connected to a receiver with the same point mobility as the source, i.e., $\mathbf{Y}_{22}^{\mathrm{B}} = \mathbf{Y}_{22}^{\mathrm{A}}$. Inserting this expression into Equation 3.27 and Equation 3.28 yields:

$$S_{2,\mathrm{Mirror}} = \frac{1}{8}\left(\mathbf{f}_2^{\mathrm{bl}}\right)^{\mathrm{H}} \mathbf{Y}_{22}^{\mathrm{A}} \mathbf{f}_2^{\mathrm{bl}}, \tag{3.31}$$

$$S_{2,\mathrm{Mirror}} = \frac{1}{8}\left(\mathbf{v}_2^{\mathrm{free}}\right)^{\mathrm{H}} \left(\mathbf{Y}_{22}^{\mathrm{A}}\right)^{-\mathrm{H}} \mathbf{v}_2^{\mathrm{free}}, \tag{3.32}$$

where the first expression again corresponds to the formulation using blocked forces and the second to that using free velocities. In Figure 3.5, the Mirror Power corresponds to the power at $Y_{22}^{\mathrm{B}}/Y_{22}^{\mathrm{A}} = 1$ and a relative phase $\varphi = 0$.
Another way to derive a purely source-based power quantity is to form the scalar product of blocked forces and free velocities:

$$S_{2,\mathrm{Char}} = \frac{1}{2}\left(\mathbf{f}_2^{\mathrm{bl}}\right)^{\mathrm{H}} \mathbf{v}_2^{\mathrm{free}}, \tag{3.33}$$

which is referred to as the Characteristic Power $S_{2,\mathrm{Char}}$. Using the relation $\mathbf{v}_2^{\mathrm{free}} = \mathbf{Y}_{22}^{\mathrm{A}} \mathbf{f}_2^{\mathrm{bl}}$ (see Equation 3.6), one obtains the alternative expressions:

$$S_{2,\mathrm{Char}} = \frac{1}{2}\left(\mathbf{f}_2^{\mathrm{bl}}\right)^{\mathrm{H}} \mathbf{Y}_{22}^{\mathrm{A}} \mathbf{f}_2^{\mathrm{bl}}, \tag{3.34}$$

$$S_{2,\mathrm{Char}} = \frac{1}{2}\left(\mathbf{v}_2^{\mathrm{free}}\right)^{\mathrm{H}} \left(\mathbf{Y}_{22}^{\mathrm{A}}\right)^{-\mathrm{H}} \mathbf{v}_2^{\mathrm{free}}. \tag{3.35}$$

Comparing the equations for the Mirror Power and the Characteristic Power it becomes evident that the Characteristic Power is exactly four times the Mirror Power. Both metrics therefore contain the same physical information about the source. This could already be observed for the one-dimensional case in Section 2.2.1 (see Table 2.2). In Figure 3.5, the Characteristic Power is found exactly where the two asymptotes $Y_{22}^{\mathrm{B}}/Y_{22}^{\mathrm{A}} \to 0$ and

$Y_{22}^{\mathrm{B}}/Y_{22}^{\mathrm{A}} \rightarrow \infty$ intersect. As already evident from the analytical expression, the figure also confirms that the value of $S_{2,\mathrm{Char}}$ is exactly four times that of $S_{2,\mathrm{Mirror}}$.
The Characteristic Power is a theoretical power quantity that cannot be directly measured, since a source cannot be simultaneously "blocked" and "free," and the transmitted power is zero in both cases. Nevertheless, as argued in [86], the Characteristic Power provides a meaningful and practically relevant descriptor. Although, it is not a strict theoretical upper limit for the power delivered, it serves as a practical maximum in most situations.
A further advantage of the Characteristic Power, as also noted in [86], lies in the robustness of its determination. The Maximum Available Power $S_{2,\mathrm{MAP}}$, which may appear more suitable at first glance, has the drawback that its determination requires inversion of the real part of the mobility matrix $\mathbf{Y}_{22}^{\mathrm{A}}$ (see Equation 3.30), which is itself subject to measurement errors.
Taken together, these properties make the Characteristic Power the most reliable receiver-independent descriptor. It provides a compact, physically meaningful measure that captures the effective excitation strength of a SBN source in a single power quantity.
It is important to note that for determining power quantities a consistent definition of the interface is essential, since the force and velocity DoF must coincide. In a typical measurement setup for the In Situ Blocked Force method, however, the excitation points do not generally coincide with the sensor positions. Consequently, the measured forces and velocities must be transformed into appropriate coordinates. The VPT can again be used for this purpose, and the expression for the Characteristic Power from Equation 3.33 then becomes, in VP coordinates:

$$S_{2,\mathrm{Char}} = \frac{1}{2}\left(\mathbf{m}_2^{\mathrm{bl}}\right)^{\mathrm{H}} \mathbf{q}_2^{\mathrm{free}}. \tag{3.36}$$

4 Approaches for Assessing Structure-Borne Noise Excitation by Axial Piston Pumps

The relationships among Transfer Path Analysis (TPA), Virtual Point Transformation(VPT), and the Characteristic Power introduced in the previous chapter provide the theoretical foundation for assessing the SBN of hydraulic pumps. On this basis, the following sections present three methodological approaches for assessing the SBN of an axial piston pump. A prerequisite for any such assessment is a clear definition of the interface of the investigated pump using VPT. Following this, two source-specific evaluation methods are introduced. The first aggregates the blocked forces and blocked torques at the interface into one force-based and one torque-based metric, whereas the second employs the previously introduced Characteristic Power as a single-valued metric. In the final part of the chapter, a receiver-dependent approach is presented, in which the assessment is based on a freely defined receiver point in an actual application, such as a microphone placed inside the operator cabin.

4.1 Interface Description of the Investigated Axial Piston Pump

The pump under investigation is a 9-piston axial piston pump of swash-plate type with a variable displacement volume, suitable for use in a 6-ton excavator. The pump features a flange with two mounting points in accordance with ISO 3019-1:2001 and employs a splined shaft as the shaft-hub connection to the corresponding motor. The pump housing, including the mounting flange, is made of cast steel.

Two different interface definitions were examined for the axial piston pump, as illustrated in Figure 4.1. The first option describes the interface by means of a single VP (single-VP configuration), located at the intersection of the shaft axis and the contact plane between the pump and the motor. In the second interface definition, the pump is described using two VPs (dual-VP configuration), each located at one of the pump's mounting points. Accordingly, the source characterization comprises 6 DoF for the single-VP configuration and 12 DoF for the dual-VP configuration.

The single-VP configuration has the advantage that the interface description involves fewer quantities, which simplifies the characterization. This is particularly beneficial because the excitation at a single VP is easier to interpret, as no interactions between multiple VPs occur. Another advantage is that a central VP can be defined for any pump, regardless of the number of mounting points or the dimensions of the mounting flange. In contrast, the dual-VP configuration offers the advantage that the VPs are located directly at the mounting points, where the main SBN transmission is expected. Moreover, due to the higher number of descriptive quantities, an interface representation using multiple VPs may allow the description of the SBN excitation up to higher frequencies. Determining which interface definition is better suited for the investigated axial piston pump is therefore one of the central research questions addressed in this work.

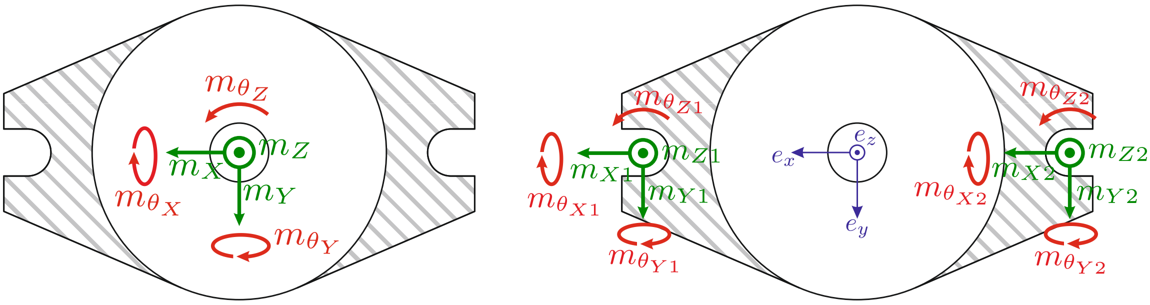

Figure 4.1: Schematic illustration of different interface definitions for the investigated axial piston pump. Left: single-VP configuration. Right: dual-VP configuration.

It is important to note that hydraulic pumps exhibit an additional SBN interface at the charge and discharge ports, where hoses or pipes are connected. These interfaces were not considered further in the present work. A major challenge when applying the In Situ Blocked Force approach to such interfaces is that the measured SBN response on the receiving structure (i.e., on the hose or pipe, measured via an accelerometer) consists of a component transmitted through the mechanical interface and a component generated by the pressure pulsations within the hose or pipe itself. Thus, the receiving structure cannot be regarded as passive. Applying TPA methods to this type of interface therefore represents an area for future research.

4.2 Source-Specific Assessment Using Aggregated Blocked Loads

Assuming that the blocked loads can be reliably determined in VP-coordinates using In Situ Blocked Force method and VPT, a direct assessment of source strength can initially be formulated at the level of the individual force and torque components. However, a 6 DoF (single-VP) or even 12 DoF (dual-VP) representation is often impractical for comparative analysis, optimization, or target-setting, as it yields a large number of evaluation parameters. A scalar condensation is therefore desirable in order to reduce the dimensionality of the descriptor while preserving the essential physical information.
For the single-VP configuration, the VP is characterized by three translational and three

rotational components. These components can be combined using the Euclidean norm as follows:

$$\|\mathbf{m}^{\mathrm{bl}}_{\mathrm{T,1VP}}\| = \sqrt{\left(m^{\mathrm{bl}}_{X}\right)^2 + \left(m^{\mathrm{bl}}_{Y}\right)^2 + \left(m^{\mathrm{bl}}_{Z}\right)^2}, \tag{4.1}$$

$$\|\mathbf{m}^{\mathrm{bl}}_{\mathrm{R,1VP}}\| = \sqrt{\left(m^{\mathrm{bl}}_{\theta_X}\right)^2 + \left(m^{\mathrm{bl}}_{\theta_Y}\right)^2 + \left(m^{\mathrm{bl}}_{\theta_Z}\right)^2}. \tag{4.2}$$

This reflects an aggregation in an energetic sense but also leads to the loss of phase information. To simplify the representation of the assessment metrics, the subscript $(\cdot)_2$, which indicates that the quantity pertains to the interface, is omitted in Equations 4.1 and 4.2 and in the following, as all introduced source-specific assessment metrics are based on interface quantities.

The dual-VP configuration introduces additional complexity because forces and torques are associated with different, spatially displaced VPs. Consequently, the force components and the torque components cannot be directly combined into one force and one torque quantity using vector norms. Moreover, the coupling between the two VPs must be taken into account. Unlike in the single VP case, where only one VP emits vibration power, the two VP setup also involves power exchange between the VPs.

In general, for SBN sources described by multiple contact points or VPs, two special cases may occur. The first case arises when the VPs are not coupled, i.e., they behave completely independently. If this holds, each individual VP can be considered as an individual SBN source. In such cases, torques resulting from coupling between the VPs can be neglected, and the individual force and torque components of the different VPs may be combined using a Root-Sum-Square (RSS) approach. For the dual-VP configuration, this is given by:

$$\overline{\mathbf{m}}^{\mathrm{bl}}_{\mathrm{T,2VP}} = \sqrt{\left(m^{\mathrm{bl}}_{X1}\right)^2 + \left(m^{\mathrm{bl}}_{Y1}\right)^2 + \left(m^{\mathrm{bl}}_{Z1}\right)^2 + \left(m^{\mathrm{bl}}_{X2}\right)^2 + \left(m^{\mathrm{bl}}_{Y2}\right)^2 + \left(m^{\mathrm{bl}}_{Z2}\right)^2}, \tag{4.3}$$

$$\overline{\mathbf{m}}^{\mathrm{bl}}_{\mathrm{R,2VP}} = \sqrt{\left(m^{\mathrm{bl}}_{\theta_{X1}}\right)^2 + \left(m^{\mathrm{bl}}_{\theta_{Y1}}\right)^2 + \left(m^{\mathrm{bl}}_{\theta_{Z1}}\right)^2 + \left(m^{\mathrm{bl}}_{\theta_{X2}}\right)^2 + \left(m^{\mathrm{bl}}_{\theta_{Y2}}\right)^2 + \left(m^{\mathrm{bl}}_{\theta_{Z2}}\right)^2}. \tag{4.4}$$

This also represents an aggregation in an energetic sense with a loss of the phase information, but does not correspond to the Euclidean norm, as quantities of different vectors are included.

The neglect of the coupling between contact points has been shown to be a valid assumption for sources coupled to the receiving system via multiple resilient mounts, as in ISO 9611:1996. However, as discussed in Section 2.2.3, the mounting of hydraulic pumps is substantially different from that of resiliently mounted machines. Thus, it is expected that the pump's steel flange behaves like a rigid body over a broad frequency range, resulting in strong coupling between the two VPs of the dual-VP configuration.

The second special case, which is therefore considered more relevant for the investigated axial piston pump, is that the VPs of the SBN source behave as points on a rigid body. In this case, the loads of the two VPs can be geometrically combined into one resultant force vector and one resultant torque vector as follows:

$$\mathbf{m}^{\mathrm{bl}}_{\mathrm{T,2VP}} = \mathbf{m}^{\mathrm{bl}}_{\mathrm{T,2VP\text{-}1}} + \mathbf{m}^{\mathrm{bl}}_{\mathrm{T,2VP\text{-}2}}, \tag{4.5}$$

$$\mathbf{m}^{\mathrm{bl}}_{\mathrm{R,2VP}} = \mathbf{m}^{\mathrm{bl}}_{\mathrm{R,2VP\text{-}1}} + \mathbf{m}^{\mathrm{bl}}_{\mathrm{R,2VP\text{-}2}} + \mathbf{r}_{\mathrm{2VP\text{-}1}} \times \mathbf{m}^{\mathrm{bl}}_{\mathrm{T,2VP\text{-}1}} + \mathbf{r}_{\mathrm{2VP\text{-}2}} \times \mathbf{m}^{\mathrm{bl}}_{\mathrm{T,2VP\text{-}2}}, \tag{4.6}$$

where $\mathbf{m}^{\mathrm{bl}}_{\mathrm{T,2VP\text{-}1}}$ and $\mathbf{m}^{\mathrm{bl}}_{\mathrm{T,2VP\text{-}2}}$ contain the translational components of the blocked load vector of the VPs, while $\mathbf{m}^{\mathrm{bl}}_{\mathrm{R,2VP\text{-}1}}$ and $\mathbf{m}^{\mathrm{bl}}_{\mathrm{R,2VP\text{-}2}}$ contain the rotational components. The vectors $\mathbf{r}_{\mathrm{2VP\text{-}1}}$ and $\mathbf{r}_{\mathrm{2VP\text{-}2}}$ denote the relative vectors from a reference point to each respective VP. Assuming rigid-body behavior is fully satisfied, the resulting force vector $\mathbf{m}^{\mathrm{bl}}_{\mathrm{T,2VP}}$ and torque vector $\mathbf{m}^{\mathrm{bl}}_{\mathrm{R,2VP}}$ are coherently combined in phase. A key difference in this approach is that the total torque in Equation 4.6 introduces terms of the form $\mathbf{r} \times \mathbf{m}_{\mathrm{T}}$, which represent torques arising from the rigid coupling of the VPs [87].
After the resulting vectors $\mathbf{m}^{\mathrm{bl}}_{\mathrm{T,2VP}}$ and $\mathbf{m}^{\mathrm{bl}}_{\mathrm{R,2VP}}$ are determined, the Euclidean norms $\|\mathbf{m}^{\mathrm{bl}}_{\mathrm{T,2VP}}\|$ and $\|\mathbf{m}^{\mathrm{bl}}_{\mathrm{R,2VP}}\|$ can be calculated in the same manner as in Equation 4.1 and Equation 4.2, resulting in one force-based and one torque-based metric. However, it is evident that this second approach of combining forces and torques of the dual-VP configuration negates the primary advantage of describing the source with two VPs, which is to require the rigid body condition to be fulfilled only for each of the two VPs separately.
When neither of the two special cases—independence between the individual VPs or fulfillment of the rigid-body condition—is met, a straightforward aggregation of the blocked loads of the dual-VP configuration into one force and torque metric is not possible.

4.3 Source-Specific Assessment Using Characteristic Power

An extended evaluation approach is based on the Characteristic Power introduced in Section 3.3.2. For the reasons discussed there, primarily its receiver independence, physical interpretability, and robustness, it represents the most promising power-based metric for a source-specific assessment. Power-based metrics in general, and thus also the Characteristic Power, offer the substantial advantage that rotary and translatory DoF can be combined, allowing the total SBN excitation to be condensed into a single evaluation metric. Moreover, for the case of multiple contact points, such as in the dual-VP configuration, the dynamic transmission behavior between the contact points can be taken into account. This stands in contrast to the aggregation on load level, where either a rigid-body coupling or no coupling between the VPs had to be assumed. As a result, it is also possible to analyze the power exchanged between the contact points. For example, in [88] it was demonstrated that the transmission behavior between multiple contact points of a resiliently mounted source can be neglected, which is consistent with the assumptions of ISO 9611:1996.
To calculate the Characteristic Power according to Equation 3.36, both the blocked loads in VP coordinates and the free velocities of the pump in VP coordinates are required. For an axial piston pump this is particularly challenging, because an external motor is required to drive the pump, and operation under free-suspended conditions is therefore not feasible. One possible solution is to determine the free velocities from the blocked loads and the point admittance of the source according to Equation 3.6. In VP coordinates, the relationship used to compute the Characteristic Power is then given by:

$$S_{\mathrm{Char}} = \frac{1}{2}\left(\mathbf{m}_2^{\mathrm{bl}}\right)^{\mathrm{H}} \mathbf{q}_2^{\mathrm{free}} = \frac{1}{2}\left(\mathbf{m}_2^{\mathrm{bl}}\right)^{\mathrm{H}} \mathbf{Y}^{\mathrm{A}}_{22,\mathrm{qm}} \mathbf{m}_2^{\mathrm{bl}}, \tag{4.7}$$

and accordingly the real part of the Characteristic Power then becomes:

$$P_{\text{Char}} = \text{Re}\left\{\frac{1}{2}\left(\mathbf{m}_2^{\text{bl}}\right)^{\text{H}} \mathbf{Y}_{22,\text{qm}}^{\text{A}} \mathbf{m}_2^{\text{bl}}\right\}. \tag{4.8}$$

The point admittance of the pump $\mathbf{Y}_{22,\text{qm}}^{\text{A}}$ can be obtained via an impact-hammer or shaker measurement performed on the freely suspended pump, followed by a VPT of the measured admittance matrix. For this purpose, the pump must also be freely suspended, as in the case of direct free velocity measurement, but it does not need to be operated. Nevertheless, this test requires considerable additional effort in an industrial environment, especially if the hydraulic connections of the pump must remain installed. The investigation of whether this additional effort is justified is one of the points addressed in this thesis.

4.4 Receiver-Dependent Assessment

The source-specific evaluation of noise is an important tool in the development of components, and corresponding receiver-independent assessment methods have been established for ABN, FBN, and SBN. However, as discussed previously, the properties of the receiving system play a particularly significant role in the case of SBN. Component-based TPA methods, such as the In Situ Blocked Force method, provide a framework for digitally combining source excitation described by blocked forces with separately measured or simulated receiver systems, thereby enabling advanced concepts for receiver-dependent assessment such as a Virtual Acoustic Prototyping (VAP). The transferability principle introduced in Section 3.1.3.2 can be used not only for validating the source description via the blocked forces, but also for combining a source described by blocked forces with any arbitrary receiver, provided that their interface definitions are consistent, which can usually be assured when using VPT.
A common procedure to build a VAP is therefore to determine the blocked forces at a specially designed test rig, denoted by $(\cdot)^{\text{R}}$, and to combine them with a separately measured or simulated receiver behavior $(\cdot)^{\text{E}}$. It should be noted that, both on the test rig and during receiver characterization, the source and receiver are coupled, meaning that the measurements or simulations are actually performed in the coupled sytems $(\cdot)^{\text{AR}}$ and $(\cdot)^{\text{AE}}$. Although in theory it should not matter whether the blocked forces are determined on a dedicated test rig or in an actual application, the determination of the blocked forces on a test rig using the In Situ Blocked Forces methods provides several advantages:

- The test rig can be optimized specifically for the determination of blocked forces.
- The interface is easier to access compared to that in a mobile working machine.
- Disturbances from other noise sources present in a mobile working machine are avoided.
- A geometric model of the test rig is typically available, improving the accuracy of the VPT.

- Operating conditions can be well controlled and reproduced.

These advantages typically improve the accuracy and reliability of the blocked forces. Once determined at the test rig, the blocked forces can then be combined with the receiver behavior $(\cdot)^{AE}$. For the experimental determination of $(\cdot)^{AE}$, the interface between source and receiver is typically excited using an impact hammer or shaker, and the response is measured at a specific sensor on the receiver. Depending on the application, this may be an accelerometer or directly an airborne acoustic quantity, for example the sound pressure in the operator cabin measured with a microphone. In this way, the effect of SBN excitation of a source on a very specific target metric can be evaluated, and the multi-dimensional interface excitation involving 6 or 12 VP DoF is effectively condensed into a single evaluation quantity.

If experimental measurement of the receiver system is not possible, for instance because the mobile working machine is still in an early development phase or the interface is not accessible, the measured blocked forces can instead be inserted into a structural-dynamic Finite Element Model. The resulting propagation of SBN induced by the source can then be analyzed numerically, and potential design improvements can be derived in a virtual environment. Another promising approach for representing receiver behavior is the combination of individual receiver subcomponents by means of *Frequency-Based Substructuring* (FBS). Depending on the properties of each subcomponent, the modelling can be carried out experimentally or numerically. This approach offers substantial potential and has already been successfully applied in the automotive sector [89]–[94].

One might assume that if the receiver is simulated, the source could be simulated as well. The fundamental difference lies in the difficulty of accurately modelling the internal excitation mechanisms of the source. In structural dynamics, such internal mechanisms are often challenging to reproduce [57], [59]. For the special case of an axial piston pumps, hydrodynamic contacts, such as those between the cylinder block and valve plate, and nonlinear effects pose particular challenges in numerical simulations [36], [46], [95]. In contrast, the behavior of a passive receiver system is often easier to model with sufficient accuracy. This is the reason why the excitation of the source is often easier to determine experimentally, whereas the behavior of the receiver can also be represented through a simulation model [62].

For the receiver-dependent evaluation in this thesis, the transmission behavior of the receiver was determined experimentally for an electrified excavator and is combined with the blocked forces of an axial piston pump measured on the test rig. A schematic illustration of the setup in the excavator is provided in Figure 4.2. In general, an arbitrary number and variety of receiver sensors, such as accelerometers or microphones, can be installed when experimentally determining the receiver behavior. In practice, however, the most relevant quantity is often the sound pressure level (SPL) inside the operator cabin. For this reason, this quantity is used as the primary receiver-dependent assessment metric. The procedure to combine the blocked forces from the test rig with the receiver behavior of the excavator essentially corresponds to that of the Transferability Validation. Nevertheless, for the prediction of the cabin noise, so-called vibro-acoustic transfer functions have to be employed. These transfer functions describe the transmission behavior between an excitation load and a resulting sound pressure signal. Mathematically, the entire process of determining the blocked loads on a test bench and combining them with the vibro-acoustic transfer function can be expressed as follows:

$$\mathbf{m}_2^{\mathrm{bl}} = \left(\mathbf{Y}_{42,\mathrm{um}}^{\mathrm{AR}}\right)^+ \mathbf{u}_4 \quad \text{with} \quad \mathbf{Y}_{42,\mathrm{um}}^{\mathrm{AR}} \in \mathbb{C}^{n_\mathrm{u} \times n_\mathrm{m}}, \tag{4.9}$$

$$p_3 = \mathbf{H}_{32,\mathrm{um}}^{\mathrm{AE}} \mathbf{m}_2^{\mathrm{bl}} \quad \text{with} \quad \mathbf{H}_{\mathrm{um}} \in \mathbb{C}^{1 \times n_\mathrm{m}}. \tag{4.10}$$

Equation 4.9 describes the determination of the blocked loads in VP coordinates on the test bench, while Equation 4.10 describes their combination with the receiver behavior $\mathbf{H}_{32,\mathrm{um}}^{\mathrm{AE}}$. Specifically, $\mathbf{H}_{32,\mathrm{um}}^{\mathrm{AE}}$ denotes the vibro-acoustic transfer function between a load excitation at the interface in VP coordinates and the microphone signal in the excavator cabin. As indicated by its dimensions, all VP DoF are effectively condensed into a single sound-pressure signal p_3, which serves as the receiver-dependent evaluation metric.
The same principle applies to SBN receivers, i.e., accelerometers, for which load-velocity transfer functions are used instead of vibro-acoustic transfer functions. The corresponding prediction is given by:

$$\mathbf{u}_3 = \mathbf{Y}_{32,\mathrm{um}}^{\mathrm{AE}} \mathbf{m}_2^{\mathrm{bl}} \quad \text{with} \quad \mathbf{Y}_{\mathrm{um}} \in \mathbb{C}^{3 \times n_\mathrm{m}}. \tag{4.11}$$

Since accelerometers are typically triaxial sensors, the predicted response is a vector quantity.

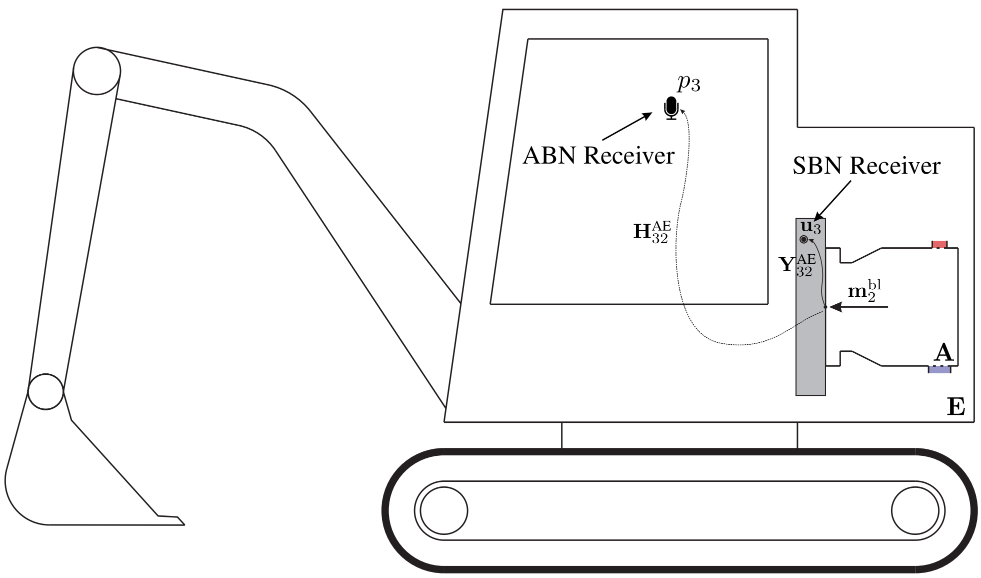

Figure 4.2: Schematic illustration of the receiver-dependent assessment approach.

5 Experimental Results

This chapter presents the results obtained for the different approaches used to assess the SBN excitation by the axial piston pump under investigation. As in the previous chapter, the analysis distinguishes between a source-specific and a receiver-dependent assessment. The source-specific evaluation is based on the implementation of the In Situ Blocked Force method on a test rig. Accordingly, the chapter first presents the corresponding results, with particular emphasis on the quality criteria introduced to verify the validity of the In Situ Blocked Force TPA. Subsequently, the load-based metrics and the Characteristic Power are evaluated for both a stationary operating point and a speed run-up.
For the receiver-dependent assessment, the test setup and the key boundary conditions for determining the receiver behavior of the electrified excavator are first described. A central aspect of this evaluation is whether the blocked loads determined on the test rig can be transferred to the excavator, i.e., whether sufficient transferability is ensured. This is examined by analyzing a stationary operating point that could be established both on the excavator and on the test rig. Subsequently, the blocked loads obtained during the speed run-up on the test rig are combined with the excavator's behavior, enabling a receiver-dependent assessment during the run-up. In the final section of the chapter, the introduced evaluation metrics are compared. Using an artificial sensitivity analysis, it is demonstrated how variations in SBN excitation influence the different metrics. Finally, the advantages and disadvantages of the various assessment approaches are discussed, with particular attention to practicality, robustness, and the explanatory capability of the metrics.

5.1 Source-Specific Assessment of the Axial Piston Pump

A fundamental prerequisite for the source-specific assessment is the determination of the blocked loads of an axial piston pump in accordance with ISO 20270-1:2019. The standard provides various guidelines as well as quality criteria that support the proper implementation of the method. The following section presents the test setup and the key results of the In Situ Blocked Force TPA carried out on the test rig.

5.1.1 In Situ Blocked Force Transfer Path Analysis at the Test Rig

As previously noted, determining the blocked loads on a test rig offers several advantages, particularly the accessibility of the interface, the availability of well-defined geometric properties of the receiver in the interface region, and the high degree of controllability of the operating conditions. For the In Situ Blocked Force TPA conducted within the scope of this thesis, the test rig is described in the following.

5.1.1.1 Test Setup

In this section, first the layout of the test facility where the In Situ Blocked Force method was implemented is described. Subsequently, the specific test setup is presented.
Figure 5.1 shows a schematic representation of the test facility that was originally designed for measurements according to ISO 4412-1:1991 (ABN characterization of hydraulic pumps). Its design provides the important benefit that the influence of the pump's drive unit on the SPL measured in the anechoic chamber is minimized. To achieve this, the engine room, the anechoic chamber, and the mounting unit for the pump that also houses the shaft bearings are located on separate foundations. In addition, the drive shaft is connected to the pump via an elastomer claw coupling, which further reduces SBN transmitted through the drivetrain.
The SBN interface is therefore located between the pump and the tube-like structure that contains the shaft bearings. This structure is supported by a deep pile foundation that is mechanically decoupled from the remainder of the test rig. Consequently, the only potential SBN source on the passive side of the system is the bearing support of the drive shaft. However, its contribution is expected to be small compared with the SBN generated by the pump itself.

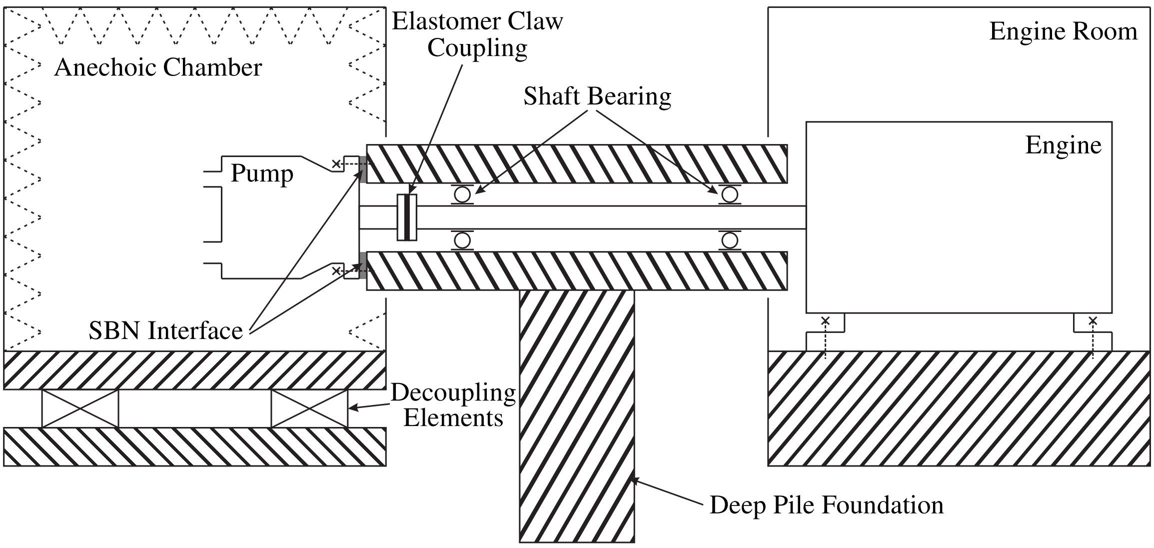

Figure 5.1: Schematic illustration of the test facility for acoustic measurements of axial piston pumps

For the implementation of the In Situ Blocked Forces method on the test rig, a custom test-bench flange was designed to connect the test pump to the tube-like receiver structure. A schematic illustration of the flange is shown in Figure 5.2. The flange is mounted to the tube-like structure using eight screws, while the pump, equipped with a two-bolt flange, is attached using two screws. The triaxial accelerometers serving as indicator sensors $\mathbf{u}_4$ are represented as green squares, and the receiver sensor $\mathbf{u}_3$ is shown as a blue square. The receiver sensor is mounted with a spatial rotation so that the measured accelerations contain a mixture of contributions from all source excitations in all three spatial directions, as recommended in [70]. The six indicators can theoretically be positioned anywhere downstream of the interface on the receiver. However, as suggested by [57], they should be positioned in close proximity to the interface to ensure a high signal-to-noise ratio (SNR) when measuring the transfer functions—also referred to as frequency response functions (FRFs).

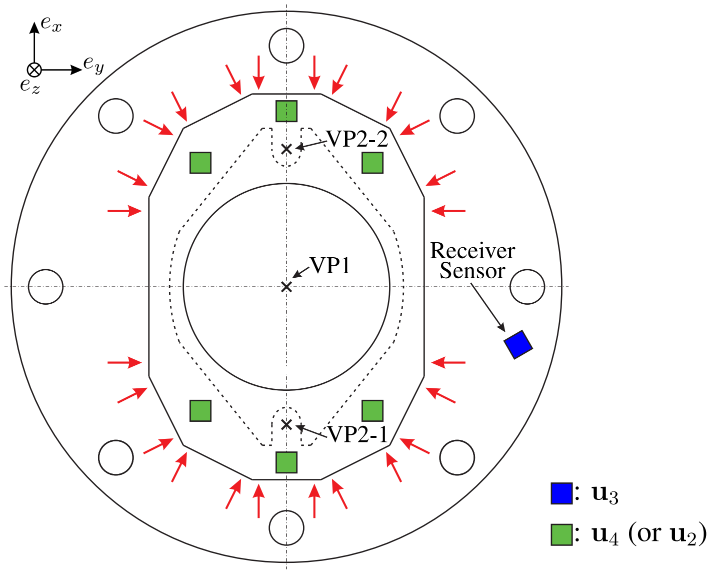

Figure 5.2: Schematic illustration of the test setup for the In Situ Blocked Force TPA

As mentioned earlier, in an In Situ Blocked Force TPA, the source and receiver remain coupled throughout the entire procedure. Therefore, excitation cannot be applied directly at the interface, but only in its vicinity. For this reason, the excitation points are arranged around the interface. In Figure 5.2 the 24 excitation points for the impact hammer or shaker are schematically indicated by red arrows. In addition to a rotation about the axial z-axis, the excitation points are also rotated about the x- and y-axes, which cannot be directly seen in the two-dimensional representation in Figure 5.2. A major advantage of the In Situ Blocked Forces method is that the calculated blocked forces are independent of the receiver's behavior. This independence allows for flexible receiver design, enabling its geometry to be chosen such that the structure can be properly excited with an impact hammer or shaker. Although the positions of the excitation points depend on the receiver's geometry around the interface, this dependency can be resolved later through a VPT.
The arrangement of the six indicator accelerometers and the 24 excitation points enables a characterization of the pump using one or two VPs, consistent with the interface definition in Section 4.1. Therefore, as recommended in Section 3.2.1, the 24 forces are transformed into VP coordinates prior to the calculation of the blocked loads, thereby reducing the

number of interface loads to six (single-VP configuration) or twelve (dual-VP configuration). For the single-VP configuration (VP1 in Figure 5.2), all 18 indicator signals are used to estimate the six VP DoF, resulting in a threefold overdetermination of the admittance matrix $\mathbf{Y}^{\mathrm{AR_B}}_{42,\mathrm{um}}$. For the dual-VP configuration (VP2-1 and VP2-2 in Figure 5.2), where the VPs coincide with the mounting points, the same number of indicators is available while the number of VP DoF doubles, yielding a 1.5-fold overdetermination of $\mathbf{Y}^{\mathrm{AR_B}}_{42,\mathrm{um}}$.
To facilitate a straightforward Transferability Validation, the In Situ Blocked Force TPA was performed in two different setups. The first test setup $\mathbf{AR_B}$ ($\mathbf{Y}^{\mathrm{AR_B}}_{42}$) is the standard configuration with eight mounting screws. The second test setup $\mathbf{AR_C}$ ($\mathbf{Y}^{\mathrm{AR_C}}_{42}$) was modified by removing four of the eight screws, thereby altering the receiver's behavior.

5.1.1.2 General Information and Conditions

Using the described test setup, an In Situ Blocked Force TPA was performed for the axial piston pump under investigation. As discussed in Chapter 3, several approaches exist to assess the quality of TPA results. Before analyzing these quality criteria, it is essential to provide some general information and boundary conditions related to the measurements.
The determination of FRFs in the initial step of the In Situ Blocked Force TPA can be performed using either an impact hammer or a shaker. Both excitation methods were examined in this study and found to be feasible. The impact hammer provides a rapid and flexible excitation, whereas the shaker requires more extensive mounting efforts. Nevertheless, due to its superior reproducibility, the shaker was considered the preferred method. Consequently, all FRFs reported in this study were obtained using a compact inertial shaker (approx. dimensions ⌀25 mm × 30 mm).
For measuring the vibration response, standard piezoelectric triaxial accelerometers with a valid frequency range of 2 Hz to 5 kHz were used. This range adequately covers the lower target frequency limit of the investigation, defined as 140 Hz. This value is 10 Hz lower than the first harmonic of a nine-piston axial piston pump operating at 1000 rpm, ensuring that the first harmonic at this rotational speed is included. An upper target frequency was not specified since the assessment of the upper frequency limit forms part of this study and no definite guidance was found in the literature. For instance, Muench [46] specifies an upper limit of 5 kHz for acoustic analysis of axial piston pumps, whereas Vesikar [54] reports 2 kHz as the upper limit for noise analysis in tractors and excavators without a specific focus on hydraulic pumps. ISO 9611:1996, which addresses the characterization of resiliently mounted SBN sources, identifies the most relevant frequency range for practical SBN problems as 20 Hz to 1 kHz. Therefore, part of the present analysis includes estimating an appropriate frequency range for blocked load determination of the investigated pump.
Data processing was performed using the Python programming language, with particular emphasis on the *pyFBS* package [109]. This package is specifically designed for FBS and TPA and provides detailed documentation and example scripts for implementing VPT and In Situ Blocked Force TPA. It was developed by the *Laboratory for Dynamics of Machines and Structures* at the University of Ljubljana and the *Chair of Applied Mechanics* at the Technical University of Munich, as described in [96]–[98].

5.1.1.3 Virtual Point Transformation

The first quality criteria that do not directly evaluate blocked load determination are the Consistency criteria of the VPT, introduced in Sections 3.2.2.1 and 3.2.2.2. Of particular interest is the comparison between the two interface definitions. For the In Situ Blocked Force TPA, the Impact Consistency is more relevant, as usually only the excitation DoF are transformed into VP coordinates, whereas the measured movements at the indicator sensors remain in original coordinates. However, Sensor Consistency is also analyzed as it provides additional insight into the dynamic behavior of the interface.
It is important to note that the indicator sensors $\mathbf{u}_4$ in the In Situ Blocked TPA do not necessarily have to be located near the interface, but anywhere downstream of the interface on the receiver. However, in the chosen test setup, the indicators are positioned in close proximity to the interface, making $\mathbf{u}_4$ equivalent to the interface motion $\mathbf{u}_2$. Accordingly, the admittance matrix $\mathbf{Y}_{42}^{\mathrm{AB}}$ also corresponds to the admittance matrix $\mathbf{Y}_{22}^{\mathrm{AB}}$.
Figure 5.3 illustrates the Overall Sensor Consistency on the left and the Overall Impact Consistency on the right. Up to approximately 4.3 kHz, Sensor Consistency exhibits nearly identical behavior for both interface definitions. Beyond this frequency, the single-VP configuration shows a decline, whereas the dual-VP configuration maintains a higher level.

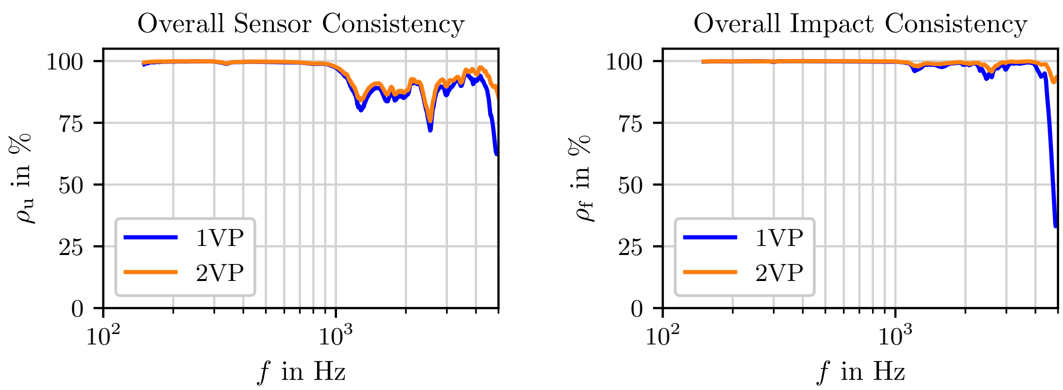

Figure 5.3: Overall Consistency of the two different interface definitions for the In Situ Blocked Force TPA at the test rig. Left: Sensor Consistency. Right: Impact Consistency.

Below 4.3 kHz, Sensor Consistency remains at 100 % up to 1 kHz, then decreases to approximately 80 %. This behavior may result from flexible interface modes violating the rigid-body assumption, from measurement uncertainties, or inaccuracies in sensor positioning, which become significant at higher frequencies. The identical trend for both interface definitions suggests that measurement or positioning inaccuracies, rather than rigid-body assumption violations, are the primary cause. In contrast, the divergence above 4.3 kHz indicates that motion is better represented by the dual-VP configuration, potentially indicating some degree of flexible behavior at the interface. Thus, the dual-VP configuration offers a clear advantage only beyond this frequency.
This observation is even more pronounced for Impact Consistency. The sharp decline of the single-VP configuration at 4.3 kHz strongly supports the previous interpretation. Up to

this point, Impact Consistency remains at nearly 100 % for both configurations, confirming that the rigid-body condition for load transformation is satisfied.
In summary, the more complex modeling using two VPs becomes beneficial only above 4.3 kHz. Impact Consistency is fully maintained up to this frequency, whereas Sensor Consistency decreases to approximately 80 % above 1 kHz. These findings also highlight an advantage of the one-sided VPT during the In Situ Blocked Force TPA, where only forces are transformed into VP coordinates (see Equation 3.17). By avoiding transformation of motions, errors associated with imperfect Sensor Consistency are mitigated.

5.1.1.4 On-Board Validation

The OBV represents the most straightforward quality criterion of In Situ Blocked Force TPA and is also included in ISO 20270-1:2019, which also recommends performing the OBV for an artificial excitation. As outlined in Section 3.1.3.1, this typically involves applying a known, controllable excitation on the source side. For the In Situ Blocked Force TPA of the axial piston pump, an easily accessible point on the pump housing was excited using the same inertial shaker. Figure 5.4 illustrates the OBV result obtained for this excitation, showing both the measured and predicted signal of one receiver sensor channel (other channels exhibit similar behavior). Since the force excitation signal is known and can serve as a reference, a FRF comprising both magnitude and phase can be computed.

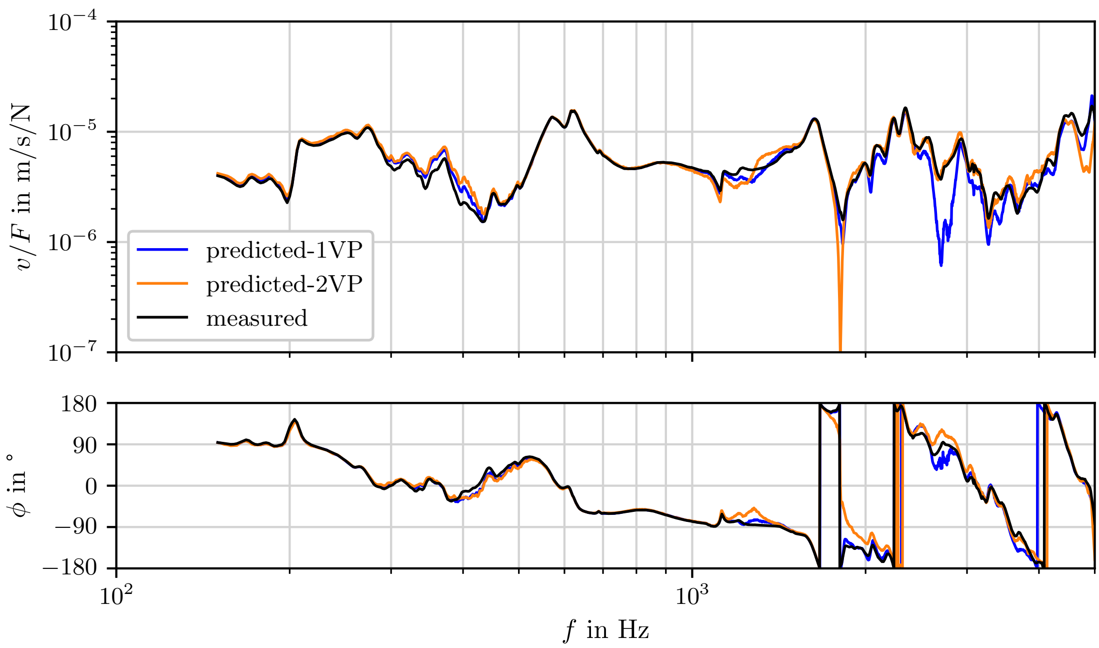

Figure 5.4: Results of OBV at the test rig for an artificial excitation on the pump housing

It can be observed that both interface definitions accurately predict the motion at the receiver sensor. Magnitude and phase of the prediction and the reference measurement agree well across most of the frequency range. However, between 2.5-3 kHz, the six blocked loads of the single-VP configuration are not sufficient to accurately predict the receiver motion. The significant drop for the dual-VP configuration observed around 1.8 kHz is likely the result of an ill-conditioned admittance matrix at the antiresonance, combined with reduced overdetermination in the dual-VP configuration. Overall, Figure 5.4 demonstrates that the chosen test configuration and interface definition are suitable for describing a source-side SBN excitation using blocked loads. For this kind of excitation the modeling using the dual-VP configuration is advantageous for frequencies above 2.5 kHz.

In contrast to the controlled artificial excitation, the excitation during actual pump operation is significantly more complex and cannot be measured. Figure 5.5 presents the OBV for the stationary operating point of the pump at n = 2000 rpm, p_{H} = 200 bar and $V_d = V_{d,\mathrm{max}}$. To provide a compact representation of the overall sensor motion, the signals of the three accelerometer channels are combined using their vector norm. This representation yields a scalar measure of the total vibration amplitude while inherently omitting phase relations between the individual sensor axes. Since no defined excitation signal is available during operational measurements, a phase reference relative to the excitation cannot be established. In principle, one accelerometer channel could be chosen as a reference. However, the pump's motion during operation is the result of multiple simultaneously acting excitation mechanisms with different spatial orientations. This leads to a superposition of vibration components whose relative phase relationships are strongly dependent on the local motion at the sensor position. As a result, the inter-axis phase information lacks clear physical interpretability and does not provide meaningful insight into the overall vibration behavior. Thus, the use of the vector norm is considered appropriate, as it provides a concise and robust representation of the overall sensor motion without implying physically ambiguous phase relationships. In Figure 5.5, the magnitude of the vector norm is shown on a decibel scale with a reference value of $v_{\mathrm{ref}} = 10^{-6}$ m/s.

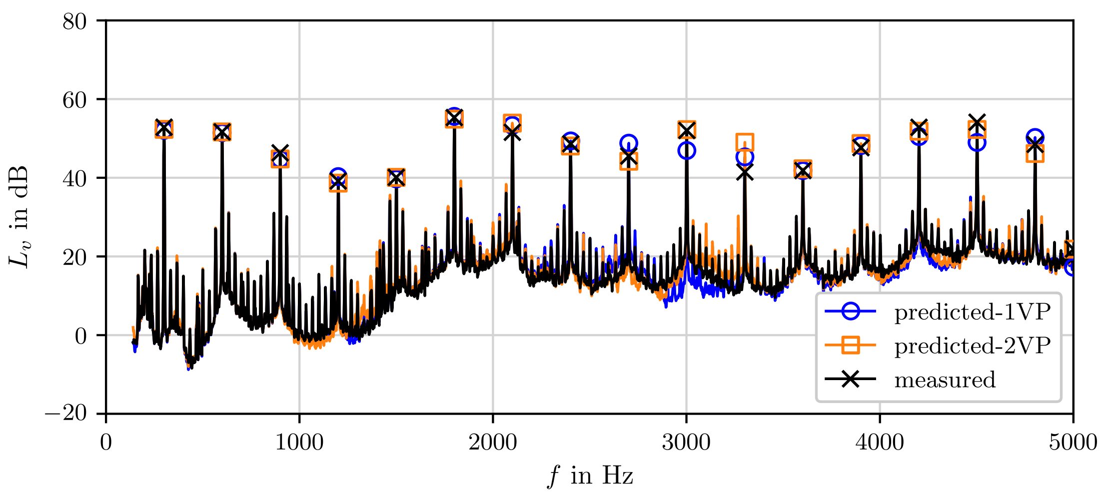

Figure 5.5: Results of OBV at the test rig for the stationary operating point: n = 2000 rpm, p_{H} = 200 bar, $V_d = V_{d,\mathrm{max}}$

The resulting velocity spectrum is typical for the noise signature of an axial piston pump. Such pumps exhibit a tonal excitation characterized by pronounced peaks at harmonics of

the piston frequency. For the operating point considered, the first harmonic, due to the nine pistons, is at 300 Hz, with higher harmonics occurring at multiples of this frequency. The maximum value at the peaks is marked with a cross for the measurement, a circle for the prediction with the single-VP configuration, and a square for prediction with the dual-VP configuration. It can be seen that predictions and measurements agree very well at harmonics up to 2.4 kHz for both configurations. At higher frequencies, minor deviations occur, with some harmonics better predicted by the single-VP configuration and others by the dual-VP configuration.
This demonstrates that the designed test setup also allows for the determination of blocked loads, which are capable of describing the pump SBN excitation during actual pump operation. Both interface definitions yield very comparable results and allow a precise prediction of the receiver movement across the entire frequency range.

5.1.1.5 Transferability Validation

The OBV is a very practical method to assess whether the determined blocked loads are capable of adequately describing the source, such that a prediction within the same test setup is possible. However, what OBV cannot indicate is whether the blocked loads are independent of the specific test setup—i.e., the receiver—which is essential for source characterization in cTPA. This aspect is addressed by the Transferability Validation introduced in Section 3.1.3.2, which is not yet included in ISO 20270-1:2019.
To facilitate a straightforward investigation of transferability at the test rig, every second screw of the eight mounting bolts on the test flange was removed (see Figure 5.2), thereby altering the structural dynamic characteristics of the receiver. The effect of this modification on the system behavior is illustrated in Fig. 5.6, which shows the FRF to the receiver point $\mathbf{u}_3$ for the configuration with eight bolts (test setup $\mathbf{AR_B}$) and the configuration with four bolts (test setup $\mathbf{AR_C}$). The excitation corresponds to the same artificial excitation applied to the pump housing in the previous section. It can be observed that removing the screws shifts the resonance originally occurring at approximately 600 Hz to about 500 Hz. A noticeable difference in the transfer behavior already occurs around 400 Hz. Consequently, this simple modification enables transferability investigations starting at 400 Hz.
The results of the Transferability Validation for an artificial excitation at the same excitation point as for the OBV are presented in Figure 5.7. The blocked loads are determined in the test setup $\mathbf{AR_B}$ and subsequently used to predict the receiver motion for the test setup $\mathbf{AR_C}$. Accordingly, the predictions for both interface definitions are compared with the measured receiver response in the test setup $\mathbf{AR_C}$. It should be noted that, although the same location on the pump housing is used for excitation, the excitation applied during blocked load determination in the test setup $\mathbf{AR_B}$ and that used for measuring the receiver response in the test setup $\mathbf{AR_C}$ are not identical. This represents a significant difference from the OBV, where blocked load determination and receiver response measurement occur in the same system under identical excitation. For a reliable Transferability Validation, the excitation signal should therefore be as similar as possible for both test setups. Shaker excitation offers an advantage over impact hammer excitation in this regard, as

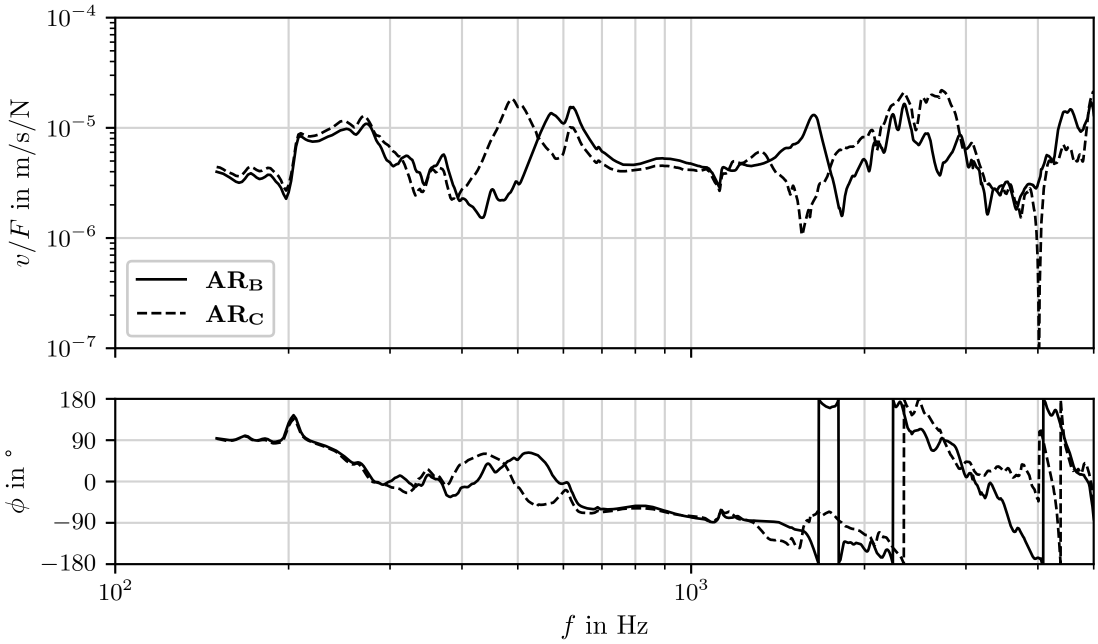

Figure 5.6: Comparison of the receiver FRFs measured for the eight-screw (**AR**$_\mathbf{B}$) and four-screw (**AR**$_\mathbf{C}$) test setups under artificial excitation applied to the pump housing.

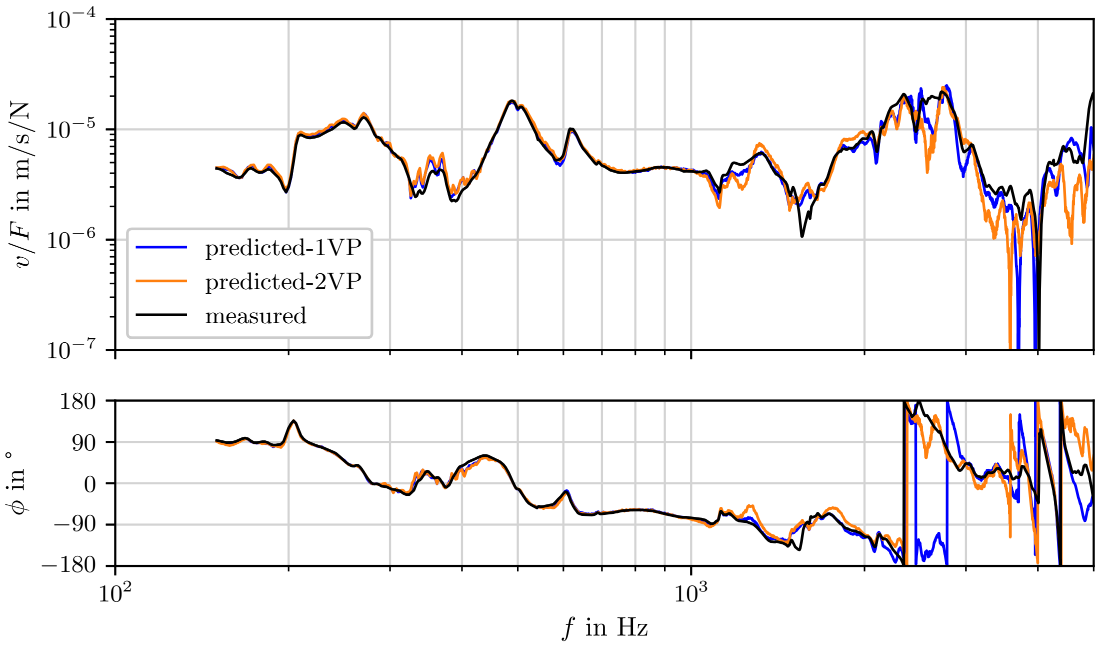

Figure 5.7: Results of Transferability Validation at the test rig for an artificial excitation on the pump housing

the excitation signal is typically highly reproducible. Furthermore, as in the OBV, in the case of artificial excitation where the input signal is known, the response signal can be normalized by the excitation signal, resulting in an excitation-independent FRF, as shown in Figure 5.7.
Up to approximately 2.5 kHz, the agreement between prediction and measurement is very good for both interface definitions. At higher frequencies, larger deviations occur in both magnitude and phase, although the overall trend remains well predicted. It can therefore be concluded that, for the artificial excitation, transferability—and thus receiver independence—is given up to 2.5 kHz, whereas below 400 Hz, no reliable Transferability Validation is possible due to similar structural dynamic behavior.
In the next step, similar to the OBV, the transferability is investigated for a stationary operating point. In this case, fulfilling the requirement of identical excitation is significantly more challenging than for artificial excitation. Furthermore, the excitation is unknown, which makes normalization using the excitation signal impossible. Therefore, the operating conditions of the pump must be adjusted precisely to achieve an internal source excitation that is as similar as possible in the test setups $\mathbf{AR}_\mathrm{B}$ and $\mathbf{AR}_\mathrm{C}$. The most critical operating parameters are rotational speed, pressure, and displacement volume, which can be controlled by the test facility. Additional influencing factors, such as oil temperature and air content in the oil, should also be kept as identical as possible.
The result of the Transferability Validation for the same operating point as in the OBV is shown in Figure 5.8. Here again, the blocked loads determined on the test setup $\mathbf{AR}_\mathrm{B}$ are employed to predict the receiver sensor motion for the test setup $\mathbf{AR}_\mathrm{C}$.

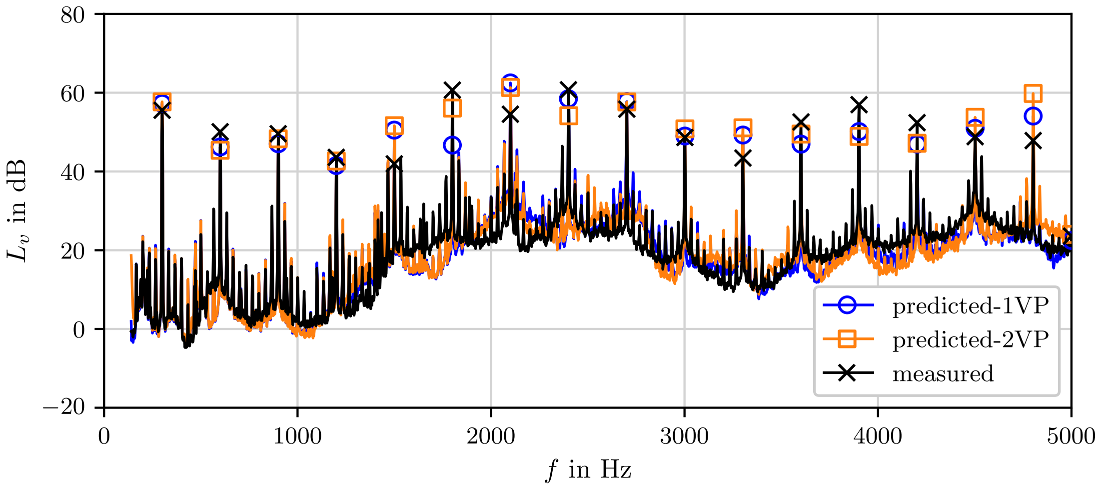

Figure 5.8: Results of Transferability Validation at the test rig for the stationary operating point: n = 2000 rpm, p_H = 200 bar, $V_d = V_{d,\mathrm{max}}$

It is evident that the agreement between prediction and measurement is significantly worse than in the OBV. For both interface definitions, a very good fit is observed for the first four harmonics, i.e., up to 1.2 kHz. For higher harmonics, deviations become substantial, reaching more than 10 dB. Both interface definitions exhibit comparable results, with no clear advantage for either definition.

When comparing these results with those obtained with the artificial excitation, it becomes clear that predictions during pump operation are considerably less accurate. This suggests that the deviations at higher frequencies in Figure 5.8 are not caused by poor admittance matrices or the In Situ Blocked Force TPA methodology itself, but rather by differences in the internal excitation mechanism of the pump.
In summary, the Transferability Validation indicates that for artificial excitation, very good transferability is achieved up to 2.5 kHz. For a stationary operating point, however, this is only valid up to approximately 1.2 kHz, which suggests that the internal pump excitation is reproducible only up to this frequency.

5.1.2 Free Velocity Determination

The previous section demonstrated that the In Situ Blocked Force TPA using the described test setup is feasible to determine the blocked loads of the axial piston pump. The accuracy of the results depends strongly on the considered frequency range and the type of excitation. To compute the Characteristic Power, as outlined in Section 4.3, both blocked loads and free velocities are required. For hydraulic pumps, free velocities cannot be measured directly. However, they can be derived from the blocked loads and the point admittance of the source according to Equation 3.6. The test setup for the determination of the source point admittance and the corresponding results achieved with this setup are presented in the following sections.

5.1.2.1 Test Setup

The source point admittance is obtained by suspending the pump freely and performing a FRF measurement at the pump interface using either an impact hammer or a shaker, similar to the first step of the In Situ Blocked Force TPA. For the axial piston pump investigated, both mounting screws were removed and the pump was suspended near its original installation position on the test rig using thin ropes and soft spring elements, resulting in a freely suspended condition. The hydraulic hoses remained connected and filled with oil throughout the procedure.
A schematic illustration of the test setup for point admittance measurement is shown in Figure 5.9. Unlike the In Situ Blocked Force TPA, sensor and excitation point placement cannot be freely designed and is largely constrained by the pump interface geometry. Nevertheless, a measurement configuration could be defined that enables point admittance determination for both interface definitions (single-VP and dual-VP configuration). In total, six triaxial accelerometers and 18 excitation points were positioned at the interface. For the single-VP configuration, where the point admittance is described by a 6×6 matrix, only four accelerometers, shown with solid outlines, and eight excitation points, shown as solid arrows, were considered. The remaining sensors and excitation points, indicated by dashed outlines and dashed arrows, were excluded based on an analysis of Sensor and Impact Consistency. For the dual-VP configuration, all six accelerometers and all 18 excitation points had to be included to determine the 12×12 admittance matrix. The same

inertial shaker and accelerometer type as those used for the In Situ Blocked Force TPA were employed to measure the FRFs.

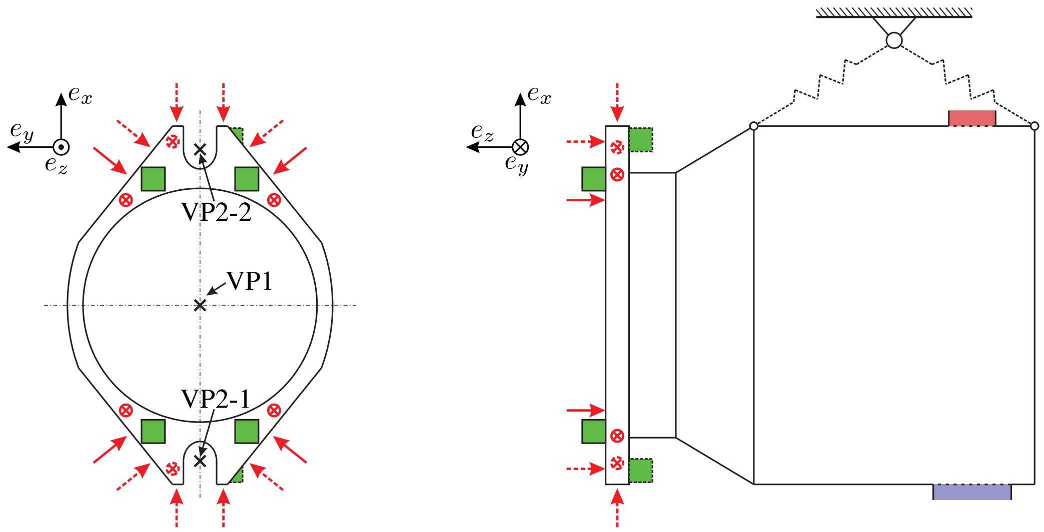

Figure 5.9: Schematic representation of the test setup for point admittance measurements of the pump under freely suspended conditions

5.1.2.2 Virtual Point Transformation

Similar to the In Situ Blocked Force TPA, the initial step involves assessing the quality of the VPT. Figure 5.10 illustrates Sensor and Impact Consistency for both interface definitions. For the interface definition using a single central VP, Consistency improves noticeably when the dashed sensors and excitation points are excluded. This can be explained by the fact that these sensors and excitation points are located relatively far from the central VP and are positioned on a comparatively thin structural region. Consequently, when they are excluded, the rigid-body assumption holds up to a higher frequency.

For both interface definitions, Sensor Consistency drops significantly above 1 kHz, possibly due to sensor positioning inaccuracies or flexible interface motion. Compared to the In Situ Blocked Force TPA, this decline is more critical, since for the determination of the source point admittance not only force but also velocity signals are transformed into VP coordinates. Based on the Sensor Consistency results, the interface motion can no longer be fully represented by the VP motion above 1 kHz. Up to approximately 2 kHz, it may still be assumed that a large portion of the motion is captured, albeit not completely. This limitation must be considered when interpreting the results and evaluating the suitability of the assessment method. Optimizing sensor placement to improve Sensor Consistency—as it is possible in the In Situ Blocked Force TPA due to the flexible receiver design—is not feasible here, because the source geometry largely constrains the sensor positioning.

In contrast to Sensor Consistency, Impact Consistency remains at a consistently high level for both interface definitions over the entire frequency range. These findings suggest that the observed drop in Sensor Consistency is not primarily caused by flexible interface

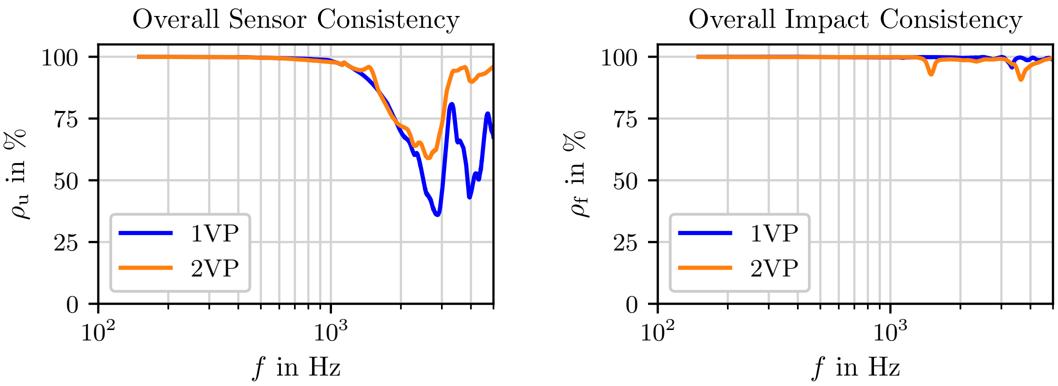

Figure 5.10: Overall Consistency of the two different interface definitions for free velocity determination setup. Left: Sensor Consistency. Right: Impact Consistency.

behavior, but rather by other sources of uncertainty, most notably sensor positioning inaccuracies. One plausible explanation is that the precise spatial alignment of sensors mounted on the pump using adhesive may be more error-prone than the positioning of excitation points. The direction of the force excitation applied by the inertial shaker is determined by the surface normal at the excitation point and can be accurately obtained from the pump's geometric model. In contrast, the sensors may be rotated around the normal direction of the adhesive surface, introducing potential misalignment errors. Furthermore, the influence of inaccurate sensor positioning may be amplified by the relatively small distances between the sensors. As a consequence, the relative motions used to determine the VP quantities are also small, particularly at higher frequencies, making the transformation more sensitive to measurement errors. This effect is more pronounced here than in the In Situ Blocked Force test setup, where the sensors are spaced further apart.
In summary, the Consistency analysis indicates that above approximately 1 kHz the interface motion can no longer be comprehensively described by the VP motion alone, and the results in this frequency range must therefore be interpreted with appropriate caution.

5.1.2.3 Quality Assessment

The determination of the pump's free velocities is based on the blocked forces and the source point mobility according to Equation 3.6, which in VP coordinates becomes:

$$\mathbf{q}_2^{\text{free}} = \mathbf{Y}_{22}^{\text{A}} \mathbf{m}_2^{\text{bl}}. \tag{5.1}$$

However, in contrast to In Situ Blocked Force TPA, no direct validation method comparable to the OBV exists. This is due to the fact that the free velocities of a hydraulic pump under operating conditions cannot be measured directly, but can only be derived from the blocked loads in combination with the source admittance. Any validation approach would therefore be circular and would not constitute an independent verification of the free velocity determination.

For artificial excitation, however, the situation is fundamentally different. Artificial excitation can be applied with the pump freely suspended, allowing the interface free velocities to be measured directly and thus to serve as an independent reference. To determine the predicted free velocities for the artificial excitation, in a first step the blocked forces for the same artificial excitation are determined in the In Situ Blocked Force TPA setup. These blocked forces are then combined with the point admittance of the source, measured under free-suspension conditions, to achieve the predicted free velocities.
Figure 5.11 shows the comparison between measured and predicted translational free velocity components for the two different interface definitions. The left plot shows the vector norm of the three translational velocity components of the central VP in the single-VP configuration $\|\mathbf{q}^{\text{free}}_{\text{T,1VP}}\|$. The right plot displays the corresponding quantities for the first of the two VPs of the dual-VP configuration $\|\mathbf{q}^{\text{free}}_{\text{T,2VP-1}}\|$. The vector norm is used to obtain a compact representation of the overall translational motion of the VP. Since the central VP of the single-VP configuration is located at a different spatial position on the source interface than the VPs of the dual-VP configuration, the velocities differ even under ideal rigid-body behavior. For this reason, the results are presented in separate plots. As with the previous figures for artificial excitation, the resulting velocity is normalized by the applied excitation signal.

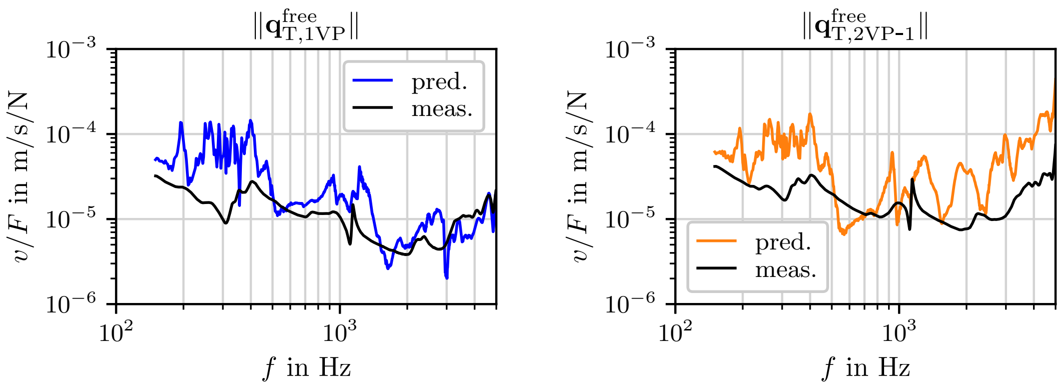

Figure 5.11: Comparison of measured and predicted vector norms of the translational free velocity components for an artificial excitation applied to the pump housing

For both setups, the agreement between prediction and measurement is limited. Up to approximately 500 Hz, the free velocities are significantly overestimated. Above this frequency range, the prediction obtained with the single-VP configuration follows the overall trend of the measured velocity, whereas the dual-VP configuration continues to yield a significant overestimation.
A similar outcome is observed when considering the vector norms of the rotational free velocities, i.e., the angular velocities at the same VPs $\|\mathbf{q}^{\text{free}}_{\text{R,1VP}}\|$ and $\|\mathbf{q}^{\text{free}}_{\text{R,2VP-1}}\|$, as shown in Fig. 5.12. The single-VP configuration exhibits comparable behavior, whereas for the dual-VP configuration the deviation between prediction and measurement is even larger than for the translational velocities.
These observations indicate that the free-velocity estimation based on blocked loads and source point admittance is highly sensitive to errors. Compared with the OBV accuracy

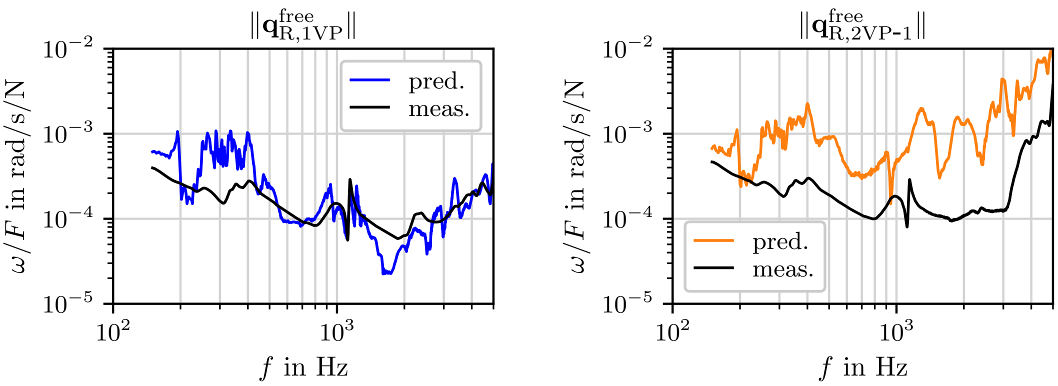

Figure 5.12: Comparison of measured and predicted vector norms of the rotational free velocity components for an artificial excitation applied to the pump housing

of the In Situ Blocked Force TPA, the agreement between predicted and measured free velocities is considerably poorer for both interface definitions. For the single-VP configuration, the global trend is captured above approximately 500 Hz, whereas for the dual-VP configuration, no meaningful prediction is achieved for the entire frequency range.
Several potential causes may contribute to the deviations between calculated and measured free velocities. Measurement inaccuracies—such as sensor and excitation-point positioning—as well as imperfections in the VPT are possible sources of error. However, based on the Consistency criteria, these effects would be expected to become dominant mainly at higher frequencies (above about 1 kHz). The significant deviations observed already below 500 Hz therefore suggest additional influences related to differences in the source behavior between the coupled state, in which the blocked loads are determined, and the free suspended state, where point admittance and free velocities are measured. These can be either practical distinctions resulting from the test setup or physical phenomena that cannot be represented by the relationship in Equation 5.1. A major distinction arises from the fact that the interface is defined solely as the flange connection between the pump and the test rig, whereas, in the coupled condition, the pump is additionally connected to its surroundings by the hoses and by the shaft-hub assembly. Although the hoses remained installed to minimize their influence, the shaft-hub connection, implemented by an elastomeric claw coupling, certainly affects the dynamic behavior of the pump. Under freely suspended conditions this effect is absent and, consequently, the source behavior changes. Both the influence of the hoses and of the shaft-hub coupling are likely more pronounced at lower frequencies, where vibration modes with larger amplitudes occur.
Moreover, additional physical coupling-related effects, such as local distortion or friction-induced damping, further modify the source dynamics in the coupled state and therefore impact the prediction [99]. The implicit consideration of coupling effects in In Situ Blocked Force TPA is also another reason why "in situ" source characterization is often preferred over that with free velocities [62], [99].
Despite these differences in source behavior, the prediction with the single-VP configuration still captures the global trend of the measured free velocities above approximately 500 Hz. For the dual-VP configuration, this is not the case. One plausible explanation is the

unfavorable location of the VPs in the dual-VP configuration. Although these positions—located at the pump mounting points—are technically appropriate for the coupled state, they are situated in regions of the pump flange with thin wall sections. As a consequence, the VPs may adequately represent the motion of these local flange sections, in accordance with the Consistency criteria, but are less representative of the global interface motion of the pump. Moreover, the structural behavior in this region is likely strongly affected by coupling-induced friction or distortion, which further degrades the quality of the free-velocity prediction for the dual-VP configuration.
Another limitation of the dual-VP interface definition arises from the fact that excitation and sensor points belonging to the same VP are located very close to each other. As a consequence, the differences in the sensor or force signals, which form the basis for the computation of the VP quantities, become small, making the VPT more sensitive to measurement and positioning errors. This effect is less critical for the measured free velocities, which exhibit a higher signal quality, but amplifies the uncertainty in the predicted free velocities.
In summary, the comparison of free velocities obtained for an artificial excitation indicates that the determination of free velocities based on blocked loads derived from the In Situ Blocked Force TPA is error-prone and inaccurate. For the single-VP configuration, the trend of the measured velocities can be reproduced above approximately 500 Hz, whereas for the dual-VP configuration no reliable prediction can be achieved.

5.1.3 Source-Specific Assessment at a Stationary Operating Point

The preceding sections on the determination of blocked loads using the In Situ Blocked Force TPA test rig, as well as the computation of free velocities via the source point admittance, form the basis for determining the source-specific assessment metrics introduced in Chapter 4. As a first step, the same stationary operating point as considered in Section 5.1.1 is analyzed.

5.1.3.1 Assessment Using Aggregated Blocked Loads

Section 4.2 introduced different approaches for assessment metrics at the load level. For the single-VP configuration, the quantities are condensed using the Euclidean norm, yielding one scalar force metric and one scalar torque metric. For the dual-VP configuration, the situation is inherently more complex, as SBN transmission occurs at two spatially separated yet interacting points. A scalar condensation of the force and torque quantities is only feasible under additional assumptions.
Assuming no interaction between the two VPs of the dual-VP configuration, the quantities can be combined in RSS fashion according to Equation 4.3 and Equation 4.4. If the other extreme case of rigid coupling is assumed, a resultant force and torque vector may instead be formed according to Equation 4.5 and Equation 4.6, followed by the computation of their Euclidean norms. However, if the rigid-body assumption is fully valid, modeling the interface using two VPs becomes unreasonable, as rigid-body conditions must then hold

for the entire interface rather than locally at each VP.
For the axial piston pump considered in this study, the results of the Consistency criteria for the In Situ Blocked Force test setup indicate rigid-body behavior of the interface, when coupled to the test rig, up to high frequencies, i.e., 4.3 kHz (see Figure 5.3). Therefore, the second special case, which assumes rigid coupling between the VPs, is considered more appropriate. To further assess whether this assumption is justified, the following consideration is made.
As discussed in Section 4.2, if the rigid-body condition is fully satisfied for the entire interface, the Euclidean norms obtained for the single-VP configuration, $\|\mathbf{m}^{\mathrm{bl}}_{\mathrm{T,1VP}}\|$ and $\|\mathbf{m}^{\mathrm{bl}}_{\mathrm{R,1VP}}\|$, must coincide with those resulting for the dual-VP configuration, namely $\|\mathbf{m}^{\mathrm{bl}}_{\mathrm{T,2VP}}\|$ and $\|\mathbf{m}^{\mathrm{bl}}_{\mathrm{R,2VP}}\|$. However, if the rigid-body condition is violated during the geometric aggregation of forces and torques of the dual-VP configuration using Equation 4.5 and Equation 4.6, an error is introduced. In this case, the resulting force and torque norms of the single-VP and dual-VP configurations will no longer coincide. Consequently, the comparison of these vector norms serves as a qualitative indicator of whether the rigid-body assumption holds during the aggregation of the dual-VP configuration, and thus for the entire interface.
Figures 5.13 and 5.14 illustrate this comparison. Figure 5.13 presents the force norms, while Figure 5.14 shows the torque norms. A reference value of 10^{-6} N for forces and 10^{-6} Nm for torques is used to define the decibel scale.

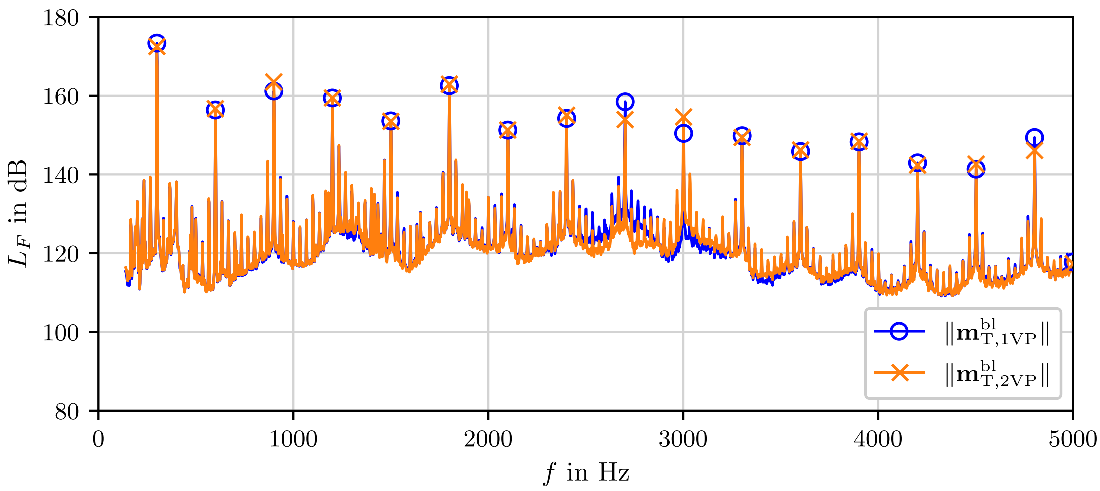

Figure 5.13: Comparison of $\|\mathbf{m}^{\mathrm{bl}}_{\mathrm{T}}\|$ for the single-VP and dual-VP configurations at the stationary operating point: n = 2000 rpm, p_{H} = 200 bar, $V_d = V_{d,\mathrm{max}}$

For the entire frequency range, the force and torque norms of both configurations agree very well at the pump harmonics. Even above 4.3 kHz, where the Impact Consistency of the single-VP configuration significantly deteriorates, a good agreement is still observed. This is likely because the Impact Consistency criterion is considerably more sensitive to violations of the rigid-body condition than the qualitative comparison of vector norms. Overall, the results indicate that the rigid-body assumption is satisfied for the entire interface up to high frequencies, and that an interface definition using a single VP is sufficient.

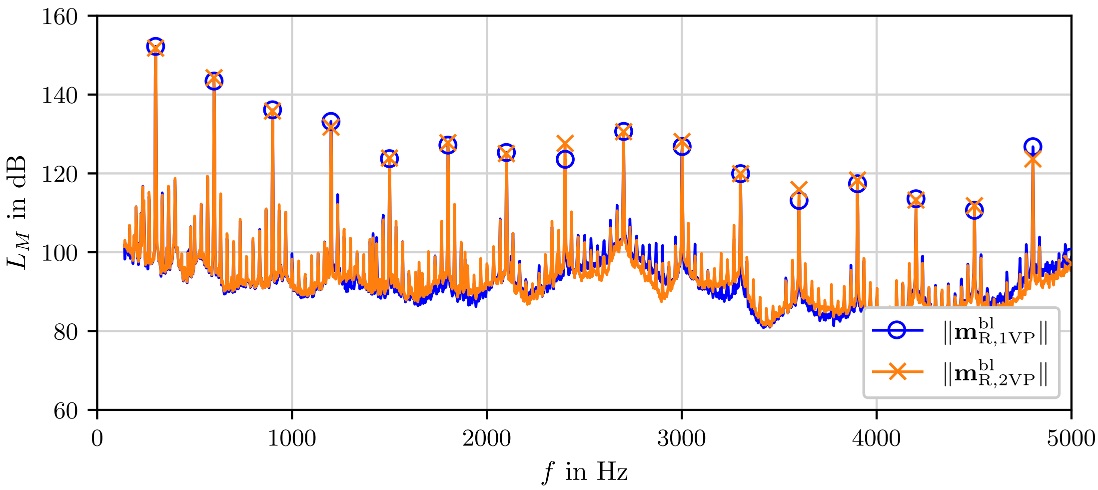

Figure 5.14: Comparison of $\|\mathbf{m}^{\mathrm{bl}}_{\mathrm{R}}\|$ for the single-VP and dual-VP configurations at the stationary operating point: n = 2000 rpm, p_{H} = 200 bar, $V_d = V_{d,\max}$

Given these findings, along with the results from previous sections where no clear advantages of the dual-VP configuration were identified, particularly during actual operation of the pump, the subsequent analysis focuses exclusively on the single-VP configuration. Consequently, the second research question regarding an appropriate interface representation can be conclusively answered. For the axial piston pump studied here, a single-VP interface description is adequate. This representation retains the benefits outlined in Section 4.1 without introducing significant losses in interface-description quality compared to the dual-VP configuration.

A fundamental prerequisite for source-specific evaluation is that the evaluation metrics are independent of the receiving system and, therefore, independent of the test setup. Consequently, the evaluation metrics obtained from the test setups $\mathbf{AR}_{\mathrm{B}}$ and $\mathbf{AR}_{\mathrm{C}}$ are expected to be identical. Figures 5.15 and 5.16 show the vector norms of the blocked forces and blocked torques for both test setups at the same operating point as discussed previously.
In contrast to the Transferability Validation, where the prediction is compared with a directly measured variable, this comparison involves two calculated quantities. As a result, potential numerical issues in the computation are not observable, as they occur equally for both quantities compared. The analysis should therefore be interpreted as a qualitative assessment of receiver independence rather than a quantitative validation. Similar to the transferability analysis, it can be assumed that significant differences in receiver behavior occur only above approximately 400 Hz. Accordingly, the comparison becomes meaningful mainly in the higher frequency range.
Both figures show a very good agreement up to the fourth harmonic at 1.2 kHz. Beyond this frequency, slightly larger deviations are observed. However, deviations remain small up to the sixth harmonic. From the seventh harmonic at 2.1 kHz onward, larger differences at some harmonics occur for $\|\mathbf{m}^{\mathrm{bl}}_{\mathrm{R,1VP}}\|$. This observation is consistent with the results of

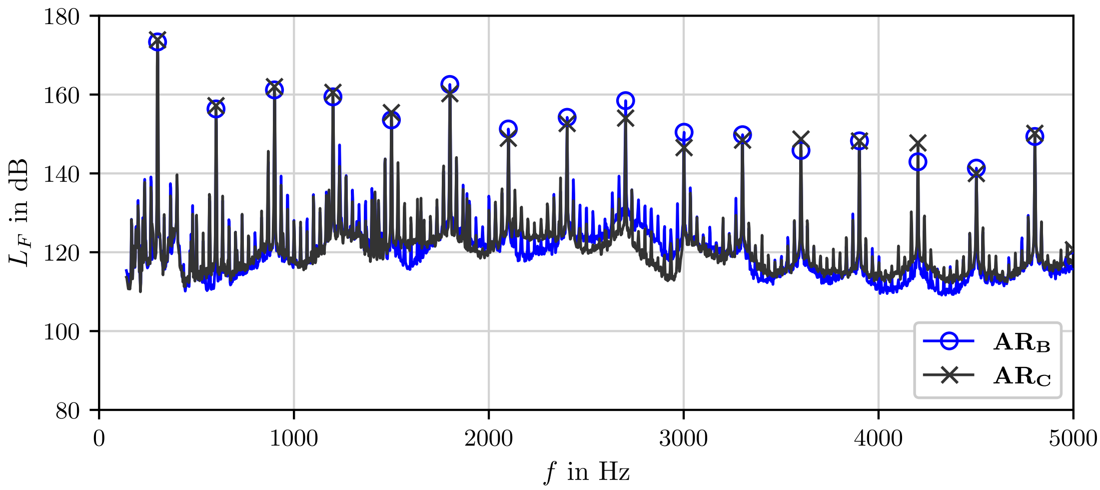

Figure 5.15: Comparison of $\|\mathbf{m}^{\mathrm{bl}}_{\mathrm{T,1VP}}\|$ determined in test setups $\mathbf{AR_B}$ and $\mathbf{AR_C}$ at the stationary operating point: n = 2000 rpm, p_{H} = 200 bar, $V_d = V_{d,\max}$

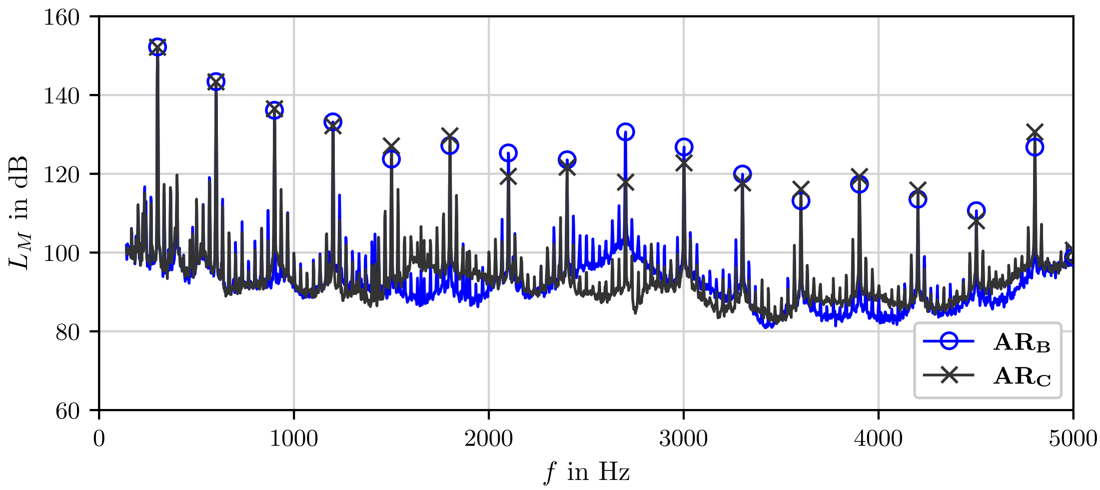

Figure 5.16: Comparison of $\|\mathbf{m}^{\mathrm{bl}}_{\mathrm{R,1VP}}\|$ determined in test setups $\mathbf{AR_B}$ and $\mathbf{AR_C}$ at the stationary operating point: n = 2000 rpm, p_{H} = 200 bar, $V_d = V_{d,\max}$

the Transferability Validation shown in Figure 5.8, where very good agreement was also found up to the fourth harmonic. Similar to the Transferability Validation, the cause for the deviations at higher frequencies is not necessarily a lack of compliance with receiver independence, but rather differences in operating conditions, because although the same operating point is considered, the measurement is not exactly identical. Additionally, the receiver independence of the first harmonic, cannot be meaningfully evaluated, since the test setups exhibit significantly different behavior only above 400 Hz. However, as the second to fourth harmonics match perfectly and larger deviations only occur at higher frequencies, it is expected that receiver independence also applies to the first harmonic. Although, conclusive validation is not possible with the applied variation of the test setup. Analyzing the evaluation metrics separately, $\|\mathbf{m}^{\mathrm{bl}}_{\mathrm{T,1VP}}\|$ is clearly dominated by the first

harmonic at 300 Hz. Its magnitude is approximately 15 dB higher than that of the remaining harmonics. At higher frequencies, the harmonic peaks tend to decrease. A similar global trend is observed for $\|\mathbf{m}^{\mathrm{bl}}_{\mathrm{R,1VP}}\|$. Nevertheless, the spectral characteristics differ significantly from those of the load-based metric. Although the first harmonic is also dominant in this case, the amplitude distribution differs markedly between the two metrics.
This demonstrates that the force-based and torque-based metrics, despite differing in their physical units, also exhibit qualitatively significant differences in their spectral characteristics. Consequently, the qualitative behavior of one metric cannot be inferred from the other, and both metrics must always be considered separately. Therefore, the load-based evaluation approach necessarily requires the consideration of two metrics. Furthermore, based on these results, it is currently not possible to identify whether the SBN excitation is dominated by a force or torque excitation.

5.1.3.2 Assessment Using Characteristic Power

The lack of direct comparability between the force- and torque-based metrics is one of the main reasons why Characteristic Power was introduced in the previous chapters.
In addition to the blocked loads, the determination of Characteristic Power requires the free velocities, which are computed from the blocked loads and the point admittance of the pump according to Equation 5.1. The validation approach based on artificial excitation presented in Section 5.1.2.3 demonstrates that the determination of the free velocities is error-prone and, consequently, also affects the accuracy of the Characteristic Power. The most likely causes are effects occurring during the coupling of source and receiver, which influence the structural dynamic properties of the source itself. Nevertheless, the validation shows that, using the single-VP interface definition, the global behavior of the free velocities can be captured for frequencies above 500 Hz. For the operating point considered here, this implies that the magnitude of the first harmonic must be treated with particular caution, as this lies at 300 Hz.
Figure 5.17 shows the real part of the Characteristic Power for the same operating conditions and for both test setups. A reference value of $P_{\mathrm{ref}} = 10^{-12}$ W is used to obtain the decibel scale. Since power levels are considered, the level is computed according to $L_W = 10\log_{10}(P/P_{\mathrm{ref}})$ rather than the relation used for the level calculation of field quantities, $L_X = 20\log_{10}(X/X_{\mathrm{ref}})$, such as forces, torques, and velocities. Consequently, a doubling of the power corresponds to an increase of approximately 3 dB in the power level, whereas a doubling of a field quantity results in an increase of approximately 6 dB.
When comparing the results for the two test setups in Figure 5.17, it should be noted that the same point mobility is used for the power calculation in both cases, while the blocked loads from the two different test setups $\mathbf{AR_B}$ and $\mathbf{AR_C}$ are applied. As a result, only differences in the blocked loads contribute to the observed deviations. Depending on the point admittance, these differences may have a strong or weak influence on the Characteristic Power. Very good agreement at the harmonic frequencies is observed up to the sixth harmonic. Beginning with the seventh harmonic at 2.1 kHz, deviations increase, with the twelfth harmonic being particularly noticeable. For the test setup $\mathbf{AR_B}$, no amplitude value is obtained at this harmonic. A closer inspection reveals that the curve is not defined at

this frequency, as the real part of the Characteristic Power becomes negative, preventing the calculation of a power level. As discussed in Section 3.3.1, the total active power is, by definition, positive, since power is transferred only from the source to the passive receiver and not vice versa. The result obtained for the twelfth harmonic is therefore unphysical. The most likely cause is an erroneous determination of the free velocity. Although not shown explicitly here, this unphysical behavior was observed over wide frequency ranges for the Characteristic Power of the dual-VP interface definition, further supporting the conclusion that the free velocities are incorrectly determined in the dual-VP configuration. The Characteristic Power exhibits a pronounced dominance of the first harmonic. On the one hand, this is consistent with the observations made for the load-based assessment metrics. On the other hand, it must be interpreted with caution, as the free velocities are significantly overestimated up to approximately 500 Hz. Similar to the load-based metrics, the magnitudes of the harmonic components of the Characteristic Power decrease with increasing frequency in a global trend. For the first three harmonics, the qualitative behavior of the Characteristic Power follows a similar pattern to that of the force-based metric $\|\mathbf{m}^{\mathrm{bl}}_{\mathrm{T,1VP}}\|$. Nevertheless, this qualitative similarity alone does not permit a reliable conclusion that the SBN excitation at this operating point is predominantly force-driven.

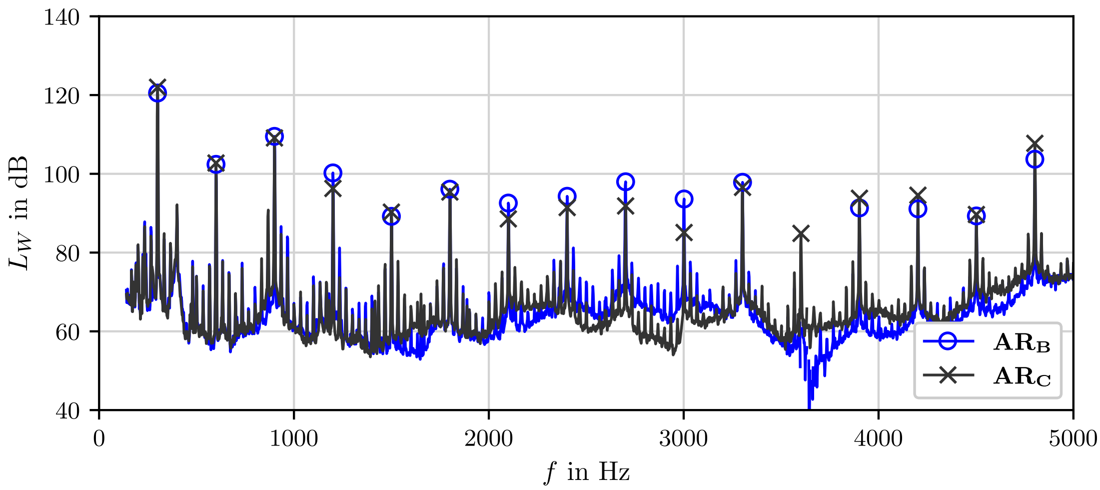

Figure 5.17: Comparison of the P_{Char} determined in test setups $\mathbf{AR_B}$ and $\mathbf{AR_C}$ at the stationary operating point: n = 2000 rpm, p_{H} = 200 bar, $V_d = V_{d,\max}$

A key advantage of the power-based metric is that the translational and rotational contributions to the Characteristic Power can be directly compared. A limitation, however, arises in the spectral power level representation, since only the real part of the total Characteristic Power is required to be positive, whereas this constraint does not necessarily hold for the translational and rotational contributions when considered individually. Therefore, the comparison of these contributions must be performed on a linear scale, which is unfavorable for spectral representations. This limitation is less critical for a run-up analysis, where the spectrum is condensed into a single scalar quantity. For this reason, the comparison of translational and rotational contributions is addressed in the following section, which analyzes source-specific metrics for a speed run-up of the pump.

5.1.4 Source-Specific Assessment during Run-Up

The analysis of a rotational speed run-up of a hydraulic pump is a well-established and essential procedure for the noise assessment of axial piston pumps. Each rotational speed results in a distinct frequency characteristic and, consequently, a different spectral distribution. For a straightforward representation of the speed run-up, the spectral information must therefore be condensed into a single representative quantity. In this context, the choice of the frequency range used for the aggregation is of particular importance. The selected range should include the dominant spectral components while, at the same time, being limited to frequency components that are considered valid and reliable.
Based on the preceding results, the available findings do not directly indicate a unique frequency range, as the different validation approaches yield differing results. The OBV and Transferability Validation under artificial excitation show very good agreement between prediction and reference measurement for the single-VP interface definition up to 2.5 kHz. Under operational conditions, however, increased deviations in transferability are observed starting from the fourth harmonic, corresponding to 1.2 kHz. The comparison of the load-based metrics likewise indicates very good agreement up to 1.2 kHz. Between 1.2 kHz and 2.1 kHz, only minor deviations are evident, while more pronounced deviations occur from the seventh harmonic, corresponding to 2.1 kHz. A comparable trend is seen for the Characteristic Power, where the agreement also deteriorates from the seventh harmonic onward. For both the Transferability Validation and the comparison of the metrics, the observed deviations may be attributed not only to the lack of receiver independence but also to differences in operating conditions. As stated at the beginning of this chapter, the lower cut-off frequency was set to 140 Hz.
Based on this, the frequency range used for the aggregation of the source-specific evaluation metrics is selected as 140-2000 Hz. The lower bound provides a small safety margin relative to the first harmonic at a rotational speed of 1000 rpm, which occurs at 150 Hz. The upper limit of 2000 Hz is derived as a reasonable boundary based on the various preceding results. This choice is primarily motivated by the observation that the source-specific evaluation metrics exhibit good agreement between the two test setups within this frequency range. Moreover, this upper limit is also consistent with the definition proposed by Vesikar et al. [54], who identified 2000 Hz as the upper cut-off frequency for noise analysis in tractors and excavators.
For the analysis during the run-up, the pump speed was continuously increased from 1000 rpm to 2000 rpm over 45 s. As previously noted, the spectral content varies with speed. Therefore, the speed ramp was segmented into individual time blocks, and one spectrum was computed for each block. In this study, the signal was divided into blocks of 0.5 s. Combined with a sampling frequency of 20 kHz, this results in a spectral frequency resolution of 2 Hz. This represents an appropriate trade-off between the time window length—required for adequate frequency resolution—and minimal speed variation within each block (approximately 11 rpm). Furthermore, the blocks overlapped by 50 %, yielding a total of 180 time blocks and, consequently, 180 individual spectra for the 45 s signal.
For each spectrum, the load-based evaluation metrics and the Characteristic Power are determined individually. The spectral quantities are then aggregated so that each time

block yields a single scalar value, which can subsequently be plotted against rotational speed. Since the aggregation procedure for the spectral quantities differs between the load-based evaluation metrics and the Characteristic Power, this is explained separately in the following sections.

5.1.4.1 Assessment Using Aggregated Blocked Loads

Since the vector norm of the blocked forces and torques in the frequency domain represents an amplitude spectrum rather than a power spectrum, the aggregation of the spectrum differs from that used for Characteristic Power.
According to Parseval's theorem, the average power of a periodic signal $x(t)$ is equal to the sum of the average powers of all its harmonic components [100]. In order to apply this concept to load quantities, these signals must be transformed into power-equivalent measures, such as the RMS value.
For a single harmonic component, the RMS value is obtained by dividing the amplitude A_k by the factor $\sqrt{2}$. Consequently, the overall RMS value of a periodic load signal can be computed from its amplitude spectrum as:

$$x_{RMS} = \sqrt{\sum_k \left(\frac{A_k}{\sqrt{2}}\right)^2} = \sqrt{\sum_k \frac{A_k^2}{2}}. \tag{5.2}$$

When this is applied to the pump speed run-up, a single scalar value is obtained for each of the 180 spectra, which can be plotted as a function of rotational speed. Figure 5.18 illustrates the results for a speed run-up from 1000 to 2000 rpm at a discharge port pressure of $p_{\mathrm{H}} = 200$ bar and at the maximum displacement volume $V_d = V_{d,\max}$ of the pump. The individual blocked load components are shown in black, while the load-based evaluation metrics are indicated in green and red. Results obtained with the $\mathbf{AR_B}$ test setup are shown using solid lines, whereas results from the $\mathbf{AR_C}$ setup are represented by dashed lines.
In the case of perfect receiver independence, the solid and dashed curves would coincide. As can be observed in the six subplots, the curves agree very well, with only minor deviations in narrow rotational speed ranges, indicating a high degree of receiver independence. This behavior can be explained by the fact that the dominant harmonics, which largely determine the RMS value, are located in the lower frequency range. In this frequency range, the agreement between the two test setups was found to be highest, as previously shown in Figures 5.15 and 5.16.
The selected representation, in which each individual blocked load component is plotted together with the corresponding load-based metric, enables a straightforward assessment of which interface load dominates the force or torque excitation at a given rotational speed for the investigated axial piston pump. For force excitation, it can be observed that the y-direction (see Fig. 5.2) contributes significantly to the overall force excitation over the entire speed range, whereas the x-direction exhibits a significant contribution only within specific speed intervals. The contribution of the z-direction to the force excitation is negligible across the full speed range. A different trend is observed for torque excitation, where torques from all spatial directions contribute to the overall excitation. Notably,

in the speed range between 1400 rpm and 1800 rpm, the torque excitation about the y-axis decreases, while that about the z-axis becomes dominant. Consequently, the torque excitation in this range is primarily governed by a torsional component.
When comparing the behavior of the two evaluation metrics $\|\mathbf{m}_{\mathrm{T}}^{\mathrm{bl}}\|$ and $\|\mathbf{m}_{\mathrm{R}}^{\mathrm{bl}}\|$, it becomes evident that they do not exhibit qualitatively similar trends. This observation supports the findings presented in Section 5.1.3.1, indicating that both metrics display different behaviors and, therefore, neither can be considered representative of the overall SBN excitation. Consequently, force and torque excitation must be analyzed separately.

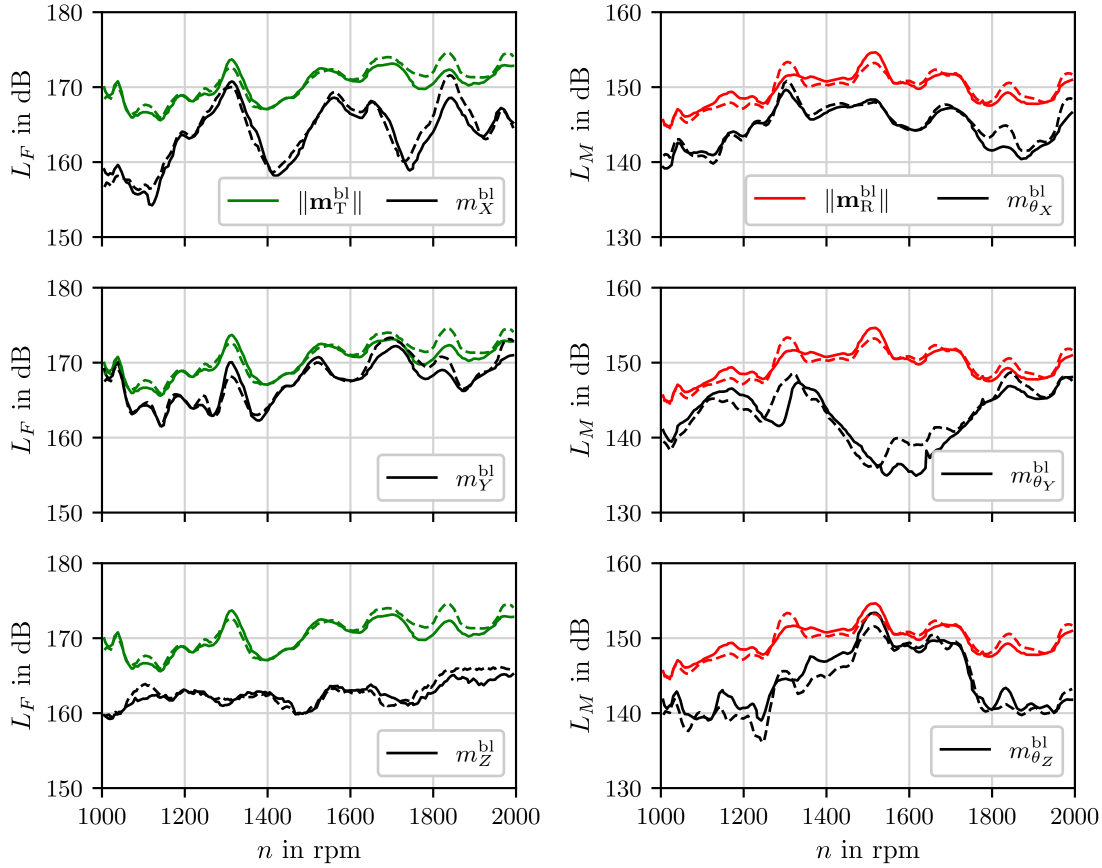

Figure 5.18: RMS value of the load-based metrics and the individual loads during a run-up with $p_{\mathrm{H}} = 200$ bar, $V_d = V_{d,\max}$ (solid line: **AR$_{\mathbf{B}}$**, dashed line: **AR$_{\mathbf{C}}$**).

5.1.4.2 Assessment Using Characteristic Power

As mentioned in the previous section, the aggregation of the spectrum at the Characteristic Power is handled differently because it represents a power spectrum, for which Parseval's theorem applies directly. Consequently, the total power of a periodic signal is simply obtained by summing all spectral components:

$$P_{\mathrm{tot}} = \sum_k P_k, \tag{5.3}$$

where P_k denotes the power contribution of the k-th harmonic component in the power spectrum.
Before analyzing the Characteristic Power during the run-up, it should be noted that Section 5.1.2.3 identified a particularly high uncertainty in the determination of the free translational and angular velocities for frequencies up to approximately 500 Hz. This uncertainty consequently affects the Characteristic Power in this frequency range. Additionally, as can be inferred from Fig. 5.17, the lower frequency range below 1 kHz is expected to contribute significantly to the total Characteristic Power P_{tot}. It can therefore be assumed that the values of P_{tot} are influenced by the error-prone determination of the translational and angular velocities in this frequency range. Accordingly, the quantitative values of the Characteristic Power should be interpreted with caution.
However, an important objective of the Characteristic Power analysis is not only the absolute quantification of P_{tot}, but also the assessment of whether the excitation is predominantly translational (force-driven) or rotational (torque-driven). As shown in Fig. 5.11 and Fig. 5.12 in Section 5.1.2.3, both the translational velocities and the rotational velocities of the single-VP configuration exhibit a comparable deviation between measurement and prediction. In addition, the Sensor Consistency analysis of the free velocity determination test setup indicates that, for frequencies below 1 kHz, the transformation into VP coordinates is performed reliably.
Based on these observations, it is reasonable to assume that the error introduced by the differing dynamic behavior of the source in the freely suspended and coupled conditions affects both the free translational and angular velocities in a similar manner. Consequently, the associated uncertainty is expected to have a comparable impact on the translational and rotational contributions to the Characteristic Power. While the resulting estimates therefore remain subject to uncertainty, they are nevertheless considered suitable for assessing whether one excitation mechanism is clearly dominant over the other, or whether neither contribution prevails.

Before analyzing the translational and rotational power contributions in detail, the overall Characteristic Power as well as the contributions of the individual interface DoF are shown as a function of rotational speed in Figure 5.19, analogous to the illustration in the previous section. Solid lines denote the test setup $\mathbf{AR_B}$, whereas dashed lines indicate the test setup $\mathbf{AR_C}$. In contrast to Figure 5.18, a linear scale is used instead of a decibel scale. This choice is motivated by the fact that the real part of the Characteristic Power associated with individual interface DoF is not necessarily positive, only the total active Characteristic Power is required to remain positive. Since decibel values cannot be defined for negative quantities, a linear representation is employed. Consequently, deviations between the two test setups are more recognizable.
Overall, a qualitatively good agreement between the two test setups is observed. Although the peak values differ quantitatively, the general shape of the curves is comparable, as the peaks occur at similar rotational speeds. Notably, the real part of the Characteristic Power of individual DoF may become negative, indicating an out-of-phase relationship between load and velocity at the respective operating points. This behavior is physically admissible as long as the real part of the total Characteristic Power remains positive.

An examination of the individual DoF contributions reveals that the translational power in the z-direction contributes only marginally to the total Characteristic Power. In contrast, all other DoF provide noticeable contributions, although in some cases only over short rotational speed ranges. The most dominant contribution originates from translational motion in the y-direction, which remains significant over nearly the entire speed range.

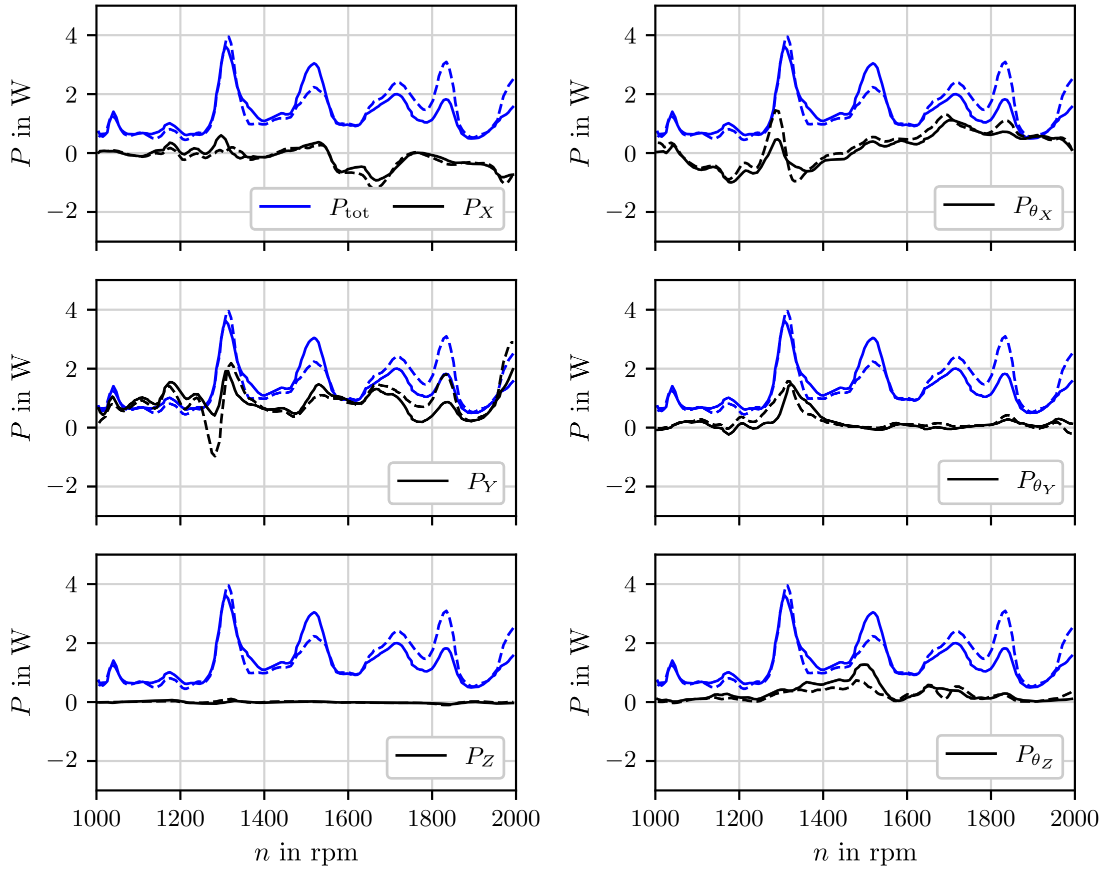

Figure 5.19: Real value of the total Characteristic Power and that of the individual DoF during a run-up with p_{H} = 200 bar, $V_d = V_{d,\mathrm{max}}$ (solid line: $\mathbf{AR_B}$, dashed line: $\mathbf{AR_C}$).

Furthermore, Figure 5.19 indicates that translational and rotational power components significantly contribute to total Characteristic Power. This observation is illustrated more explicitly in Figure 5.20, where the real part of the total Characteristic Power of the test setup $\mathbf{AR_B}$ is compared with the summed translational and rotational power contributions P_{T} and P_{R}. It is evident that both components contribute significantly to the total Characteristic Power and that neither is strictly dominant. While translational DoF prevail in the lower rotational speed range, rotational DoF become increasingly dominant at higher speeds.

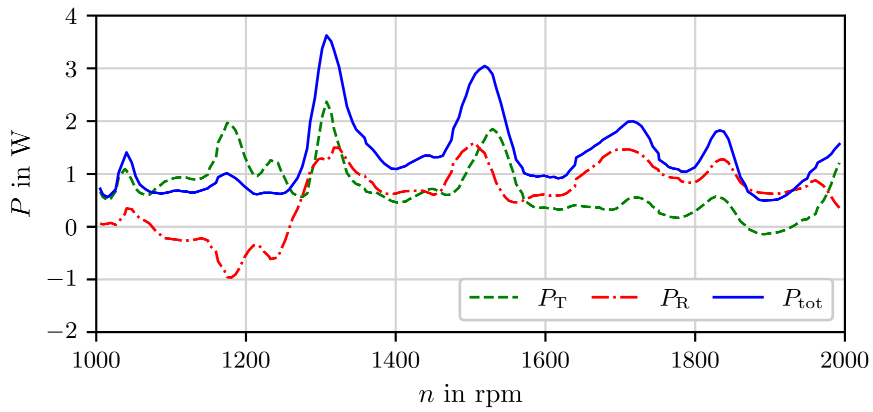

Figure 5.20: Real value of the total Characteristic Power and that of the of translational and rotational DoF of test setup $\mathbf{AR_B}$ during a run-up with $p_H = 200$ bar, $V_d = V_{d,max}$.

As discussed previously, the analysis of Characteristic Power must be interpreted with caution due to uncertainties inherent in its determination. Nevertheless, the results suggest that both excitation mechanisms, force-driven and torque-driven, contribute significantly to the SBN excitation at the interface. Consequently, both excitation types must be considered when evaluating the SBN behavior of the investigated axial piston pump.
For assessment using load-based metrics, this implies that both force-based and torque-based metric must be taken into account.

5.2 Receiver-Dependent Assessment of the Axial Piston Pump

The SBN assessment based on source-specific metrics provide a powerful tool, particularly for the component development of hydraulic pumps. It enables a receiver-independent comparison of different pumps as well as of noise mitigation measures. However, for later stages in the development process of mobile machinery, the cTPA framework described in Section 4.4 additionally allows for a receiver-dependent evaluation of hydraulic pumps. If the transfer behavior of a mobile working machine is determined experimentally or numerically, it can be combined, based on the principle of transferability, with blocked loads measured on a test rig. In this way, the response at a specific receiver point can be predicted, providing a receiver-dependent, single-valued evaluation metric.
To investigate this approach within the scope of this work, the receiver behavior of an electrified 6-ton excavator was determined experimentally. Accordingly, the following sections first describe the experimental setup and results of the determination of the excavator behavior. Subsequently, the results obtained by combining the blocked loads measured on the test rig with the dynamic behavior of the excavator are presented.

5.2.1 Determination of the Excavator Behavior

In order to determine the dynamic behavior of the excavator, a shaker or impact hammer measurement is performed to identify the transfer behavior, i.e., the FRFs, from the source interface to the specific receiver point. Additionally, a reference measurement during pump operation should be conducted. The comparison between the predicted response, which is obtained by combining the blocked loads measured on the test rig with the experimentally determined excavator FRFs, and the directly measured excavator signal during pump operation serves as a validation of the proposed approach. This validation is essentially a Transferability Validation of the test rig blocked loads with the excavator as an alternative receiver.
However, both the measurement of FRFs and the measurements during pump operation are significantly more challenging than the In Situ Blocked Force TPA measurements performed on the test rig, for the reasons outlined in Section 4.4. In summary, these challenges include limited accessibility to the source, the absence of a geometric model of the interface, reduced control over operating conditions, and disturbances from additional noise sources. The latter is particularly critical in mobile working machines. In addition to auxiliary units such as cooling fans or air-conditioning compressors, a major challenge for applying cTPA to hydraulic pumps arises from the direct mechanical coupling between the pump and the drive motor.
In contrast to the dedicated hydraulic pump test rig, where significant design effort is made to minimize the influence of the drive unit and to isolate the pump noise, in mobile working machines the hydraulic pump is typically flange-mounted directly to the drive motor. For a reliable Transferability Validation, the receiver, i.e. all structures downstream of the source, must exhibit passive behavior. This condition is only met if the excitation caused by all other noise sources, including the drive motor, is significantly lower than the excitation generated by the hydraulic pump. For diesel engine-driven systems, this assumption is hard to meet, as diesel engines transmit a high level of SBN, particularly in the low-frequency range. In contrast, electric motors typically generate significantly less noise, which is why in electrified mobile working machines hydraulic noise is often perceived as dominant. This observation is supported by the investigations of Fiebig [8] on electrically driven industrial hydraulic systems, which indicate that noise excitation by the electric motor plays a minor role.
Based on these considerations, an electrified excavator was selected for the present investigation. The machine is equipped with a pump that is identical in design but not the same individual unit as the pump used in the test rig measurements. The experimental setup used for the determination of the excavator behavior is described in detail in the following section.

5.2.1.1 Test Setup

The investigated excavator was converted within the scope of a research project from a diesel-powered drivetrain to a battery-electric drivetrain. For this purpose, the diesel tank and internal combustion engine were replaced by a battery system, power electronics, and

an electric motor.
Figure 5.21 shows a schematic illustration of the excavator test setup. The investigated axial piston pump is mounted directly to the electric motor, which is attached to the vehicle frame via rubber mounts for vibration isolation. In order to investigate only the SBN transmitted to the vehicle through the pump interface, the discharge port of the pump is not connected to the excavator hydraulic system as in standard operation. Instead, the hydraulic oil is pumped directly back to the tank through an external pressure relief valve. This configuration is intended to minimize SBN and ABN generated by pressure pulsations within the hydraulic system.

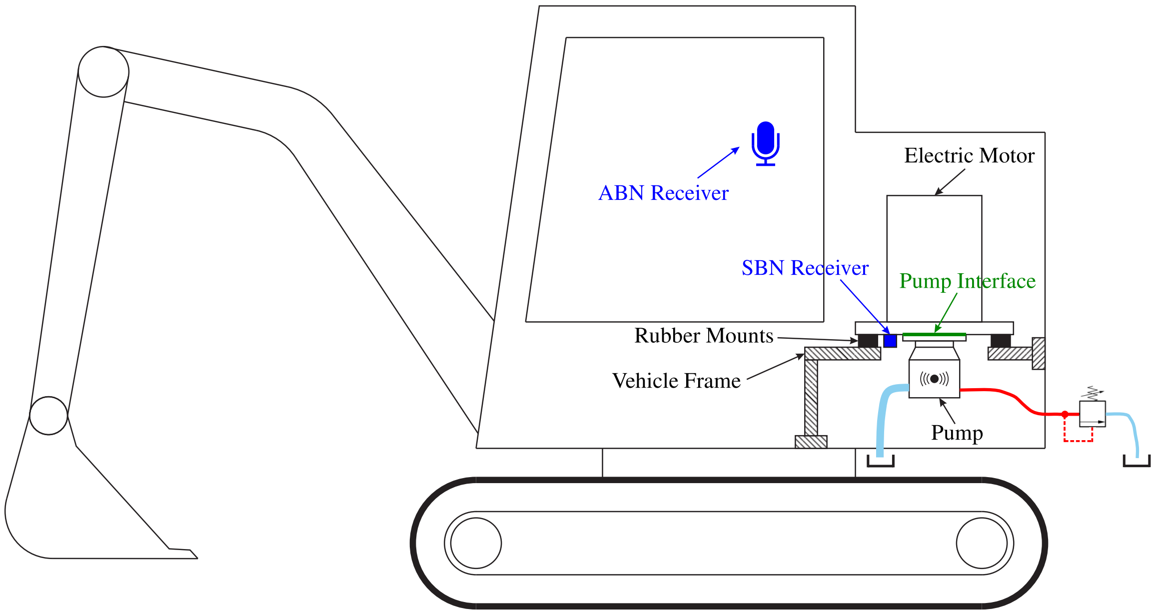

Figure 5.21: Schematic illustration of the test setup for the determination of the excavator behavior

Several SBN and ABN receivers are installed in the excavator. The sensors considered in the following analysis are the SBN receiver and the ABN receiver shown in Figure 5.21. The SBN receiver, i.e., the accelerometer, is positioned directly on the motor flange of the electric motor and is therefore located immediately downstream of the pump interface. The ABN receiver, i.e., the microphone, is installed inside the cabin in close proximity to the driver's left ear.
During operation, the pump emits not only SBN through the mounting but also direct ABN from the pump housing. To minimize this contribution, the cabin door was kept closed at all times and potential openings were sealed using insulation material. However, it should be noted that the operator cabin of the excavator exhibits significantly poorer ABN insulation compared to modern passenger vehicles. In addition, the cabin featured small openings for cables required to monitor the operating conditions of the electrified powertrain from the driver's seat. These openings were difficult to seal completely. Consequently, a contribution from the ABN path cannot be entirely excluded.

The transfer behavior from the interface to the receiver points is determined by exciting close to the interface using an impact hammer or a shaker and measuring the responses at the receiver locations. As known from the test rig results, the SBN excitation of the investigated axial piston pump can be described using one VP. Consequently, the excitation points around the interface must be positioned such that all six DoF of the single central VP can be identified.

In contrast to the FRF measurements conducted on the test rig, the accessibility of the interface in a mobile working machine is significantly more limited. Additionally, the receiver structure cannot be freely selected, as it is largely defined by flange of the electric motor. In particular, excitation of the interface in-plane using an impact hammer or shaker is not possible. For this reason, two bracket-shaped adapter structures were designed and glued to the electric motor flange using an epoxy adhesive with high stiffness and good load-transfer properties. These adapters allow excitation in all three spatial directions and enable the mounting of accelerometers close to the interface.

A schematic illustration of the pump interface, including the adapter structures and excitation points, is shown in Figure 5.22. In this figure, the electric motor flange is shown in white, the pump housing in gray, and the additional adapter structures in yellow. The bracket-shaped adapters are glued to the motor flange in such a way that they do not contact the pump housing and can therefore be considered part of the receiver.

It should be noted that no additional accelerometers at the interface, shown as green squares in Figure 5.22, are required for determining the transfer behavior to the receiver points. These sensors were used as indicator sensors to perform a In Situ Blocked Force TPA in the mobile working machine. The results of this analysis are not discussed in detail here, as this would exceed the scope of the thesis and essentially follow the same procedure as the implementation of the method on the test rig, only in a different test environment. Instead, the following sections directly focuses on the results obtained by combining the blocked loads measured on the test rig with the transfer behavior of the excavator.

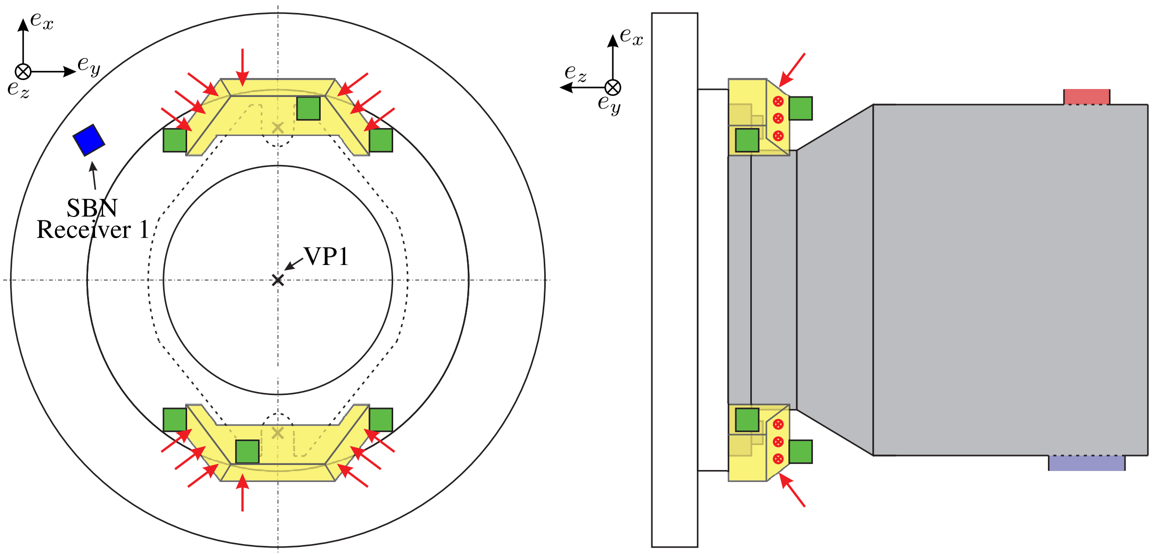

Figure 5.22: Schematic illustration of the pump interface in the excavator

In Figure 5.22, the excitation points are again shown as red arrows. During the positioning of these, it became apparent that excitation using an impact hammer was not feasible due to limited space around the interface. Therefore, the same inertial shaker used in the test rig measurements was employed. Using this shaker, excitation was applied at a total of 14 locations, which are exemplarily shown in Figure 5.22. The information required for the VPT, namely the spatial positions and orientations of the excitation points, is subject to significantly higher uncertainty compared to the test rig measurements. This is primarily due to the absence of an accurate geometric model of the receiver flange and the difficulty of precisely gluing the adapters because of limited accessibility.
Again, the same inertial shaker and accelerometer types as used in the test rig measurements were employed. As the ABN receiver, a Class 1 electret condenser measurement microphone was employed. Its free-field frequency response extends from 3.5 Hz to 20 kHz and therefore sufficiently covers the frequency range of interest. Data analysis was again performed using the Python programming language with the pyFBS package.

5.2.1.2 Virtual Point Transformation

As in the previous sections, the first quality criterion is the Consistency of the VPT. Figure 5.23 again shows the Sensor and Impact Consistency, where the results for the excavator test setup are shown in light orange and those for the In Situ Blocked Force TPA on the test rig are shown in blue for comparison. For the determination of Consistency, the indicator sensors shown as green squares in Figure 5.22 were used. Although these sensors are not required for determining the transfer behavior to the receiver sensors, they can be used to assess the quality of the VPT. As in the In Situ Blocked Force TPA, the overall Impact Consistency is the most relevant criterion, since only the forces are transformed into the VP coordinates. Nevertheless, the Sensor Consistency again provides additional insight into the interface behavior.

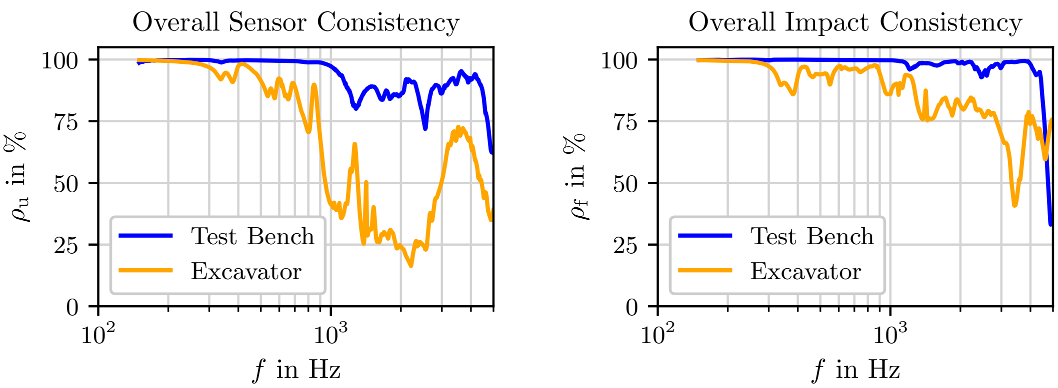

Figure 5.23: Overall Consistency of the two different interface definition for the test rig and the excavator setup. Left: Sensor Consistency. Right: Impact Consistency.

When looking at the Sensor Consistency, it can be observed that, for the excavator setup, it begins to decrease slightly at approximately 300 Hz. It then fluctuates between 70 %

and 100 % before dropping significantly at around 900 Hz. At frequencies above this threshold, it must be assumed that the projection of the measured indicator signals into the VP coordinates is no longer reliable. The Impact Consistency for the excavator setup is, as observed in the previous sections, consistently higher than the Sensor Consistency over the entire frequency range. Here, a first decrease is also observed at approximately 300 Hz. However, the Impact Consistency remains above 90 % up to about 900 Hz, and the significant drop to values below 50 % only occurs above 3 kHz. It can be assumed that the fluctuations observed below 900 Hz are primarily caused by errors in the positioning of the excitation points, which are mainly a consequence of the inaccurate attachment of the bracket-shaped adapters. At higher frequencies, various effects can influence the quality of the VPT. However, based on the trend of the Impact Consistency, it may be concluded that above approximately 3 kHz the VP loads are no longer able to describe the SBN excitation of the pump with sufficient accuracy.

In general, it can be stated that the quality of the VPT for the excavator measurements is significantly lower than that achieved for the test rig measurements, where a pronounced decrease in both Sensor and Impact Consistency is only observed at approximately 4.3 kHz. The main reasons for this are most likely inaccuracies in the positioning of sensors and excitation points, as well as the structural dynamic behavior of the bracket-shaped adapters. Due to the design constraints, these adapters have a relatively thin-walled profile. As a result, it can be assumed that they undergo elastic deformation at significantly lower frequencies compared to the massive test rig flange (see Figure 5.2). Furthermore, the adhesive layer used for bonding the adapters may also contribute to the observed deviations due to its own compliance and damping characteristics. The exact influence of the various error sources cannot be quantified retrospectively. However, it can be concluded that the rigid body assumption is violated at lower frequencies for the VPT of the excavator setup compared to the test rig setup.

In summary, the quality of the VPT for the excavator setup is clearly worse to that of the test rig setup. Nevertheless, based on the results for the Impact Consistency, within the frequency range of primary interest (140-2000 Hz), it can be assumed that the VP loads are capable of describing the main SBN excitation.

5.2.1.3 Quality Evaluation Receiver Transfer Functions

One aspect that had already been considered as critical prior to the measurements on the excavator was whether the excitation provided by the compact inertial shaker would be sufficient to determine the receiver transfer functions with adequate quality. If the transfer behavior to the receivers cannot be measured reliably, no robust prediction of the vibro-acoustic response can be made. In order to assess whether the receiver transfer functions can be obtained with sufficient quality, the following figures show, for each receiver, the measured response under shaker excitation at the interface as well as the corresponding noise floor recorded with the excavator switched off. Specifically, Figure 5.24 shows the response at the SBN receiver located at the electric motor flange together with its noise floor, both expressed on a decibel scale. To represent the overall sensor motion, the vector norm of all sensor channels is shown.

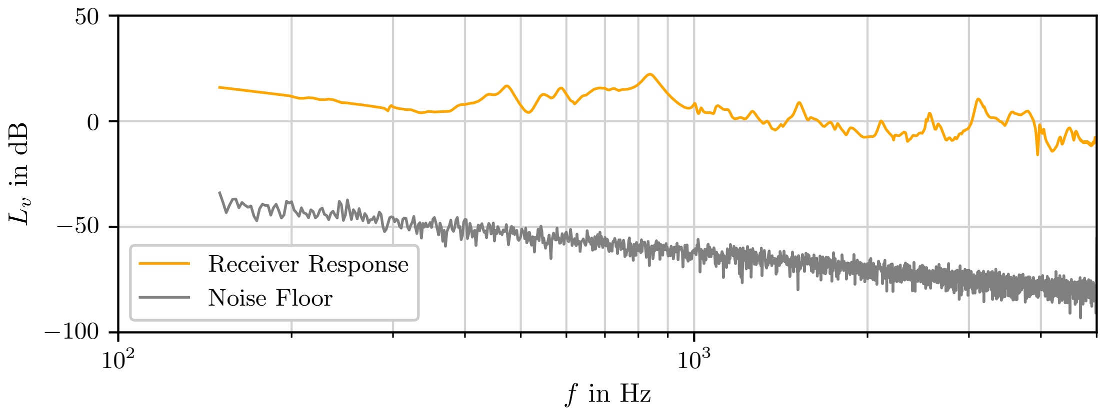

Figure 5.24: Investigation of the SNR of the SBN Receiver during Excitation in the Interface using the Inertial Shaker

As can be observed, the noise floor is approximately 50 dB or more below the measured response over the entire frequency range. In experimental practice, a minimum SNR of about 10 dB between the measured signal and the noise floor is commonly regarded as sufficient for a reliable evaluation. Below this level, the measured signal is expected to be strongly influenced by background noise, and the resulting data cannot be considered robust. It should be emphasized that the value of 10 dB does not represent a strict or normative threshold, but rather a pragmatic guideline that has proven useful in practice. For the SBN receiver, it is therefore evident that this requirement is exceeded by a large margin. Consequently, the limited excitation power of the shaker does not pose a limitation for the measurement of the corresponding transfer function.
A different situation is observed for the microphone inside the cabin. The noise floor and the response to the same excitation are shown in Figure 5.25. For this representation, the typical reference value of $p_{\mathrm{ref}} = 20\ \mu\mathrm{Pa}$ was used to calculate the decibel scale. Compared to the SBN receiver, the difference between the response signal and the noise floor is significantly reduced. This is expected because the microphone is located at a considerably further distance from the pump interface, and the excitation signal is transmitted through the electric motor decoupling and the massive machine structure before reaching the ABN receiver. It can be seen that, in the frequency range below approximately 300 Hz, the criterion of a SNR of 10 dB is not met, and therefore no reliable statements can be made in this range. Above 300 Hz, the SNR improves significantly and reaches values of approximately 10-15 dB on average. However, local drops of the response can still be observed, where the 10 dB difference is not achieved.
These results indicate that the shaker's excitation power is too low to allow highly reliable determination of the transfer function to the cabin microphone. Nevertheless, for frequencies above 300 Hz it can be assumed that the background noise no longer dominates the measured signal. Consequently, although affected by increased uncertainty, meaningful interpretations of the receiver response remain possible in this frequency range.

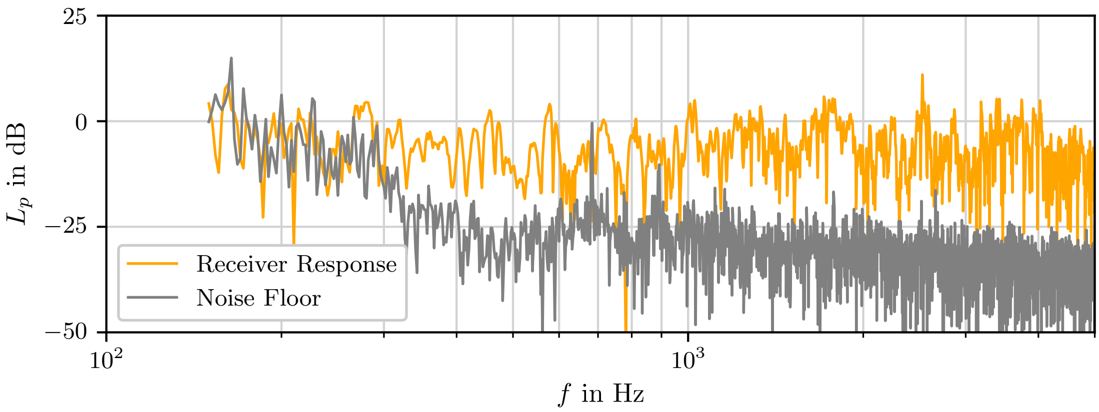

Figure 5.25: Investigation of the SNR of the ABN Receiver during Excitation in the Interface using the Inertial Shaker

5.2.2 Receiver-Dependent Assessment at a Stationary Operating Point

Once the FRFs from the interface to the receiver sensors have been determined, they can be combined with the blocked loads measured on the test rig. Using the relations described in Section 4.4, predictions of the SBN and ABN responses at the respective receiver sensors can then be obtained. For the case of a stationary operating point, it was possible to set operating conditions of the pump in the excavator that were comparable to those used during the test rig measurements. The responses measured at the receiver sensors under these conditions therefore serve as reference data for validating the prediction.

Figure 5.26 shows this comparison for the SBN receiver. The quantity shown is the vector norm of the velocities measured by all three channels of the accelerometer. It should be noted that, in the excavator, the rotational speed could only be adjusted in increments of approximately 60 rpm, resulting in an operating speed of about 1960 rpm. In contrast, during the test rig measurements the rotational speed could be set very precisely to 2000 rpm. As a consequence, the pump harmonics in the measured signal are consistently shifted to slightly lower frequencies compared to the prediction. This effect becomes increasingly pronounced for higher-order harmonics, as can be observed in Figure 5.26. Since the frequency f_k of the k-th harmonic is an integer multiple of the pump rotational speed, given by $f_k = k \cdot 9n$, the absolute frequency offset between the corresponding harmonics of prediction and measurement increases linearly with increasing harmonic order k.

A comparison of the predicted and measured responses at the SBN receiver reveals several notable observations. First, the prediction significantly overestimates the vibration response from the eighth harmonic onward, corresponding to frequencies above approximately 2.4 kHz. This confirms the previously introduced limitation of the valid frequency range to approximately 140 Hz to 2 kHz. Furthermore, it is clearly evident that up to 1 kHz the sidebands—the spectral peaks located between the harmonics—are much more pronounced in the measurement performed on the excavator than in the prediction using the blocked loads obtained on the test rig. For example, at the second harmonic, the amplitudes of the first two sidebands in the measured signal exceed that of the harmonic

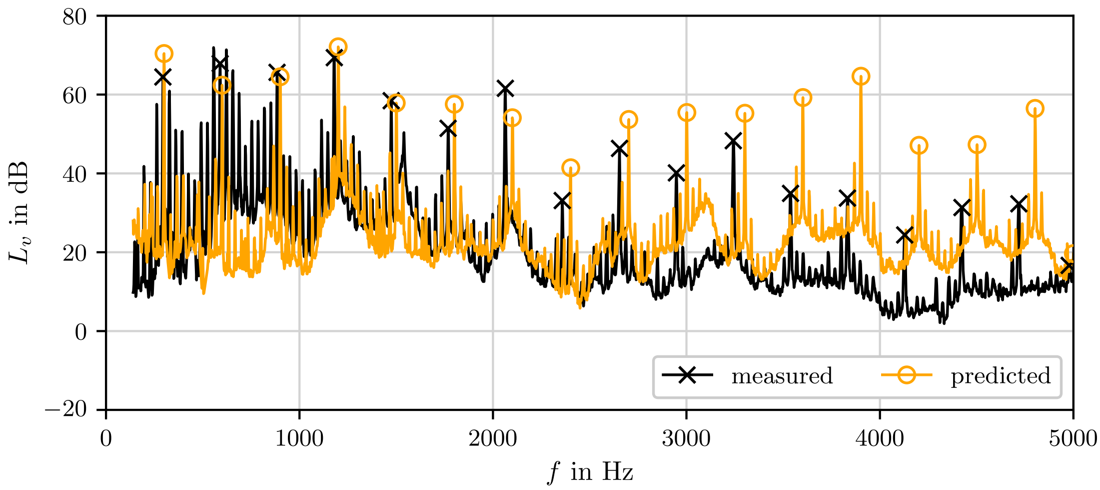

Figure 5.26: Comparison of the predicted and measured velocity at the SBN receiver in the excavator at the stationary operating point: n = 2000 rpm, p_{H} = 200 bar, $V_d = V_{d,\mathrm{max}}$

itself, whereas in the prediction the second harmonic is approximately 20 dB higher than its first sidebands.

Sidebands are a common phenomenon in rotating machinery and can originate from various sources. Typical causes include irregularities such as manufacturing tolerances in the pump drive unit or mass imbalances, which manifest at the rotational frequency and its multiples [101]. Accordingly, the frequency spacing between the sidebands in Figure 5.26 corresponds to the rotational frequency of approximately 33 Hz. The spectral shape of the predicted signal, featuring a dominant harmonic peak with several significantly lower sidebands, represents the expected behavior. In contrast, the measured signal, in which the sidebands partially exceed the harmonic amplitudes, is unusual and indicates the presence of additional effects specific to this application. A definitive identification of the root cause is not possible in retrospect, as several mechanisms may contribute. One potential cause is the occurrence of periodic disturbances arising from the coupling between the electric motor and the pump. These may include preload effects in the drivetrain, imbalances, or mechanical looseness leading to rattling, all of which can disturb the rotational motion of the pump and result in pronounced sidebands. Another possible cause might be an additional SBN contribution from the electric motor, even if it was expected that this plays a minor role compared to the excitation of the pump. Unlike in the test rig configuration, the motor in the excavator is directly coupled to the pump and therefore contributes to a greater extent to the SBN excitation at the interface.

Regardless of the specific cause, it can be concluded that the excitation characteristics of the pump on the test rig differ significantly from those in the excavator. As a result, the direct comparison between prediction and measurement is limited, and a close quantitative agreement cannot be expected. Nevertheless, below 2 kHz, the prediction and measurement exhibit a comparable trend at the harmonic frequencies, even though the absolute levels may differ by several decibels.

Although the previous results have already shown that the prediction and the measurements at the receiver points are only comparable to a limited extent, the receiver response at the ABN receiver is briefly examined in the following. This is of particular relevance, as the ABN inside the cabin represents the most application-relevant evaluation metric. The corresponding results are shown in Figure 5.27. It can again be clearly observed that the prediction significantly overestimates the noise levels at higher frequencies. Furthermore, also for the microphone, the sidebands up to approximately 1 kHz are much more pronounced in the measurement compared to the prediction. In addition, the broadband components of the measured signal are substantially higher than those of the prediction up to about 1 kHz. This behavior is most likely caused by contributions from other broadband ABN sources within the vehicle, such as the battery cooling system.

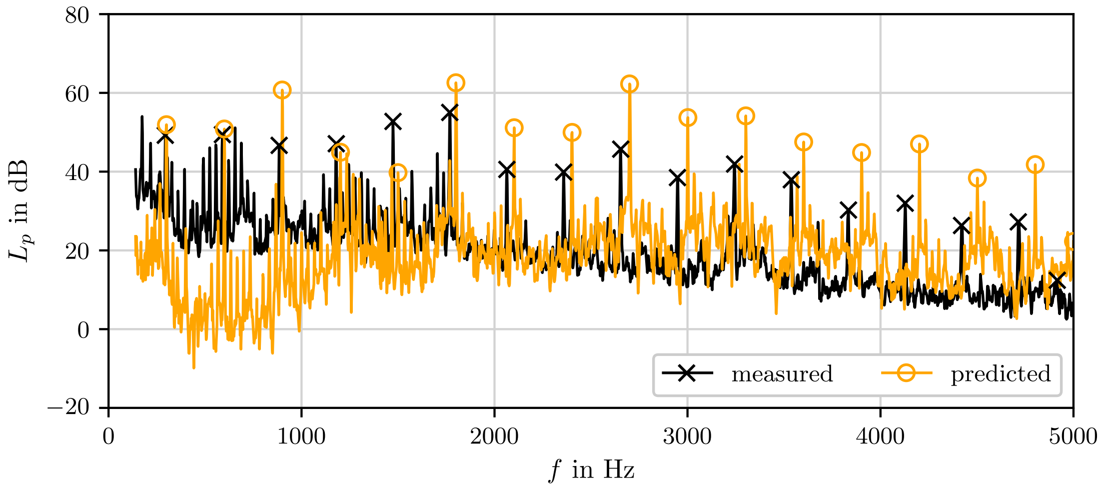

Figure 5.27: Comparison of the predicted and measured SPL at the ABN receiver in the excavator at the stationary operating point: n = 2000 rpm, p_{H} = 200 bar, $V_d = V_{d,\mathrm{max}}$

It is evident that the measured ABN level is dominated by harmonic components below 2 kHz, which further supports the previously defined upper limit of the considered frequency range. Within this range, the prediction agrees very well with the measurement at some harmonics, while deviations of up to approximately 15 dB occur at others. Consequently, a robust validation is not possible in case of the ABN receiver. In addition to the differing excitation characteristics between the excavator measurements and the test rig measurements, further factors may contribute to the observed discrepancies. These include the influence of other noise sources as well as direct ABN radiation from the pump housing. Moreover, errors in the VPT or insufficient quality of the FRFs due to inadequate SNR can also affect the results.

Overall, it can be concluded that the validation of the receiver-dependent assessment approach was not fully successful, especially for the ABN in the driver's cabin. This is primarily due to various disturbances and error sources that are inherently associated with measurements in mobile working machines. Key challenges include limited accessibility to the interface, the suppression of other noise sources, and the ability to ensure comparable operating conditions. The direct mechanical coupling between the pump and the electric

motor leads to significantly different boundary conditions compared to the test rig, which further limits the comparability of the results. Therefore, for measurements in electrified mobile working machines, a more appropriate source definition is likely the combined electric motor and pump assembly, treating both components jointly as the source.
In this case, the SBN interface would be located at the mechanical mounting points of the electric motor, either upstream or downstream of the isolator elements. For the investigated electrified excavator, the motor mounting points were significantly more accessible, and in-plane excitation using a shaker would likely be easier to realize. This interface also corresponds to that of a classically resiliently mounted SBN source, which has been investigated in numerous studies in the field of TPA [102]–[106]. At the same time, this approach offers the potential to optimize the isolator elements based on the observed dynamic behavior.
Based on the presented results, it can therefore be concluded that the transferability of the blocked loads of the axial piston pump from the test rig to a mobile working machine is not given. For a cTPA conducted within a mobile working machine, the combined motor-pump assembly is likely the more suitable source definition.

5.3 Comparison of the Assessment Metrics for a Run-Up

In the previous sections, several assessment metrics were introduced. For the load-based metrics, it was shown that they can be determined reliably using the developed test rig setup. In contrast, for the determination of the receiver-independent Characteristic Power, it became apparent that the estimation of the free velocities is particularly error-prone. Consequently, the results of the Characteristic Power can only be analyzed qualitatively.
For the receiver-dependent assessment metrics, which essentially represent a prediction of the noise at a specific receiver point, it was found that these could not be determined reliably under operating conditions in the application due to various disturbances. Thus, the predictions at the receiver points do not constitute a robust assessment metric. However, the results of the receiver-dependent metrics provide valuable insight into how receiver-dependent and receiver-independent assessment metrics differ in their characteristics.
For this reason, this section compares the results of all assessment metrics for a speed run-up. As the receiver-dependent assessment metric, the A-weighted SPL of the predicted cabin noise is used. This represents a highly application-relevant metric and also allows the human perception of sound to be considered in a straightforward manner. As already noted, this value cannot be regarded as an accurate noise prediction for the excavator. Instead, it serves to provide a qualitative impression of how the characteristics of a receiver-dependent assessment metric differ from those of receiver-independent metrics.
Figure 5.28 shows the four different assessment metrics for the same speed run-up as presented in Section 5.1.4. As in that section, the spectra of the load-based quantities were condensed using RMS values, while the Characteristic Power was obtained by summing all spectral contributions. For the calculation of the overall A-weighted SPL, the individual sound pressure spectra were first A-weighted and then combined using the RMS value. For all assessment metrics, a frequency range from 140 to 2000 Hz was considered.

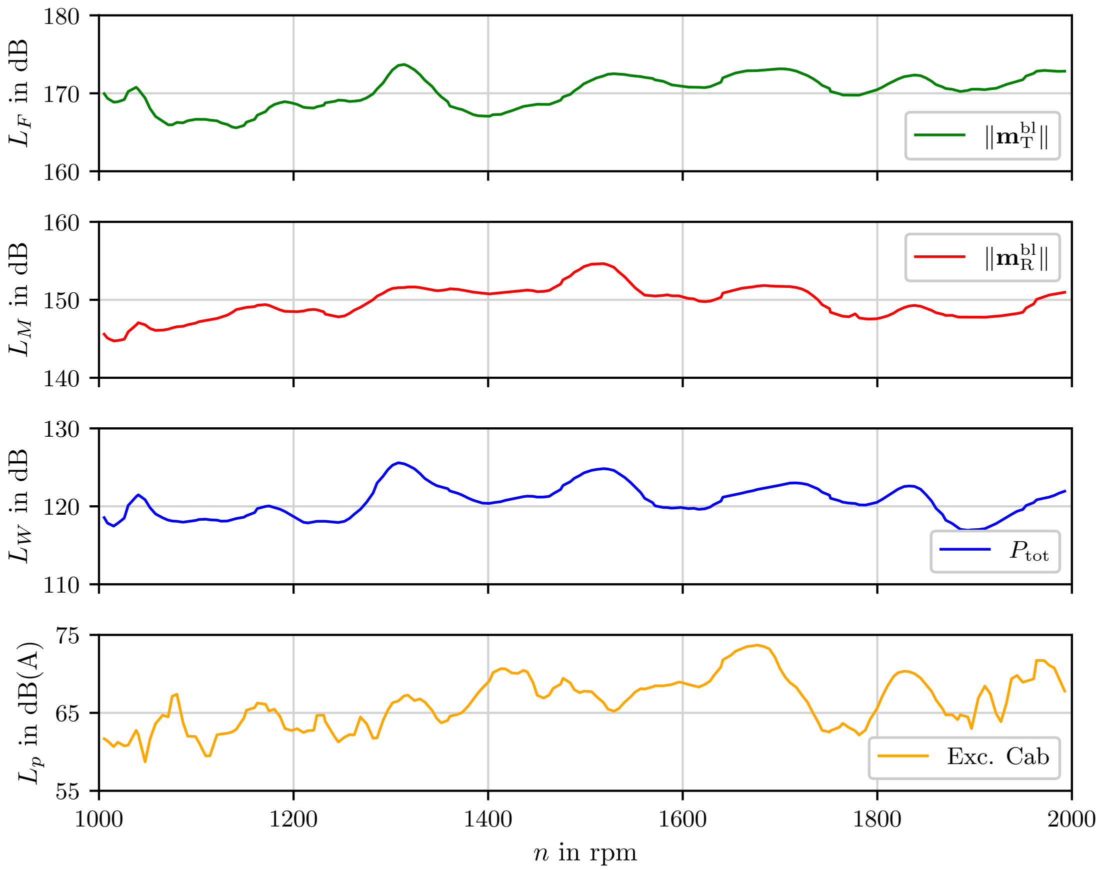

Figure 5.28: Comparison of the different assessment metrics for a speed run-up with $p_{\mathrm{H}} = 200$ bar, $V_d = V_{d,\mathrm{max}}$

A comparison of the source-specific assessment metrics shows that the Characteristic Power essentially combines the two load-based metrics. Local maxima of the Characteristic Power occur when either the blocked-force-based or the blocked-torque-based metric exhibits a local maximum. In contrast, when comparing these trends with that of the receiver-dependent metric L_p, it becomes evident that the predicted noise inside the excavator cabin exhibits a markedly different behavior. First, the noise level fluctuates much more, resulting in a higher number of local extrema. Second, no direct correlation with any of the source-specific metrics can be identified. It is important to note that identical blocked loads and blocked torques were used for the calculation of the SPL as for the other metrics. Consequently, the observed differences mainly originate from the transfer behavior between the pump interface and the microphone in the operator cabin. This observation clearly demonstrates that the transfer behavior has a major influence on the pump noise perceived in the cabin. Peaks in the predicted cabin noise do not necessarily occur where the excitation generated by the pump is strongest, but rather where the transfer path exhibits particularly effective transmission.
This effect can also be illustrated by a brief sensitivity analysis with respect to the excitation DoF. In Section 5.1.4, for the source-specific metrics it was shown that the force in

the y-direction represents the dominant excitation DoF. Figure 5.29 illustrates how the individual assessment metrics change when this force component is synthetically reduced by 10 dB. It can be observed that both the load-based force metric and the Characteristic Power are significantly reduced over nearly the entire speed range. In contrast, the predicted cabin noise is only noticeably reduced in the speed range immediately after 1000 rpm and between approximately 1900 rpm and 2000 rpm. This indicates that even if this DoF is dominant in the SBN excitation, it does not significantly influence the predicted cabin SPL because this excitation is not effectively transferred to the cabin.

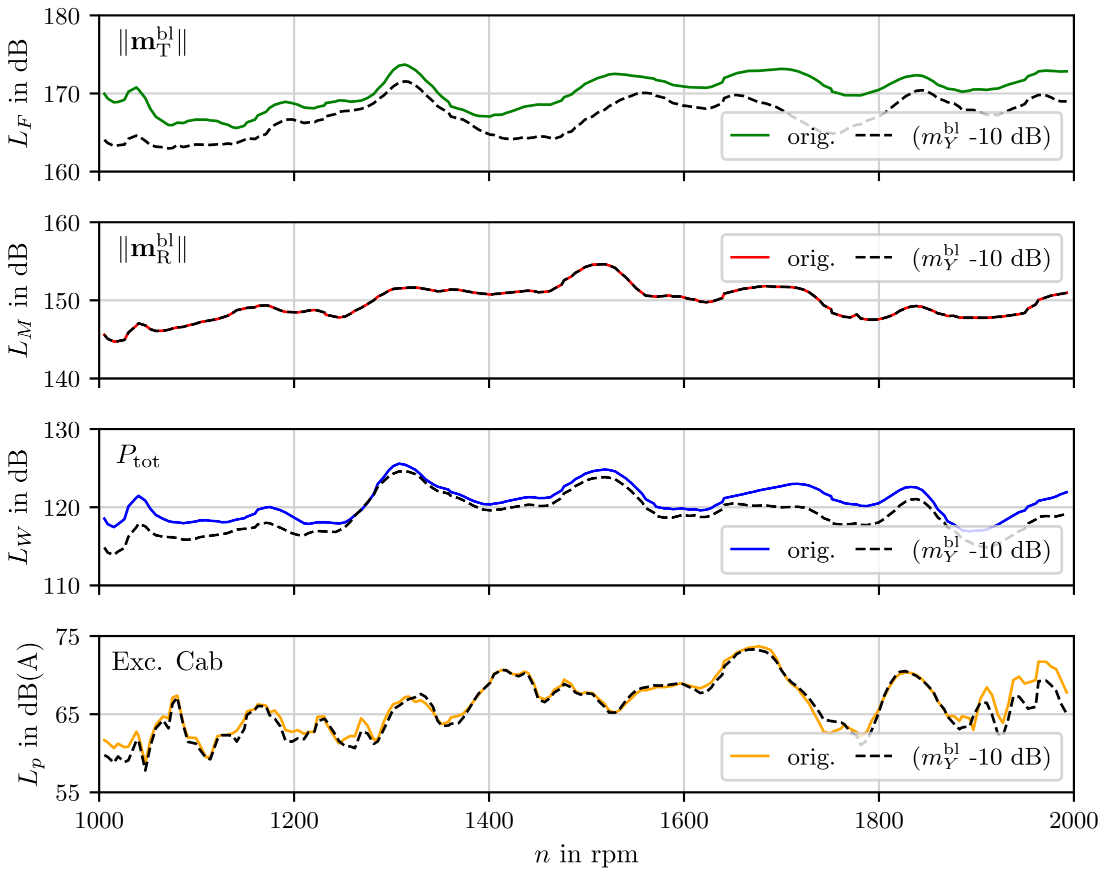

Figure 5.29: Influence of m_Y^bl on the assessment metrics during a speed run-up with p_H = 200 bar, $V_d = V_{d,\max}$

Applying the same procedure to the axial torque in the z-direction yields the trends shown in Figure 5.30. In contrast to the previous case, the reduction of this torque component similarly affects all metrics except the force-based metric. Within the speed range of approximately 1400 rpm to 1700 rpm, a clear reduction in these metrics is recognized, which shows that reducing the axial torque in this speed range would also effectively reduce the predicted cabin noise.

From these two exemplary results, it becomes evident that for optimal acoustical performance of an axial piston pump within a mobile working machine, both the excitation of the pump and the transfer behavior of the vehicle must be considered.

Beyond identifying the influence of individual excitation DoF, the sensitivity analysis clearly highlights the potential offered by the introduced assessment metrics. A modification of the SBN excitation, as artificially applied in the sensitivity analysis, can correspond to a practical noise mitigation measure. Using the proposed assessment metrics, it is possible to evaluate how such a measure affects the SBN excitation. Conversely, even prior to developing a concrete mitigation measure, the metrics can be used to assess which type of modification is likely to be most effective, for example whether a measure should primarily influence the force component in the y-direction or reduce the torque component in the z-direction.
This becomes particularly powerful when the transfer behavior of the receiver is known, as measures can then be specifically developed to reduce the noise within an application. Furthermore, this knowledge enables an evaluation of how the receiver's structural behavior could be modified to achieve noise reduction. However, information about the receiver is often not available during pump development. In such cases, the introduced source-specific assessment metrics represent a suitable and practical tool for the assessment of SBN excitation by the pump.

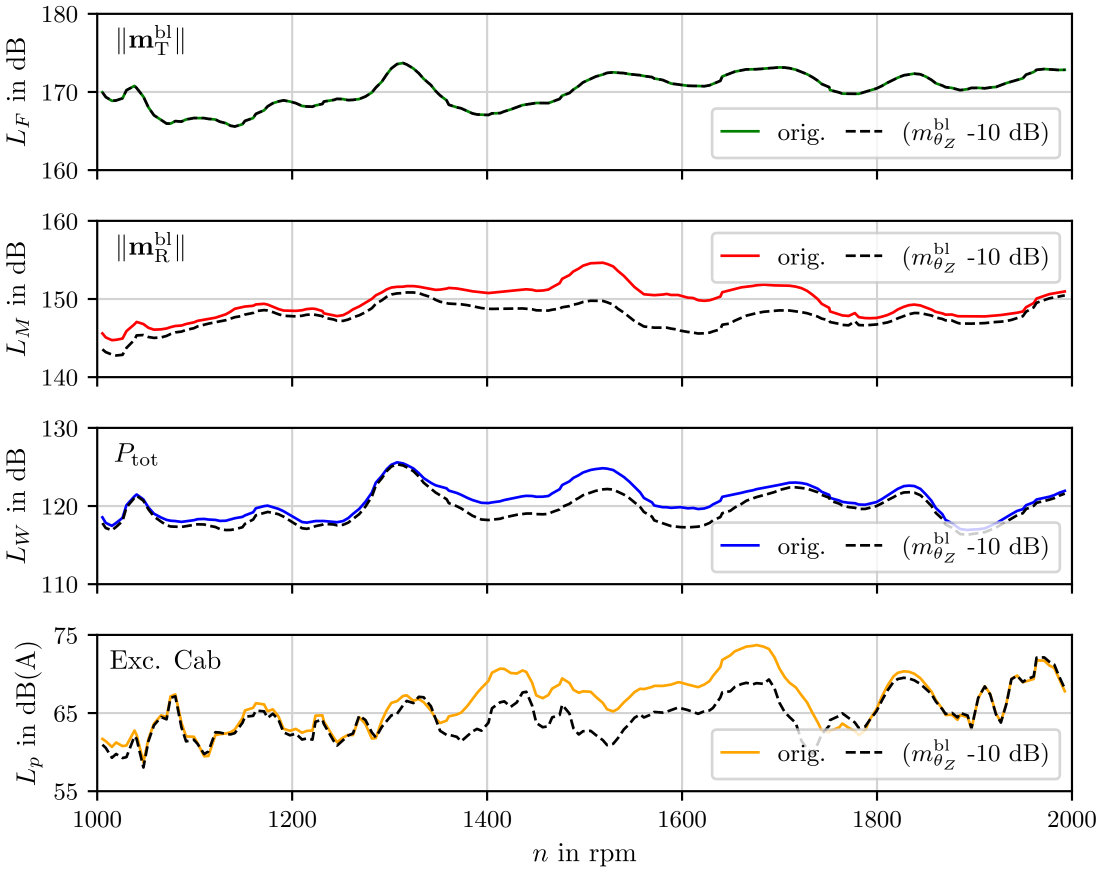

Figure 5.30: Influence of $m_{\theta_Z}^{\mathrm{bl}}$ on the assessment metrics during a speed run-up with $p_{\mathrm{H}} = 200$ bar, $V_d = V_{d,\max}$

5.4 Discussion

As a conclusion of this chapter, the advantages and limitations of the introduced assessment metrics are discussed based on the presented results, with particular emphasis on their practicality, robustness, and explanatory capability.

Source-Specific Assessment Using Aggregated Blocked Loads
The derivation of the load-based evaluation metrics relies on the reliable determination of blocked loads in VP coordinates at the test rig. Based on the applied quality criteria for the In Situ Blocked Force method and the VPT, the results indicate that the blocked loads in VP coordinates can be determined with a high degree of reliability at the test rig up to frequencies of approximately 1.2 kHz under operating conditions. The increased deviations observed in the transferability analysis at higher frequencies—used here as an indicator of receiver independence—are likely attributable to variations in operating conditions rather than to an insufficient characterization of the source by the blocked loads. This interpretation is supported by the observation that, under artificial excitation of the pump housing, good transferability is maintained up to approximately 2.5 kHz.
The comparison of different interface definitions, namely single-VP and dual-VP configurations, suggests that a single VP located at the center of the interface is sufficient to describe the SBN excitation of the investigated axial piston pump in its assembled state at the test rig. In this configuration, the pump SBN excitation can be described in a compact and physically intuitive manner using the six excitation DoF of a single VP. These DoF can subsequently be reduced by means of vector norms to one resultant force quantity and one resultant torque quantity, which form the two load-based evaluation metrics. The analysis of these metrics for two different test rig configurations, both under steady-state operating conditions and during a speed ramp, indicates that they constitute robust and largely receiver-independent measures for assessing the SBN excitation of the investigated axial piston pump. Within the scope of the present investigation, a frequency range of approximately 140 to 2000 Hz was identified as the range in which the dominant SBN excitation can be reliably assessed using these metrics.
The application of these load-based metrics offers several notable advantages. In particular, they can be determined with comparatively high accuracy and robustness. This is primarily due to the fact that only the determination of blocked loads in VP coordinates at the test rig using the In Situ Blocked Force method is required, without the need for additional experimental measurements. Measurements at the test rig are advantageous, as they provide good accessibility to the interface, well-defined geometric properties of the receiver in the interface region, and a high level of control over the operating conditions. Consequently, the blocked loads of the axial piston pump can be determined with high measurement quality. Given the comparatively low experimental effort required to obtain the two load-based metrics, this approach can be regarded as highly practical. This practicality is further supported by the standardization of the In Situ Blocked Force method in ISO 20270-1:2019, which provides an established framework for blocked force determination.

A limitation of this assessment approach is that it yields two metrics based on physically different units which cannot be directly compared. The results of this study indicate that, for the investigated axial piston pump, both translational force excitation and rotational torque excitation contribute significantly to the overall SBN excitation. Accordingly, both metrics must be considered when assessing the excitation characteristics.

Source-Specific Assessment Using Characteristic Power
In contrast, the power-based evaluation approach using the Characteristic Power allows translational and rotational contributions to be compared directly and combined into a single assessment quantity. From a theoretical standpoint, this represents a convenient source-specific evaluation metric. However, the determination of the Characteristic Power requires not only the blocked loads but also the free velocities of the pump. Since these velocities cannot be measured directly during operation, they were derived in this work from the blocked loads and the point admittance of the pump. The latter had to be determined through an extensive FRF measurement under freely suspended conditions.
The results indicate that the experimental determination of the point admittance is both time-consuming and prone to uncertainties. The pump, including the connected hoses, must be suspended freely, and sensors as well as excitation points must be positioned within the limited space available at the interface. Furthermore, investigations based on artificial excitation of the pump housing suggest that the estimation of free velocities from blocked loads and point mobilities is particularly sensitive to errors. A likely contributing factor is the difference in dynamic behavior between the pump in the freely suspended condition and in the coupled state. This observation further emphasizes the benefit of in situ source characterization in the coupled condition, as coupling effects influencing the source behavior are implicitly taken into account. In addition, it was found that the transformation of sensor signals into VP coordinates for point mobility determination is only reliable up to approximately 1 kHz. In this respect, the load-based metrics offer a clear advantage, as only the forces—rather than the forces and sensor signals—must be transformed into VP coordinates, thereby eliminating an additional potential source of uncertainty.
Overall, the results suggest that while the Characteristic Power constitutes a theoretically attractive assessment quantity, its practical determination is associated with considerable experimental effort and sensitivity to uncertainties. Consequently, this method cannot be considered robust or practical within the scope of the present study. Nevertheless, its determination allowed a qualitative estimation indicating that both translational and rotational excitation components are of comparable relevance for the investigated axial piston pump.

Receiver-Dependent Assessment
Finally, an assessment approach based on a receiver-dependent metric was investigated, using the SPL in the cabin of an electrified excavator as the target quantity. Strictly speaking, this approach does not directly evaluate the SBN excitation itself, but rather its effect within a specific receiver. In this approach, the receiver-independent blocked loads determined at the test rig are virtually coupled with a separately identified receiver

behavior, enabling a virtual prediction of the receiver response to the source excitation. Such an approach appears particularly promising in later development stages of mobile machinery, as it allows source and receiver characteristics to be jointly optimized with respect to the overall acoustic behavior of the machine.
However, for the approach implemented in this work—where the receiver behavior, i.e., the transfer behavior from the pump interface to a microphone in the excavator cabin, was determined experimentally—several practical challenges became evident. Due to the presence of multiple disturbance and error sources, as well as general practical challenges, a satisfactory agreement between the predicted and the measured cabin noise levels could not be achieved. Consequently, this evaluation approach could not be validated and must be regarded as having limited practicality for axial piston pumps in its current form. Nevertheless, the results demonstrate that both the receiver behavior and the excitation characteristics have a significant influence on the resulting SBN impact at the receiver. A brief artificial sensitivity analysis further provided a theoretical outlook on how a targeted acoustic optimization could be performed using a virtual source-receiver representation. Thus, while this approach can be considered theoretically powerful for the acoustic optimization of systems equipped with hydraulic pumps, it cannot be regarded as practical or robust in the form investigated here.
Within the scope of this study, it was observed that the experimental determination of receiver behavior in mobile machinery is strongly affected by other noise sources within the system. In particular, the direct coupling between the pump and the electric drive motor challenges the assumption of receiver passivity. Therefore, especially for electrified machines, defining the electric motor-pump assembly as a single source, with interfaces located at vibration-isolated mounting points of the motor, appears to be a more appropriate source definition. Moreover, the determination of the transfer behavior from the pump interface to the ABN in the vehicle cabin is subject to increased uncertainty due to the long transmission path and the presence of decoupling elements. A critical challenge in the experimental characterization of receiver behavior is therefore the provision of sufficiently strong excitation that can be applied within the severely constrained space around the interface. An alternative approach would be to represent the passive receiver behavior numerically, thereby eliminating this limitation. In such a case, restricted interface accessibility within the mobile working machine and additional disturbance sources would also no longer pose significant obstacles. Especially the second aspect represents a major advantage. In a mobile working machine, the hydraulic pump is typically directly coupled to other SBN sources such as a drive motor or a gearbox, which makes it difficult to experimentally separate the contribution of the hydraulic pump itself. The combination of the blocked forces measured on the test bench with the numerical model of the mobile working machine enables an isolated assessment of the hydraulic pump noise contribution. Moreover, this approach is particularly attractive within the development process of a mobile working machine, as it allows the SBN propagation of a pump to be investigated in advance by simulation, enabling structural optimizations of the machine already during the design phase.

In summary, among the assessment approaches investigated in this work, the blocked load-based approach emerges as the most practical and robust method for assessing the SBN excitation of the investigated axial piston pump. The remaining approaches, based on characteristic power and predicted receiver noise, are theoretically promising. However, uncertainties in their experimental determination currently limit their practical applicability, particularly with respect to accuracy and robustness.

6 Conclusion and Outlook

6.1 Summary

The objective of this thesis was to introduce different approaches for the assessment of SBN excitation of axial piston pumps and to assess their practical applicability. This work is primarily motivated by the continuously increasing acoustic requirements for hydraulic pumps. In particular, within the context of the electrification of mobile working machines, these requirements become more stringent, as the hydraulic system is perceived as the dominant noise source due to the absence of masking noise from internal combustion engines. While FBN and ABN of hydraulic pumps can already be evaluated in a standardized and comparable manner, no such established methods currently exist for the specific assessment of SBN excitation of hydraulic pumps.

For this reason, the second chapter first reviewed the state of the research. In addition to general approaches for the characterization of SBN sources, an overview of established methods for the characterization of FBN and ABN of hydraulic pumps was provided. This review clearly shows that previous research on hydraulic pumps has focused predominantly on the characterization of ABN and FBN, resulting in well-established and robust assessment methods. In contrast, the characterization of SBN excitation of hydraulic pumps has received relatively little attention to date. However, a comparison with general SBN source characterization approaches reveals significant similarities to the established FBN characterization methods used for hydraulic pumps.

Based on this, the third chapter introduced the theoretical foundations of SBN source characterization, which form the basis for the assessment metrics used in this thesis. Of particular importance was the introduction of the In Situ Blocked Force TPA and its associated quality criteria, as the determination of receiver-independent blocked forces constitutes the foundation of all evaluation approaches presented. To ensure a distinct interface description—an essential requirement for SBN source characterization—the VPT was introduced, enabling the projection of interface quantities onto one or more clearly defined interface points. The final part of this chapter presented power-based approaches for SBN characterization, highlighting in particular the strong influence of the receiver system on the transmitted SBN power. Nevertheless, approaches from the literature were discussed that allow for the estimation of receiver-independent power quantities.

Subsequently, two source-specific and one receiver-dependent assessment approaches were introduced. In the first source-specific approach, the SBN excitation of the pump is condensed into one receiver-independent force and one torque quantity, resulting in an evaluation approach based on two metrics. The second, power-based assessment approach further reduces the SBN excitation to a single source-specific metric, namely the

Characteristic Power. In the final assessment approach, the receiver-independent blocked loads of the source are used to predict the interior noise in the cabin of an electrified excavator. This predicted cabin noise represents a practically relevant evaluation metric and inherently depends on the excavator's structural dynamic behavior, which clearly makes this approach receiver-dependent.
In the results chapter, the introduced evaluation metrics were determined for the investigated axial piston pump and assessed with respect to their practicality, robustness, and explanatory capability using various validation approaches. A substantial part of this chapter was dedicated to the presentation of the experimental setups required to obtain the necessary quantities. For the determination of the blocked loads, a specially developed test rig was used to implement the In Situ Blocked Force TPA in accordance with ISO 20270-1:2019 for an axial piston pump. The determination of the Characteristic Power additionally required a measurement setup for the identification of the free velocities, and the prediction of the excavator cabin noise necessitated an extensive measurement of the transfer behavior within the excavator.
Based on the results obtained from the three evaluation metrics, it can be concluded that, within the scope of this thesis, the first load-based assessment approach provides a practical and robust assessment of the SBN excitation by the investigated axial piston pump. This approach enables a reliable assessment of the dominant SBN excitation up to approximately 2 kHz. The analysis using these evaluation metrics is particularly powerful during a speed run-up of the pump, where critical operating points and excitation DoF can be identified. Although the other introduced assessment metrics are theoretically highly potent, their experimental determination is significantly more challenging and prone to uncertainties, which currently limits their suitability for robust quantitative evaluation in the investigated form. Nevertheless, their application provided valuable insights despite the associated uncertainties. The Characteristic Power analysis indicated that both translational and rotational excitation components of the pump are relevant, while the investigation of the cabin noise clearly highlighted the influence of the receiver system on the resulting noise within an application.

6.2 Scientific Contribution

In order to evaluate the scientific contribution of this thesis, the research questions formulated in Section 2.3 are addressed in the following.

Is the In Situ Blocked Force method according to ISO 20270-1:2019 suitable for experimentally characterizing the structure-borne noise excitation by an axial piston pump?

The experimental implementation of the method on a dedicated test rig, as well as the analysis of the associated quality criteria, were presented in detail in Section 5.1.1. It was shown that, using the developed test setup, the blocked loads of the axial piston pump could be determined robustly under operating conditions. The results of the OBV, which

represents a key validation procedure within ISO 20270-1:2019, demonstrate very good agreement between the response predicted using the blocked loads and the corresponding reference measurements up to approximately 2.5 kHz. In addition, a Transferability Validation was conducted, which is currently not part of ISO 20270-1:2019. This validation indicates that the receiver-independence of the blocked loads under operating conditions is well fulfilled up to approximately 1.2 kHz. The larger deviations at higher frequencies may be attributed to differing operating conditions between prediction and reference measurement, since within this validation approach the reference cannot be the exact same operating measurement, but rather a different measurement under operating conditions that are as similar as possible.
Overall, it can therefore be concluded that the In Situ Blocked Force method is suitable for characterizing the SBN excitation of an axial piston pump. At the same time, it must be emphasized that the successful application of the method strongly depends on the favorable boundary conditions provided by the test bench. These include good accessibility of the interface, well-defined geometric properties of the receiver in the interface region, and a high degree of controllability of the operating conditions.
In contrast, the application of the method to an axial piston pump installed in a mobile working machine is considerably more challenging, as these conditions are typically not fulfilled. In particular, the direct coupling to the drive motor often violates the passivity requirement of the receiver system, which represents a fundamental assumption of the method and thus limits its applicability. Consequently, the In Situ Blocked Force method according to ISO 20270-1:2019 is particularly well suited for laboratory-based investigations on dedicated test rigs, whereas its direct application under real operating conditions in mobile working machines is significantly more challenging.

What is an appropriate interface definition for describing the structure-borne noise excitation by an axial piston pump?

Within the scope of this thesis, two interface definitions that appear reasonable for the mounting geometry of the investigated axial piston pumps were introduced in Section 4.1 and subsequently compared in various analyzes presented in Chapter 5. The first interface definition, referred to as the single-VP configuration, uses one VP located at the center of the interface and describes the SBN excitation by six excitation DoF. The second definition, the dual-VP configuration, employs two VPs, each located at one of the mounting points of the two-bolt pump flange. The results of multiple analyzes show that the extended interface description using two VPs does not provide a significant advantage over the single-VP configuration. Consequently, the increased complexity of the dual-VP approach is not justified for the investigated axial piston pump. In addition, the single-VP configuration offers several advantages:

- The description of the SBN excitation using the six DoF of a single VP is intuitive and facilitates straightforward physical interpretation.

- A single VP located at the center of the source can be defined distinctly for common hydraulic pumps, independent of the number of mounting points or the specific geometry of the mounting flange.
- The determination of the introduced source-specific metrics is significantly simplified, as there is no need to distinguish between quantities at spatially different positions, which considerably simplifies their aggregation.

For these reasons, the description of the SBN excitation using a single central VP is identified as a suitable interface definition for the investigated axial piston pump. Based on the results obtained in this thesis, no general statement can be made for hydraulic pumps with substantially different dimensions or design characteristics. However, since the mounting flanges of hydraulic pumps are standardized according to ISO 3019-1:2001 and thus exhibit comparable interface properties, it is expected that a single VP representation constitutes an appropriate interface description for a wide range of hydraulic pumps, particularly in view of the advantages outlined above.

How can the structure-borne noise excitation by an axial piston pump, described using multiple interface quantities, be summarized into a straightforward assessment metric?

To address this research question, the three assessment approaches introduced in Chapter 4 were investigated. In the first source-specific approach, the blocked loads expressed in VP coordinates are aggregated into one receiver-independent force metric and one receiver-independent torque metric. In the second source-specific approach, the evaluation is further condensed into a single power-based metric, which requires the additional experimental determination of the free velocities of the pump. In the introduced receiver-dependent approach, the source description based on blocked loads is used to predict the noise in the cabin of an excavator resulting from the SBN excitation of the pump. In this case, the multi-dimensional excitation is condensed into a single microphone signal.
From a theoretical perspective, all three approaches are suitable for assessing SBN excitation. However, the first evaluation approach, based on receiver-independent force and torque metrics, proved to be particularly robust and practical for the investigated axial piston pump. This is mainly due to the fact that this approach relies exclusively on the blocked loads and blocked torques, which can be determined reliably on the dedicated test bench. In contrast, the other two assessment approaches rely on additional experimentally determined quantities that are subject to significantly higher uncertainties. As a result, these two approaches are less robust and limited in their suitability for reliable quantitative assessment in the investigated form. Nevertheless, their determination has yielded important insights for the analysis of SBN excitation by axial piston pumps.

6.3 Future Research

Based on the investigations conducted within the scope of this thesis and the presented results, the following topics can be identified as promising directions for future research:

- *Characterization of SBN excitation at the hydraulic line interfaces of a hydraulic pump*
  In this thesis, only the SBN interface at the mounting flange of the pump was considered, while the interfaces at the suction and discharge ports of the hydraulic pump were neglected. In practical applications, particularly when the pump is connected to the hydraulic system via rigid pipes, it can be expected that SBN is also transmitted to the receiver system through these interfaces. Future investigations could therefore examine the relevance of these additional transmission paths and, if necessary, develop suitable methods for their characterization. This task is particularly challenging because, in addition to SBN transmitted through the mechanical interface, hydraulic lines are also excited by pressure pulsations, which subsequently lead to SBN. A clear separation of these excitation mechanisms would therefore be required.
- *Validation of pump models using blocked loads*
  As discussed at the beginning of this thesis, accurately modeling the internal noise excitation mechanisms of a SBN source, such as a hydraulic pump, remains a significant challenge. Consequently, source characterization is often performed experimentally, for example using the In Situ Blocked Force method. As demonstrated by the results of this thesis, the blocked loads of the investigated axial piston pump can be determined robustly on the developed test bench. These receiver-independent blocked loads could therefore serve as reference quantities for the validation of numerical pump models aimed at simulating SBN excitation. Such validated models would enable a more efficient investigation of noise mitigation measures already in early stages of the pump development process. A particularly interesting research question would be whether existing pump models for noise excitation are capable of accurately predicting the blocked loads.
- *Integration of measured blocked loads into numerical simulation models of mobile working machines*
  The investigations presented in this thesis show that the experimental determination of the receiver behavior of a mobile working machine is, for several reasons, highly challenging and prone to uncertainties. A promising alternative is the use of numerical structural-dynamic simulation models to represent the mobile working machine. In contrast to source modeling, only the passive properties of the receiver need to be represented in such models. From a technical perspective, the numerical modeling of mobile working machines is already feasible. It therefore represents an interesting research direction to investigate whether the combination of experimentally measured receiver-independent blocked loads and a numerical simulation model of the machine enables accurate prediction of the resulting noise radiation. Such an approach could significantly improve the efficiency of acoustic optimization processes for mobile working machines.

- *SBN characterization of an electric motor-pump assembly*
  As mentioned in the discussion section of the results chapter, the experimental investigation of the electrified excavator indicated that, for electrified mobile working machines, the electric motor-pump assembly, with an interface defined at the mounting points of the electric motor, may represent a more appropriate source definition. While the SBN characterization of electric motors has already been addressed in previous research and therefore does not constitute a fundamentally new research field, it would nevertheless be of considerable interest to investigate whether a robust virtual source-receiver model of a mobile working machine can be established based on such a combined source definition.

- *SBN characterization of an entire hydraulic system in a mobile working machine*
  An even more challenging task than the characterization of an electric motor-pump assembly—and therefore clearly a topic for future research—is the SBN characterization of an entire hydraulic system in a mobile working machine. A hydraulic system consisting of pumps, valves, actuators, and additional components is coupled to the machine structure at multiple locations. Vibrations in these components are often induced by fluid pulsations and subsequently lead to SBN that is transmitted to the machine structure via their mounting interfaces. A potential future research approach would therefore be to characterize the SBN excitation at all mounting interfaces of the hydraulic system using blocked loads, with the aim of determining the overall SBN excitation of a hydraulic system in a mobile working machine.

List of Figures

List of Tables

Bibliography

[1] European Commission, "The European Green Deal", European Commission, Brussels, Belgium, Communication from the Commission COM(2019) 640 final, 2019.

[2] L. Schmidt and A. H. Hansen, "Estimating the global emission impact of mobile & industrial hydraulic machinery", AAU Energy, Aalborg University, Aalborg, Denmark, Technical Report, 2024.

[3] M. Geimer, Ed., *Mobile Working Machines*, SAE International, Dec. 31, 2020, ISBN: 978-0-7680-9432-9. DOI: 10.4271/9780768094329.

[4] T. Pietrzyk *et al.*, "Psychoacoustic evaluation of hydraulic pumps", *Sustainability*, vol. 13, no. 13, Jun. 30, 2021, article-number: 7320, ISSN: 2071-1050. DOI: 10.3390/su13137320.

[5] L. Danes and A. Vacca, "A tandem axial-piston unit based strategy for the reduction of noise sources in hydraulic systems", *Energies*, vol. 13, no. 20, Oct. 15, 2020, article-number: 5377, ISSN: 1996-1073. DOI: 10.3390/en13205377.

[6] M. Lenz, P. Zuppke, and J. Weber, "Particle dampers for pump noise mitigation: Experimental investigation of the effects on airborne and structure-borne noise and sound perception on an axial piston pump", in *Proceedings of 19th Scandinavian International Conference on Fluid Power, SICFP'25*, Linköping, Sweden, 2025, pp. 312–331. DOI: 10.13052/rp-9788743808251A22.

[7] T. Heeger and L. Ericson, "Simulation study on harmonic torque injection for suppressing flow pulsations in electrified axial piston pumps", in *Proceedings of 19th Scandinavian International Conference on Fluid Power, SICFP'25*, Linköping, Sweden, 2025, pp. 130–141. DOI: 10.13052/rp-9788743808251A13.

[8] W. Fiebig, "Schwingungs- und Geräuschverhalten der Verdrängerpumpen und hydraulischen Systeme: Vorgehensweise, Massnahmen und Potential zur Geräuschminderung", VDI Verlag, Düsseldorf, Germany, Fortschritt-Berichte VDI, Nr. 337, 2008.

[9] R. Klop, "Investigation of hydraulic transmission noise sources", Ph.D. dissertation, Purdue University, West Lafayette, IN, USA, 2010.

[10] R. Klop and M. Ivantysynova, "Investigation of noise sources on a series hybrid transmission", *International Journal of Fluid Power*, vol. 12, no. 3, pp. 17–30, Jan. 2011, ISSN: 1439-9776. DOI: 10.1080/14399776.2011.10781034.

[11] A. Waitschat *et al.*, "Enhanced toolbox for the combined analysis of fluid- and structure-borne noise of hydraulic systems", in *Proceedings of BATH/ASME 2016 Symposium on Fluid Power and Motion Control*, Bath, UK: American Society of Mechanical Engineers, Sep. 7, 2016, ISBN: 978-0-7918-5006-0. DOI: 10.1115/FPMC2016-1701.

[12] T. Opperwall and A. Vacca, "A transfer path approach for experimentally determining the noise impact of hydraulic components", in *Proceedings of SAE 2015 Commercial Vehicle Engineering Congress*, West Lafayette, IN, USA, 2015. DOI: 10.4271/2015-01-2854.

[13] H. Theissen, "Volumenstrompulsation von Kolbenpumpen", *Ölhydraulik und Pneumatik*, vol. 24, no. 5, 1980.

[14] T. Nafz, "Aktive Ventilumsteuerung von Axialkolbenpumpen zur Geräuschreduktion hydraulischer Anlagen", ISBN: 978-3-8440-0511-0, Ph.D. dissertation, RWTH Aachen, Aachen, Germany, 2011.

[15] K. A. Edge and T. J. Wing, "The measurement of the fluid borne pressure ripple characteristics of hydraulic components", *Proceedings of the Institution of Mechanical Engineers, Part B: Management and engineering manufacture*, vol. 197, no. 4, pp. 247–254, Nov. 1983, ISSN: 0263-7146. DOI: 10.1243/PIME_PROC_1983_197_066_02.

[16] U. Heisel and J. Rothmund, "Verfahren zur Messung der Druckpulsation von Verdrängerpumpen", *Fluidtechnik*, 1989. DOI: 10.18419/opus-4249.

[17] D. N. Johnston and J. E. Drew, "Measurement of positive displacement pump flow ripple and impedance", *Proceedings of the Institution of Mechanical Engineers, Part I: Journal of Systems and Control Engineering*, vol. 210, no. 1, pp. 65–74, Feb. 1996, ISSN: 0959-6518, 2041-3041. DOI: 10.1243/PIME_PROC_1996_210_437_02.

[18] E. Kojima, J. Yu, and T. Ichiyanagi, "Experimental determining and theoretical predicting of source flow ripple generated by fluid power piston pumps", in *Proceedings of International Off-Highway and Powerplant Congress and Exposition*, Milwaukee, WI, USA, Sep. 11, 2000. DOI: 10.4271/2000-01-2617.

[19] B. Müller and H. Baum, "Impedance measurement in a hydrostatic drive", in *Proceedings of 12th International Fluid Power Conference*, Dresden, Germany: Technische Universität Dresden, Jun. 25, 2020, pp. 513–522. DOI: 10.25368/2020.58.

[20] D. N. Johnston, "Measurement and prediction of the fluid borne noise characteristics of hydraulic components and systems", Ph.D. dissertation, University of Bath, Bath, United Kingdom, 1987.

[21] International Organization for Standardization, *ISO 10767-2:1999 Hydraulic fluid power – Determination of pressure ripple levels generated in systems and components – Part 2: Simplified method for pumps*, 1999.

[22] International Organization for Standardization, *ISO 10767-1:2015 Hydraulic fluid power – Determination of pressure ripple levels generated in systems and components – Part 1: Method for determining source flow ripple and source impedance of pumps*, 2015.

[23] K. A. Edge and D. N. Johnston, "The 'secondary source' method for the measurement of pump pressure ripple characteristics part 1: Description of method", *Proceedings of the Institution of Mechanical Engineers, Part A: Journal of Power and Energy*, vol. 204, no. 1, pp. 33–40, Feb. 1990, ISSN: 0957-6509, 2041-2967. DOI: 10.1243/PIME_PROC_1990_204_006_02.

[24] K. A. Edge, "The 'secondary source' method for the measurement of pump pressure ripple characteristics part 2: Experimental results", *Proceedings of the Institution of Mechanical Engineers, Part A: Journal of Power and Energy*, vol. 204, no. 1, pp. 41–46, Feb. 1990, ISSN: 0957-6509, 2041-2967. DOI: 10.1243/PIME_PROC_1990_204_007_02.

[25] K. Weddfelt, "Measurement of pump source characteristics by the two-microphone method", in *Proceedings of The Second Tampere International Conference on Fluid Power*, Tampere, Finland, 1991.

[26] E. Kojima, "A new method for the experimental determination of pump fluid-borne noise characteristics", in *Proceedings of 5th Bath International Fluid Power Workshop, Circuit, Component and System Design*, Bath, England, 1992, pp. 111–135.

[27] S. Choi, I. Lee, and S. Ji, "Measurement of flow ripple in positive displacement pumps (effect of approximation model of discharge passage in pump)", in *Proceedings of the 10th JFPS International Symposium on Fluid Power 2017*, Fukuoka, Japan, 2017.

[28] A. F. *et al.*, "Experimental measurement and numerical validation of the flow ripple in internal gear pumps", *Energies*, vol. 15, no. 24, Dec. 18, 2022, ISSN: 1996-1073. DOI: 10.3390/en15249607.

[29] C. Bramley and N. D. Johnston, "Comparison of methods for measuring pump flow ripple and impedance", in *Proceedings of ASME/BATH 2017 Symposium on Fluid Power and Motion Control*, Sarasota, FL, USA: American Society of Mechanical Engineers, Oct. 16, 2017, ISBN: 978-0-7918-5833-2. DOI: 10.1115/FPMC2017-4223.

[30] D. E. Bowns, K. A. Edge, and D. G. Tilley, "The assessment of pump fluid borne noise", in *Proceedings of I. Mech. E. Conf.-Quiet Oil Hydraulic Systems*, London, England, 1977.

[31] P. Larsson, "Fluid power attenuators analysis, measurements and performance optimization", in *Proceedings of the JFPS International Symposium on Fluid Power*, Tokyo, Japan, 1989.

[32] D. Becher, "Untersuchungen an einer Axialkolbenpumpe mit Ringsystem zur Minderung von Pulsationen", Ph.D. dissertation, TU Dresden, Dresden, Germany, 2004.

[33] E. Kojima, T. Yamazaki, and K. Edge, "Development of standard testing procedure for experimentally determining inherent source pulsation power generated by hydraulic pump", *International Journal of Fluid Power*, vol. 10, no. 1, pp. 27–35, Jan. 2009, ISSN: 1439-9776, 2332-1180. DOI: 10.1080/14399776.2009.10780965.

[34] H. Theissen and W. Risken, "Messung der Volumenstrompulsation von Hydraulikpumpen", *Ölhydraulik und Pneumatik*, vol. 27, no. 5, 1983.

[35] B. Müller, “Einsatz der Simulation zur Pulsations- und Geräuschminderung hydraulischer Anlagen”, ISBN: 978-3-8322-0793-9, Ph.D. dissertation, RWTH Aachen, Aachen, Germany, 2002.

[36] U. Bittner, “Strukturakustische Optimierung von Axialkolbeneinheiten: Modellbildung, Validierung und Topologieoptimierung”, ISBN: 978-3-86644-938-1, Ph.D. dissertation, Karlsruher Institut für Technologie, Karlsruhe, Germany, 2013.

[37] B. Xu, S. Ye, and J. Zhang, “Numerical and experimental studies on housing optimization for noise reduction of an axial piston pump”, *Applied Acoustics*, vol. 110, pp. 43–52, Sep. 2016, ISSN: 0003682X. DOI: 10.1016/j.apacoust.2016.03.022.

[38] Y. Pan *et al.*, “Noise source identification and transmission path optimisation for noise reduction of an axial piston pump”, *Applied Acoustics*, vol. 130, pp. 283–292, Jan. 2018, ISSN: 0003682X. DOI: 10.1016/j.apacoust.2017.10.009.

[39] J. Zhang *et al.*, “Experimental investigation on the noise reduction of an axial piston pump using free-layer damping material treatment”, *Applied Acoustics*, vol. 139, pp. 1–7, Oct. 2018, ISSN: 0003682X. DOI: 10.1016/j.apacoust.2018.04.013.

[40] M. Haarhaus, “Geräuschentstehung und Geräuschminderung bei Axialkolbenpumpen in Schrägscheibenbauweise”, Ph.D. dissertation, RWTH Aachen, Aachen, Germany, 1984.

[41] A. Johansson, J. Övander, and J. O. Palmberg, “Experimental verification of cross-angle for noise reduction in hydraulic piston pumps”, *Proceedings of the Institution of Mechanical Engineers, Part I: Journal of Systems and Control Engineering*, vol. 221, no. 3, pp. 321–330, May 1, 2007, ISSN: 0959-6518, 2041-3041. DOI: 10.1243/09596518JSCE208.

[42] G. K. Seeniraj and M. Ivantysynova, “Multi-objective optimization tool for noise reduction in axial piston machines”, *SAE International Journal of Commercial Vehicles*, vol. 1, no. 1, pp. 544–552, Oct. 7, 2008, ISSN: 1946-3928. DOI: 10.4271/2008-01-2723.

[43] T. Kim and M. Ivantysynova, “Active vibration control of axial piston machine using higher harmonic least mean square control of swash plate”, in *Proceedings of 10th International Fluid Power Conference*, Dresden, Germany, 2016.

[44] T. Kim and M. Ivantysynova, “Active vibration/noise control of axial piston machine using swash plate control”, in *Proceedings of ASME/BATH 2017 Symposium on Fluid Power and Motion Control*, Sarasota, FL, USA: American Society of Mechanical Engineers, Oct. 16, 2017, ISBN: 978-0-7918-5833-2. DOI: 10.1115/FPMC2017-4304.

[45] S. Ye, J. Zhang, and B. Xu, “Noise reduction of an axial piston pump by valve plate optimization”, *Chinese Journal of Mechanical Engineering*, vol. 31, 2018, article-number: 57, ISSN: 1000-9345, 2192-8258. DOI: 10.1186/s10033-018-0258-x.

[46] H. Münch, “Akustisch erweiterte Virtualisierung von Industrieprodukten”, Ph.D. dissertation, FAU Erlangen-Nürnberg, Erlangen, Germany, 2021. DOI: 10.25593/978-3-96147-387-8.

[47] W. Kassing, “Untersuchungen zum Schwingungs-und Körperschallverhalten rotationssymmetrischer Maschinenstrukturen und Übertragung der Ergebnisse auf die Geräuschentwicklung von Axialkolbeneinheiten”, Ph.D. dissertation, TU Darmstadt, Darmstadt, Germany, 1975.

[48] E. Lechner, *Untersuchung des Betriebs- und Geräuschverhaltens einer verstellbaren Axialkolbenpumpe mit Ventil-Vorsteuerung*. Berlin, Heidelberg: Springer Berlin Heidelberg, 1980, ISBN: 978-3-540-10127-7.

[49] D. He *et al.*, “Simultaneous transfer path analysis of axial piston pump lumped parameter model results”, in *Proceedings of 2024 International Maha Fluid Power Conference*, West Lafayette, IN, USA: River Publishers, 2024, pp. 221–240, ISBN: 978-87-7004-745-6. DOI: 10.13052/rp-9788770047456.016.

[50] International Organization for Standardization, *ISO 4412-2:1991 Hydraulic fluid power – Test code for determination of airborne noise levels – Part 2: Motors*, 1991.

[51] International Organization for Standardization, *ISO 3744:2010 Acoustics – Determination of sound power levels and sound energy levels of noise sources using sound pressure – Engineering methods for an essentially free field over a reflecting plane*, 2010.

[52] P. B. Vesikar *et al.*, “Pass by noise analysis method extended for mitigation solution development on earth moving machinery”, in *Proceedings of Noise and Vibration Conference & Exhibition*, Grand Rapids & Online, MI, United States, Aug. 31, 2021. DOI: 10.4271/2021-01-1071.

[53] P. B. Vesikar *et al.*, “Excavator exterior noise contribution analysis using angle-based operational acoustic load synthesis”, in *Proceedings of Noise & Vibration Conference & Exhibition*, Grand Rapids, MI, United States, May 5, 2025. DOI: 10.4271/2025-01-0062.

[54] P. B. Vesikar, J. Edgington, and J. Drabison II, “Evaluation of invariant structural and acoustic loads estimation methods to be used in vehicle platform development independent to the boundary conditions of load generation”, in *Proceedings of Noise & Vibration Conference & Exhibition*, Grand Rapids, MI, United States, May 5, 2025. DOI: 10.4271/2025-01-0053.

[55] S. Woo and A. Vacca, “Experimental characterization and evaluation of the vibroacoustic field of hydraulic pumps: The case of an external gear pump”, *Energies*, vol. 13, no. 24, Dec. 16, 2020, article-number: 6639, ISSN: 1996-1073. DOI: 10.3390/en13246639.

[56] S. Park, J. Cho, and S. Park, “Reduction of structure-borne noise in hydraulic power unit with elastic mounting by evaluating structural acceleration level”, *Journal of Advanced Marine Engineering and Technology*, vol. 44, no. 6, pp. 422–430, Dec. 31, 2020, ISSN: 2234-7925. DOI: 10.5916/jamet.2020.44.6.422.

[57] J. W. R. Meggitt, “An introduction to the in-situ blocked force method for vibration source characterisation”, Acoustics Research Centre - University of Salford, 2022. DOI: 10.13140/RG.2.2.11488.97288.

[58] T. ten Wolde and G. Gadefelt, "Development of standard measurement methods for structureborne sound emission", *Noise Control Engineering Journal*, vol. 28, no. 1, pp. 5–14, 1987, ISSN: 07362501. DOI: 10.3397/1.2827676.

[59] A. T. Moorhouse, A. S. Elliott, and J. W. R. Meggitt, "Virtual acoustic prototyping - a story of four decades", in *Proceedings of Inter-Noise 2022*, Glasgow, 2022.

[60] International Organization for Standardization, *ISO 9611:1996 Acoustics – Characterization of sources of structure-borne sound with respect to sound radiation from connected structures – Measurement of velocity at the contact points of machinery when resiliently mounted*, 1996.

[61] German Institute for Standardization, *DIN EN 15657:2017 Akustische Eigenschaften von Bauteilen und von Gebäuden – Messung des Körperschalls von haustechnischen Anlagen im Prüfstand für alle Installationsbedingungen*, 2017.

[62] M. Haeussler, "Modular sound and vibration engineering by substructuring", Ph.D. dissertation, Technical University of Munich, Munich, Germany, 2020. DOI: 10.13140/RG.2.2.33547.41766.

[63] B. M. Gibbs, R. Cookson, and N. Qi, "Vibration activity and mobility of structure-borne sound sources by a reception plate method", *The Journal of the Acoustical Society of America*, vol. 123, no. 6, pp. 4199–4209, Jun. 1, 2008, ISSN: 0001-4966, 1520-8524. DOI: 10.1121/1.2904469.

[64] M. M. Späh and B. M. Gibbs, "Reception plate method for characterisation of structure-borne sound sources in buildings: Installed power and sound pressure from laboratory data", *Applied Acoustics*, vol. 70, no. 11, pp. 1431–1439, Dec. 2009, ISSN: 0003682X. DOI: 10.1016/j.apacoust.2009.04.011.

[65] M. M. Späh and B. M. Gibbs, "Reception plate method for characterisation of structure-borne sound sources in buildings: Assumptions and application", *Applied Acoustics*, vol. 70, no. 2, pp. 361–368, Feb. 2009, ISSN: 0003682X. DOI: 10.1016/j.apacoust.2008.03.001.

[66] F. Schoepfer, A. Mayr, and U. Schanda, "Experimental investigation of a single reception plate method to obtain two source quantities required to predict structure-borne sound transmission in buildings", in *Proceedings of ICA 2019 International Congress in Acoustics*, Aachen, Germany, 2019.

[67] International Organization for Standardization, *ISO 20270-1:2019 Acoustics – Characterization of sources of structure-borne sound and vibration – Indirect measurement of blocked forces*, 2019.

[68] A. S. Elliott *et al.*, "In-situ source path contribution analysis of structure borne road noise", *Journal of Sound and Vibration*, vol. 332, no. 24, pp. 6276–6295, Nov. 2013, ISSN: 0022460X. DOI: 10.1016/j.jsv.2013.05.031.

[69] A. S. Elliott, J. W. R. Meggitt, and A. T. Moorhouse, "Blocked forces for the characterisation of structure borne noise", in *Proceedings of Inter-Noise 2015*, San Francisco, CA, USA, 2015.

[70] M. Sturm *et al.*, “The in-situ blocked force method for characterization of complex automotive structure-borne sound sources and its use for virtual acoustic prototyping”, in *Proceedings of International Conference on Noise and Vibration Engineering (ISMA) 2016*, Leuven, Belgium, 2016.

[71] D. Lennström *et al.*, “Validation of the blocked force method for various boundary conditions for automotive source characterization”, *Applied Acoustics*, vol. 102, pp. 108–119, Jan. 2016, ISSN: 0003682X. DOI: 10.1016/j.apacoust.2015.08.019.

[72] F. Bianciardi *et al.*, “Road noise assessment using component-based TPA for a tire assembly”, in *Proceedings of SIA-CTTM Automotive NVH Comfort 2018*, Le Mans, France, 2018.

[73] K. Wienen *et al.*, “Robust NVH engineering using experimental methods - source characterization techniques for component transfer path analysis and virtual acoustic prototyping”, *SAE International Journal of Advances and Current Practices in Mobility*, vol. 1, no. 4, pp. 1766–1778, Jun. 5, 2019, ISSN: 2641-9645. DOI: 10.4271/2019-01-1542.

[74] A. El Mahmoudi *et al.*, “In-situ source characterization for NVH analysis of the engine-transmission unit”, in *Proceedings of the 38th International Modal Analysis Conference (IMAC XXXVIII)*, A. Linderholt, M. Allen, and W. D’Ambrogio, Eds., Houston, TX, USA, 2020, pp. 79–91, ISBN: 978-3-030-47629-8. DOI: 10.1007/978-3-030-47630-4_7.

[75] P. Wagner *et al.*, “High frequency source characterization of an e-motor using component-based TPA”, in *Proceedings of SIA NVH Comfort 2021*, Le Mans, France, 2021.

[76] C. L. Balogh, T. Kimpián, and T. Ungvári, “An examination of component-based TPA performance and feasibility for steering motors”, *Journal of Physics: Conference Series*, vol. 2677, no. 1, p. 012 011, Dec. 1, 2023, ISSN: 1742-6588. DOI: 10.1088/1742-6596/2677/1/012011.

[77] International Organization for Standardization, *ISO 3019-1:2001 Hydraulic fluid power – Dimensions and identification code for mounting flanges and shaft ends of displacement pumps and motors – Part 1: Inch series shown in metric units*, 2001.

[78] A. T. Moorhouse, A. S. Elliott, and T. A. Evans, “In situ measurement of the blocked force of structure-borne sound sources”, *Journal of Sound and Vibration*, vol. 325, no. 4, pp. 679–685, Sep. 2009, ISSN: 0022460X. DOI: 10.1016/j.jsv.2009.04.035.

[79] M. V. van der Seijs, D. de Klerk, and D. J. Rixen, “General framework for transfer path analysis: History, theory and classification of techniques”, *Mechanical Systems and Signal Processing*, vol. 68-69, pp. 217–244, Feb. 2016, ISSN: 0888-3270. DOI: 10.1016/j.ymssp.2015.08.004.

[80] K. Wienen, “Fast transfer path analysis using controlled electric motors as in-situ blocked force vibration sources”, Ph.D. dissertation, University of Salford, Salford, United Kingdom, 2021.

[81] M. V. van der Seijs, "Experimental dynamic substructuring: Analysis and design strategies for vehicle development", Ph.D. dissertation, Delft University of Technology, Delft, The Netherlands, 2016. DOI: 10.4233/UUID:28B31294-8D53-49EB-B108-284B63EDF670.

[82] M. V. van der Seijs *et al.*, "A robust transfer path analysis method for steering gear vibrations on a test bench", in *Proceedings of International Conference on Noise and Vibration Engineering (ISMA) 2014*, Leuven, Belgium, 2014. DOI: 10.13140/RG.2.1.4297.8647.

[83] J. W. R. Meggitt and A. T. Moorhouse, *Experimental Vibro-acoustics: In situ and blocked force methods for component-based simulation and virtual prototyping*, 1st ed. London: CRC Press, Jul. 2, 2025, ISBN: 978-1-003-39913-1. DOI: 10.1201/9781003399131.

[84] M. Sturm, "Identification and quantification of transient structure-borne sound sources in electrical steering systems", Ph.D. dissertation, University of Salford, Salford, United Kingdom, 2013.

[85] M. van der Seijs *et al.*, "An improved methodology for the virtual point transformation of measured frequency response functions in dynamic substructuring", in *Proceedings of COMPDYN 2013*, Kos Island, Greece, 2013, pp. 4334–4347, ISBN: 978-960-99994-2-7. DOI: 10.7712/120113.4816.C1539.

[86] A. T. Moorhouse, "On the characteristic power of structure-borne sound sources", *Journal of Sound and Vibration*, vol. 248, no. 3, pp. 441–459, Nov. 2001, ISSN: 0022460X. DOI: 10.1006/jsvi.2001.3797.

[87] J. L. Meriam, L. G. Kraige, and J. N. Bolton, *Engineering Mechanics*, 9th ed. Wiley, 2018, ISBN: 978-1-119-39098-5.

[88] B. M. Gibbs and M. Villot, "Structure-borne sound in buildings: Advances in measurement and prediction methods", *Noise Control Engineering Journal*, vol. 68, no. 1, pp. 1–20, Jan. 20, 2020, ISSN: 0736-2501. DOI: 10.3397/1/37681.

[89] A. El Mahmoudi, U. S. Paracha, and D. J. Rixen, "Design optimization of joint parameters using frequency based substructuring", *PAMM*, vol. 19, no. 1, Nov. 2019, article-number: e201900454, ISSN: 1617-7061. DOI: 10.1002/pamm.201900454.

[90] M. Häußler, D. Kobus, and D. J. Rixen, "Combining blocked force transfer path analysis and dynamic substructuring for acoustic design optimization", in *Proceedings of ICEDyn 2019*, Viana do Castelo, Portugal, 2019.

[91] A. El Mahmoudi, D. J. Rixen, and C. H. Meyer, "Comparison of different approaches to include connection elements into frequency-based substructuring", *Experimental Techniques*, vol. 44, no. 4, pp. 425–433, Aug. 2020, ISSN: 0732-8818. DOI: 10.1007/s40799-020-00360-1.

[92] J. O. Almirón *et al.*, "A frequency-based substructuring application on a transmission bracket", in *Proceedings of International Conference on Noise and Vibration Engineering (ISMA) 2020*, Leuven, Belgium, 2020.

[93] P. Wagner, "Application of dynamic substructuring in NVH design of electric drivetrains", in *Proceedings of International Conference on Noise and Vibration Engineering (ISMA) 2020*, Leuven, Belgium, 2020.

[94] M. van der Kooij, S. W. B. Klaassen, and A. Huelsmann, "Using dynamic substructuring and component TPA to shape the NVH experience of a full-electric vehicle", in *Proceedings of 12th International Styrian Noise, Vibration & Harshness Congress: The European Automotive Noise Conference*, Graz, Austria, Jun. 15, 2022. DOI: 10.4271/2022-01-0988.

[95] C. Schleihs, "Acoustic design of hydraulic axial piston swashplate machines", ISBN: 978-3-8440-5296-1, Ph.D. dissertation, RWTH Aachen, Aachen, Germany, 2017.

[96] T. Bregar *et al.*, "Introducing pyFBS: An open-source python package for frequency based substructuring and transfer path analysis", in *Proceedings of the 39th International Modal Analysis Conference (IMAC XXXIX)*, M. S. Allen, W. D'Ambrogio, and D. Roettgen, Eds., 2021, pp. 81–89, ISBN: 978-3-030-75909-4. DOI: 10.1007/978-3-030-75910-0_10.

[97] A. El Mahmoudi *et al.*, "A tutorial on an open-source python package for frequency-based substructuring and transfer path analysis", in *Proceedings of the 40th International Modal Analysis Conference (IMAC XL)*, M. Allen, S. Davaria, and R. B. Davis, Eds., Series Title: Conference Proceedings of the Society for Experimental Mechanics Series, Orlando, FL, USA, 2022, pp. 107–117, ISBN: 978-3-031-05404-4. DOI: 10.1007/978-3-031-05405-1_15.

[98] T. Bregar *et al.*, "pyFBS: A python package for frequency based substructuring", *Journal of Open Source Software*, vol. 7, no. 69, p. 3399, Jan. 19, 2022, ISSN: 2475-9066. DOI: 10.21105/joss.03399.

[99] A. T. Moorhouse, T. A. Evans, and A. S. Elliott, "Some relationships for coupled structures and their application to measurement of structural dynamic properties in situ", *Mechanical Systems and Signal Processing*, vol. 25, no. 5, pp. 1574–1584, Jul. 2011, ISSN: 08883270. DOI: 10.1016/j.ymssp.2010.12.016.

[100] A. V. Oppenheim, A. S. Willsky, and S. H. Nawab, *Signals & systems* (Prentice-Hall signal processing series), 2nd ed. Upper Saddle River, N.J: Prentice Hall, 1997, 957 pp., ISBN: 978-0-13-814757-0.

[101] M. Romeser and R. von Schwerin, "Data-driven serial testing of axial piston units: Integrating signal processing and machine learning for roller bearing fault detection", in *Proceedings of 19th Scandinavian International Conference on Fluid Power, SICFP'25*, Linköping University, Sweden, 2025, pp. 410–423. DOI: 10.13052/rp-9788743808251A30.

[102] S. Mathiowetz and H. A. Bonhoff, "Interface mobilities for characterization of structure-borne sound sources resiliently mounted via multiple contact points", *Journal of Sound and Vibration*, vol. 332, no. 22, pp. 5789–5803, Oct. 2013, ISSN: 0022460X. DOI: 10.1016/j.jsv.2013.05.034.

[103] A. T. Moorhouse, A. S. Elliott, and Y. Heo, “Intrinsic characterisation of structure-borne sound sources and isolators from in-situ measurements.”, in *Proceedings of ICA 2013*, Montreal, Canada, 2013. DOI: 10.1121/1.4799691.

[104] J. W. R. Meggitt and A. T. Moorhouse, “The in-situ decoupling of resiliently coupled sub-structures”, in *Proceedings of 24th International Congress on Sound and Vibration 2017*, London, UK, 2017.

[105] J. W. R. Meggitt and A. Moorhouse, “In-situ sub-structure decoupling of resiliently coupled assemblies”, *Mechanical Systems and Signal Processing*, vol. 117, pp. 723–737, Feb. 2019, ISSN: 08883270. DOI: 10.1016/j.ymssp.2018.07.045.

[106] J. Y. Oh *et al.*, “Bushing stiffness optimization method for NVH improvement using blocked force and energy-based index in suspension system”, in *Proceedings of 13th International Styrian Noise, Vibration & Harshness Congress: The European Automotive Noise Conference*, Graz, Austria, 2024. DOI: 10.4271/2024-01-2921.

Unpublished Sources

[107] Y. Bünyamin, “Optimierung des Anschlussflanschs einer Axialkolbenpumpe für die experimentelle Umsetzung der in-situ Blocked Forces Methode durch strukturdynamische FE-Simulation”, Bachelor’s thesis, Ernst-Abbe-Hochschule Jena, Jena, Germany, 2024.

[108] T. Böckle, “Charakterisierung der Körperschallemissionen von Axialkolbenpumpen”, Master’s thesis, Hochschule Esslingen, Esslingen, Germany, 2025.

Internet Sources

[109] Laboratory for Dynamics of Machines and Structures, UL FME and Chair of Applied Mechanics (AM), TUM. “pyFBS”, https://pyfbs.readthedocs.io/en/master/# (Accessed: 01/12/2026).

Own Publications

[110] M. Vogt and M. Geimer, “An approach for evaluating structure-borne noise emission of axial piston units using blocked forces”, in *Proceedings of 19th Scandinavian International Conference on Fluid Power, SICFP’25*, Linköping, Sweden, 2025, pp. 466–477. DOI: 10.13052/rp-9788743808251A35.

[111] M. Vogt and M. Geimer, “Comparison of different approaches for evaluating structure-borne noise emission of axial piston units”, in *Proceedings of DAGA 2025 (Deutsche Jahrestagung für Akustik)*, Copenhagen, Denmark, 2025.

[112] M. Vogt and M. Geimer, “An approach for evaluating structure-borne noise emission of axial piston units using blocked forces”, *International Journal of Fluid Power*, vol. 27, no. 1, pp. 225–256, 2026. DOI: 10.13052/ijfp1439-9776.2717.

[113] M. Vogt and M. Geimer, “Analysis of structure-borne noise emissions of axial piston pumps using blocked forces and virtual point transformation”, in *Proceedings of 15th International Fluid Power Conference*, Aachen, Germany, 2026.